BASIN ANALYSIS OF THE KALAHARI MANGANESE BASIN

by

SAREL JOHANNES VAN DER MERWE

SUPERVISOR: DR SW VAN DER MERWE
CO-SUPERVISOR: DR WA VAN DER WESTHUIZEN

SUBMITTED IN FULFILMENT FOR THE DEGREE OF

MAGISTER SCIENTIAE

IN THE FACULTY OF SCIENCE

DEPARTMENT OF GEOLOGY

THE UNIVERSITY OF THE ORANGE FREE STATE

BLOEMFONTEIN

June 1997

ACKNOWLEDGEMENTS

I am grateful to SAMANCOR for the opportunity to do a Basin Analysis of the Kalahari Manganese Basin and permission to use the data for a MSc. I also appreciate the financial assistance given by SAMANCOR.

I am in particular thankful for the continual guidance and support given to me by ED Swindell and Peter Harrison.

I am thankful to Dr S van der Merwe and Dr W van der Westhuizen of the University of the Orange Free State for their assistance, guidance and support during the research period.

ABSTRACT

The Proterozoic-aged Hotazel Iron Formation, within the Kalahari Manganese Basin, is host to the world's largest land-based manganese deposit. Three manganese-rich units are present, each rimmed by a hematite-lutite that grades up- and downwards into banded iron formation (BIF). Two ore types, a low-grade (30-38% Mn) Mamatwan-type, which represents the bulk of the deposit and a locally developed Wessels-type high-grade ore (> 48% Mn), are present.

The mineralogical associations within the different iron formation facies reflect the chemistry of the environment during precipitation. The depository was stratified with respect to Eh and pH which controlled the deposition of the different BIF facies and associated manganese deposits. Four major facies types were recognised, grading laterally from oxygenated shallow-water deposits which accumulated under slightly acidic conditions (hematite-chert facies BIF), through hematite-chert-carbonate and magnetite-chert-carbonate associations, into deeper water rhythmites (greenalite-magnetite-carbonate facies BIF), indicating a reduced and slightly alkaline environment. High-grade Mn ores (Wessels-type ore; hausmanite and braunite II) are restricted to the hematite-chert facies iron formation which was deposited above the wave base over intrabasinal volcanic mounds (Epsom-Olivewood paleohigh) or close to a shoreline (Wessels-type deposit). The BIF units are distinctly thin in these environments, gradually thickening deeper into the basin.

The low-grade (Mamatwan-type ore; braunite I) is hosted by evenly bedded silicate facies iron formation (greenalite-magnetite-carbonate facies) which represents the dominant facies-type in the Kalahari Basin.

The hematite, greenalite and iron-carbonate represent three primary or early diagenetic precipitates. Some of the fine-grained magnetite within the magnetite-chert-carbonate facies may also be of primary origin, but the bulk of the magnetite is clearly secondary.

Convective circulation of acidic, heated sea water is inferred to have leached iron and manganese from the Ongeluk lava pile and introduced the metals to the depository. Metal laden hydrothermal fluids, introduced along feeder channels, supplemented the metal content of the waters.

TABLE OF CONTENTS

LIST OF FIGURES

LIST OF TABLES

1. INTRODUCTION

The study area (Kalahari Manganese Basin) is situated in the Kuruman district of the Northern Cape Province and lies approximately 1 000m above sea level. The nearest towns are, Kuruman, 60km to the south east, and Kathu, approximately 55km to the south. (Fig. 1.1)

The topography varies from flat sand-covered thornveld in the south to a more undulating landscape in the north, characterised by belts of permanent dunes which grade into bushy, calcrete-covered flats. The only distinct topographic features in the area are a small inselberg at Black Rock mine, the north-south striking Kuruman Hills and the Korannaberge, which lie to the east and west of the basin respectively. The climate is semi-arid with a mean annual rainfall of 300mm, most of which falls in the summer months.

The Kalahari manganese field comprises five known erosional or structurally preserved relicts of the Proterozoic-aged Voëlwater Subgroup with interbedded manganese layers: (Fig.1.1)

(i) The Mamatwan-Wessels deposit (also known as the Main Kalahari Basin) which is the largest.
(ii) The Avontuur deposit ± 30km north of the main Kalahari Basin.
(iii) The Leinster deposit further north.
(iv) The Hotazel deposit.
(v) The Langdon Annex deposit.

The latter two are outliers which occur well to the east of the main Kalahari Basin and are generally thought to have been preserved as a result of down-faulting in grabens.

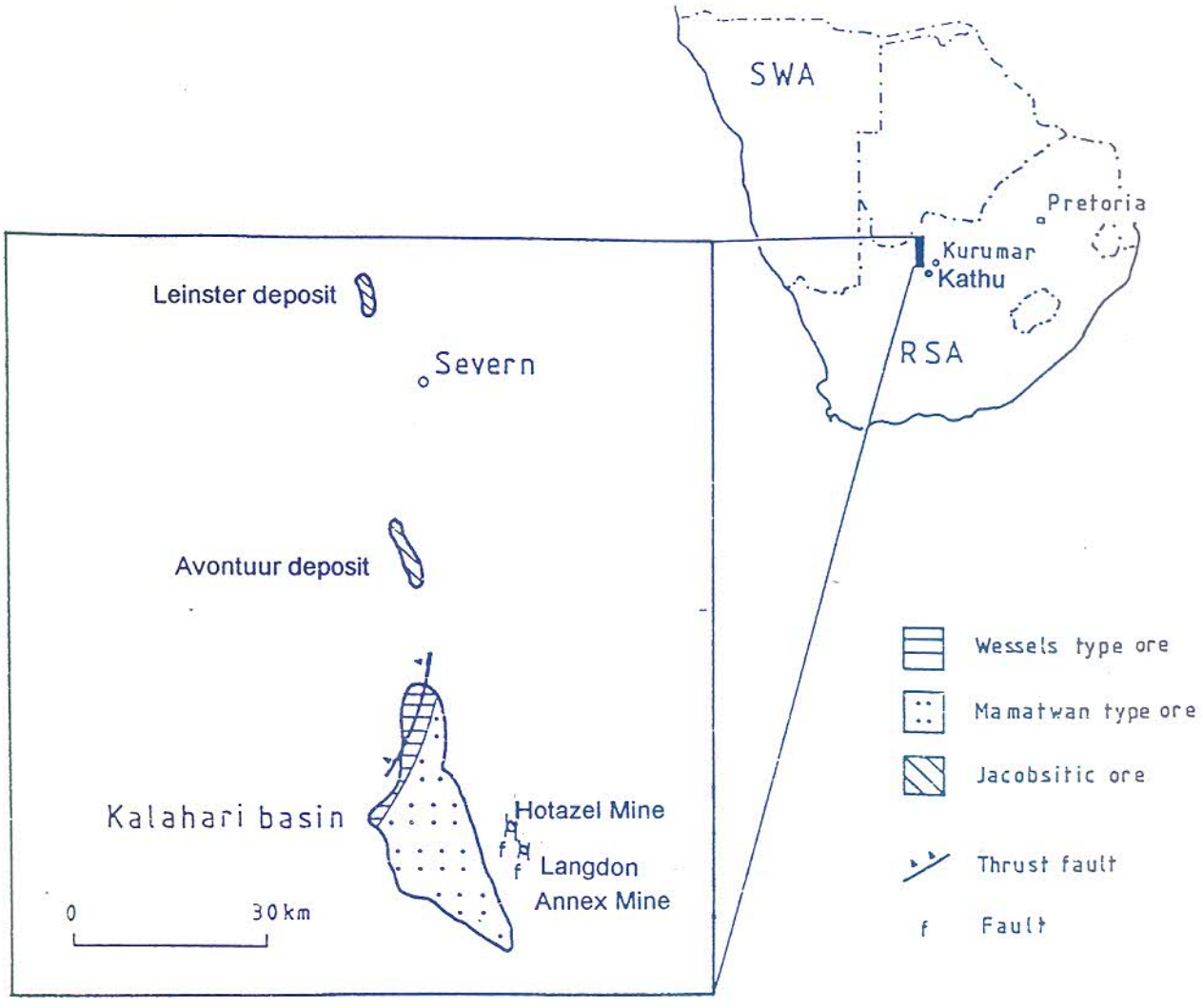

Fig. 1.1 *The locality of the study area showing the distribution of the remnants of the Kalahari basin in which the Voëlwater Subgroup has been preserved, with the various ore types encountered (After Kleyenstüber, 1984).*

Virtually the entire manganese field is covered by gravels, clays, calcrete and aeolian sand of the Tertiary-aged Kalahari Formation. The only outcrop of the Hotazel Iron Formation is on a hill at Black Rock Mine.

Commercial activities in the district are dominated by livestock and game farming as well as by mining of manganese, iron and asbestos. Manganese is currently being mined at Wessels and Mamatwan by South African Manganese Corporation (SAMANCOR) as well as by Associated Manganese at Black Rock, Nchwaning and Gloria. With the exception of Mamatwan which is an open pit, all the other mines are shallow underground operations (less than 400m deep). The Hotazel and Langdon Annex deposits have been mined out. National Manganese is currently excavating an open pit on the edge of the sub-outcrop of the main basin on the farm Langdon Annex. Middelplaats Mine, an underground operation originally commissioned by the Anglo American Corporation and subsequently purchased by Samancor, is dormant.

2. OBJECTIVES OF THE STUDY

The objectives of this study are as follows:

(i) To elucidate the palaeoenvironmental setting of the Voëlwater Subgroup, comprising lower BIF (Hotazel Formation) and upper dolomites (Mooidraai Formation) using a basin analysis approach. This has never been attempted before firstly, because the rocks can only be examined in borehole core, much of which is regarded as highly confidential by the various mining and exploration companies involved, and because previous academic research was focused on detailed mineralogy of the ores.

(ii) To establish the controls on the distribution of the Wessels-type high-grade mineralisation as opposed to that of the lower grade Mamatwan-type. This could then be used to target further exploration for shallow high-grade ore.

3. PREVIOUS STUDIES

Boardman (1964), de Villiers (1970) and Beukes (1983 & 1985) presented broad overviews of the stratigraphy, structure and regional distribution of the manganese mineralisation within the main Kalahari Basin.

De Villiers (1983) published papers on the detailed mineralogy of the manganese ores in the main Kalahari Basin. A comprehensive account of the mineralogy of some of the banded iron formations and associated ores was compiled by Kleyenstüber (1983 and 1984) at Mintek on behalf of Samancor. Nel (1984) studied the geochemical relationships and mineralogy within the Mamatwan ore body. These authors postulated genetic models for the origin of the manganese mineralisation.

Beukes and Smit (1987a) presented evidence for thrusting along the western margin of the Kalahari Basin. Miyano and Beukes (1987) evaluated the physicochemical conditions under which the low-grade diagenetic Mamatwan-type ore could have formed.

Dixon (1989) investigated sugilite and other minerals in the ores at Wessels Mine. A major petrological and geochemical study on the Ongeluk Lavas and their possible genetic relationship to the manganese ores was undertaken by Schutte (1992).

Tsikos (1994) studied the mineralogy of the banded iron formations from four bore holes along the sub-outcrop on the farm Rissik 330, to the north of Mamatwan. This study represents the first attempt to reconstruct the palaeoenvironmental setting for the deposition of the banded iron formation within the Kalahari Manganese Basin.

Burger and Beukes (1995) investigated the influence of high-angle extensional structures on the upgrading of certain of the Kalahari manganese ores.

4. REGIONAL GEOLOGICAL SETTING

4.1 Introduction

The early Proterozoic Transvaal Supergroup sequence in Griqualand West, which hosts the manganese deposits of the Kalahari field, is situated along the western margin of the Kaapvaal Craton (Fig. 4.1). The sequence is also preserved within the main Transvaal or Bushveld Basin within South Africa and south-eastern Botswana, as well as the much smaller Kanye Basin in Botswana (Eriksson *et al.*, 1993). The basin is thought to have developed in response to intracratonic extension on the then stabilised Kaapvaal-Limpopo-Zimbabwe block and comprises nearly 15 000m of relatively unmetamorphosed volcanic, clastic and chemical sedimentary rocks (Thomas *et al.*, 1993; Eriksson *et al.*, 1993).

In Griqualand West, the succession can broadly be subdivided into a basal chemical sedimentary unit, the Ghaap Group, which is overlain by a mixed volcanic-clastic-chemical unit known as the Postmasburg Group (Table 4.1). The Ghaap and Postmasburg Groups form two separate major unconformity-bounded sequences (Cheney and Winter, 1995).

According to Beukes (1983 and 1987), deposition of the Transvaal sequence in Griqualand West took place on a continental margin or trailing edge and was controlled by three major tectonic-sedimentary elements:

(i) A shallow water platform on the Kaapvaal Craton.

(ii) A platform edge (shelf margin) located parallel to the Griquatown fault zone (a growth fault across which there are a number of facies changes).

(iii) A deep basin along the western margin of the Kaapvaal Craton (Fig. 4.2).

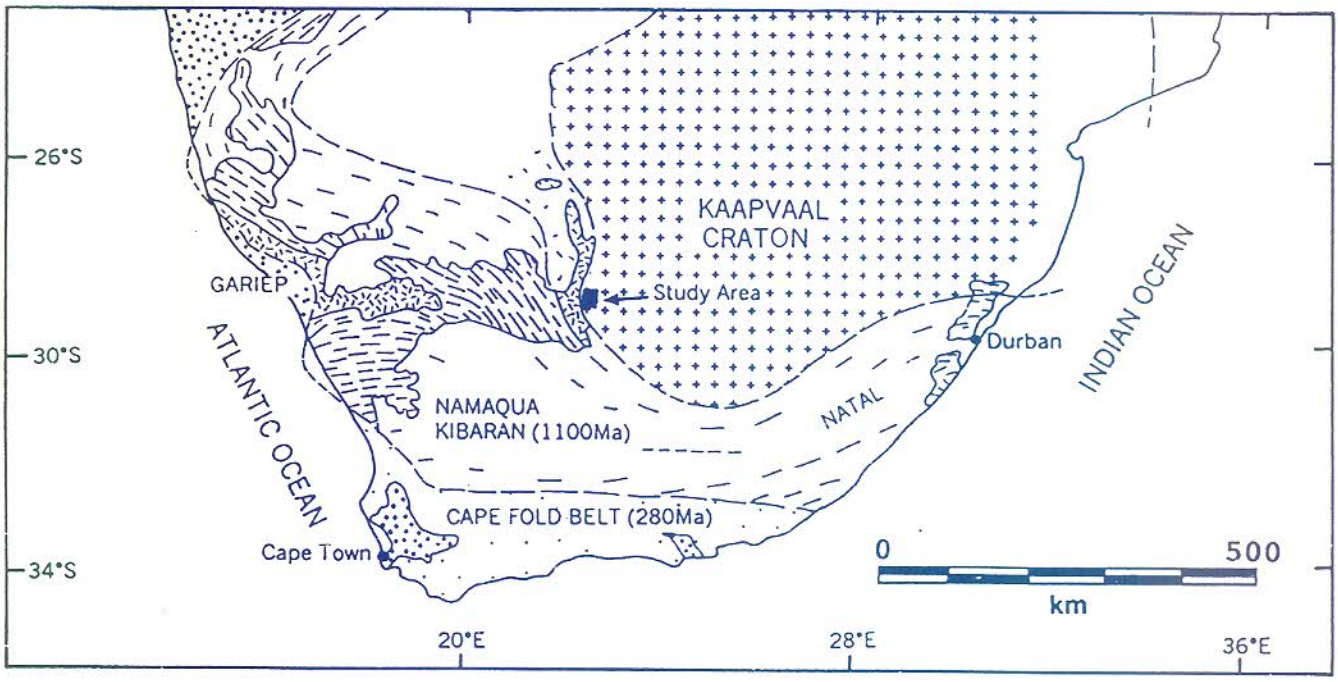

Fig. 4.1 *Location of study area in relation to the tectonic regimes of Southern Africa (after Thomas et al., 1993).*

4.2 The Ghaap Group

4.2.1 *The Campbellrand Subgroup*

The Campbellrand Subgroup consists of stromatolitic dolomite and limestone platform facies which interfinger westwards and southwestwards with laminated limestone and dolomite (Fig. 4.2) which, in part at least, may represent carbonate turbidites (Beukes 1980a and 1983); the latter have been ankeritised and silicified to produce banded ferruginous chert.

The inferred turbidites interfinger with carbonaceous shale (Prieska facies) which have been deposited in an euxinic basin in front of the carbonate platform. Regional lithofacies relationships suggest that the carbonate build-up developed

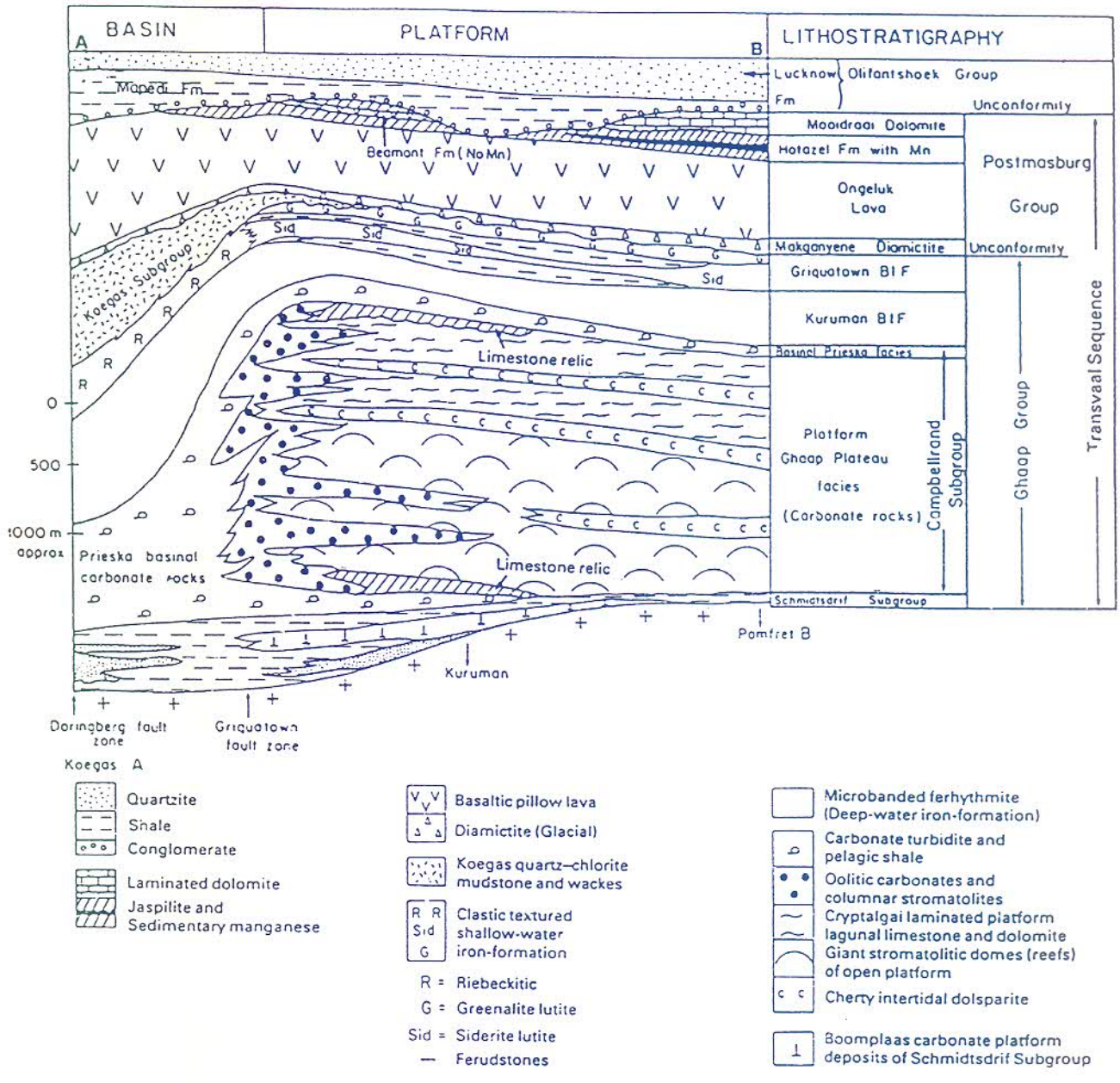

Fig. 4.2 *North-south section illustrating stratigraphic and sedimentological facies relationships in the Transvaal Supergroup in Griqualand West (after Beukes, 1986).*

from an early carbonate ramp stage to a rimmed carbonate shelf during the deposition of the upper part of the carbonate sequence (Beukes, 1987).

4.2.2 *Asbesheuwels Subgroup*

Shallow water carbonate deposition was terminated by a major transgression which drowned the shelf. The euxinic shale plus iron formation of the lower Kuruman Iron Formation were deposited in a deep shelf setting over the entire Kaapvaal Craton (Beukes, 1983, 1984 and 1987) (Fig. 4.3). The Kuruman Iron Formation comprises an upward-shallowing sequence (Fig. 4.4) which consists of the following (Beukes, 1983 and 1984):

(i) Carbonaceous shale deposited in an euxinic basin.

(ii) Ankerite-banded chert, representing distal carbonate turbidites, deposited in the transition zone between the euxinic basin and the open shelf.

(iii) Mixed stilpnomelane lutite, banded magnetite-hematite ferythmites macrocycles deposited on the deep open shelf.

(iv) Greenalite-siderite rhythmites deposited along the toe-of slope and slope areas of a shallow water platform.

(v) A clastic textured, orthochemical and allochemical iron formation (Ouplaas Member) deposited on a shallow-water platform. Volcanic ash (stilpnomelane lutite) and fumarolic sodium as well as silica were supplied to the shelf during periods of explosive volcanicity (Beukes, 1983 and 1984)

The Griquatown iron-formation overlies the Kuruman iron Formation and consists of four upward-coarsening orthochemical/allochemical units (Beukes, 1983 and 1984).

TABLE 4.1 *STRATIGRAPHY OF THE TRANSVAAL SUPERGROUP IN GRIQUALAND WEST. NORTHERN CAPE PROVINCE (after Beukes and Smit, 1987a, as amended by Hälbich et al., 1993).*

SUPER-GROUP	GROUP	SUB-GROUP	FORMATION		MAJOR LITHOLOGY	APPROX. THICNESS in m.
TRANSVAAL	OLIFANTS-HOEK	VOLOP	VERWATER		Grey quartzite	3500
			GLEN LYON — ELLIES RUS		Brown quartzite / Grey quartzite	
			FULLER		Brown quartzite	
			HARTLEY		Andesitic lava	700
			LUCKNOW		Purple and white quartzite	450
			MAPEDI		Shale, quartzite, lava Basal iron-rich conglomerate	10–1500
	POSTMAS-BURG	VOËL-WATER	MOOIDRAAI	Laterally into	Dolomite, chert,	250
			HOTAZEL	BEAUMONT	Iron-formation, manganese, lava	
			ONGELUK		Andesitic lava	900
			MAKGANYENE		Diamictite	50–150
	GHAAP	KOEGAS	ROOINEKKE & NELANI		Iron-formation, shale	300
	OLIFANTS-HOEK		GAMAGARA (Correlative of Mapedi)		Quartzite and shale, basal iron-rich conglomerate	290
TRANSVAAL	GHAAP	KOEGAS	MANGANORE*	Correlative of Asbesheuwels	Iron-formation and iron ore	0–200
			WOLHAARKOP*	Solution collapse breccia	Siliceous chert breccia	
			ROOINEKKE		Iron-formation	100
			NARAGAS		Quartz wacke, shale	240–600
			KWAKWAS		Riebeckitic slate	
			DORADALE		Iron-formation	
			PANNETJIE		Quartz wacke, shale	
		ASBES-HEUWELS	GRIQUATOWN		Clastic-textured iron-formation	200–300
			KURUMAN*	* On Maremane dome Manganore and Wolhaarkop	Microbanded iron-formation	150–750
		CAMPBELLRAND	GAMOHAAN	Laterally into NAUTE and NARAGAS	Sparry limestone, shale	1500–1700
			KOGELBEEN		Dolomite, limestone	
			KLIPPAN		Cherty dolomite	
			PAPKUIL		Dolomite	
			KLIPFONTEIN-HEUWEL		Cherty dolomite	
			FAIRFIELD		Sparry dolomite	
			REIVILO		Micritic dolomite	
			MONTEVILLE		Dolomite, limestone, shale	
		SCHMIDTS-DRIF	LOKAMMONA		Shale	10–250
			BOOMPLAAS		Dolomite, limestone, shale	
			VRYBURG		Quartzite, shale, lava	

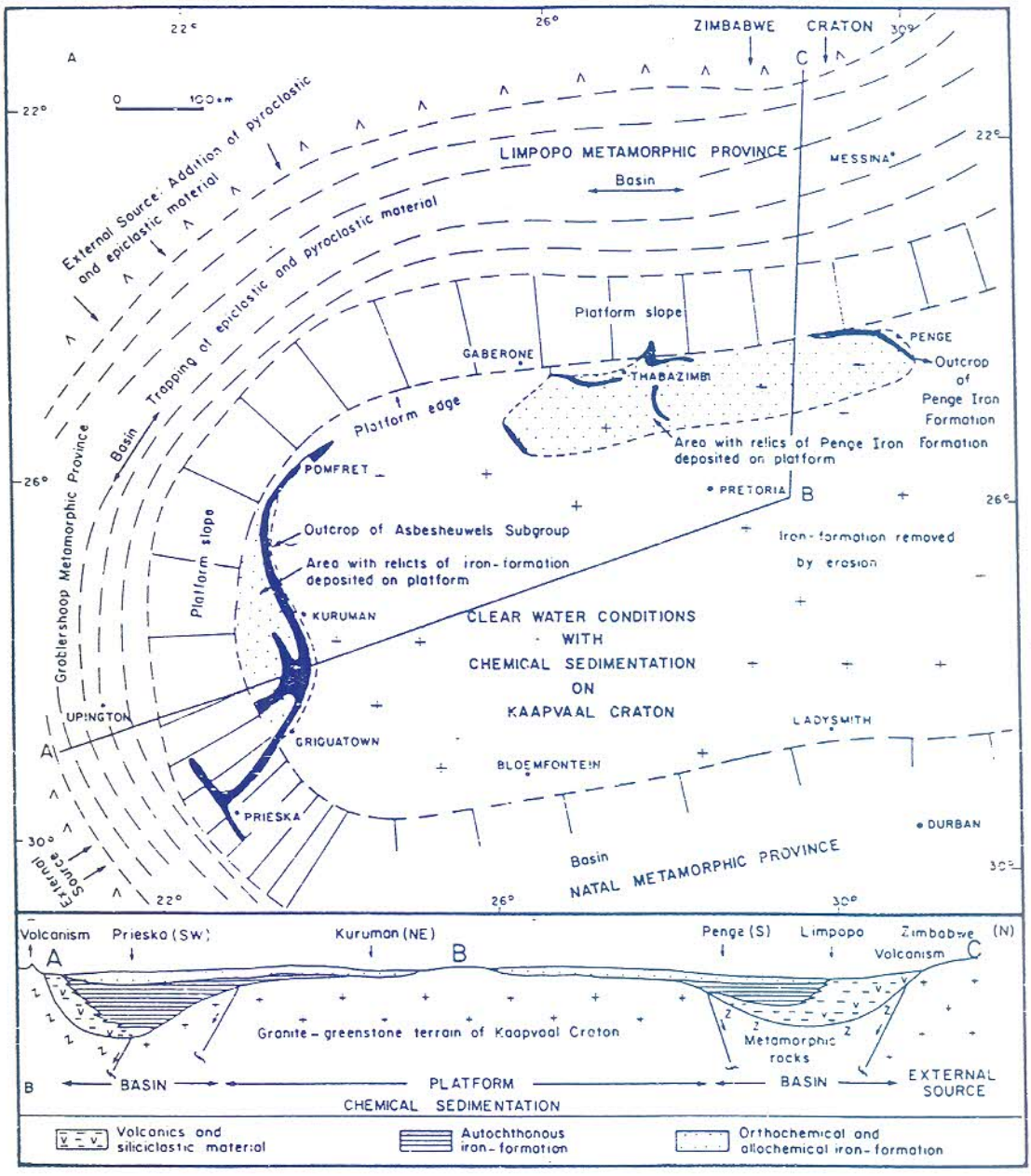

Fig. 4.3 *Nature of the depository of the Transvaal Supergroup during the deposition of the Asbesheuwels-Penge iron formation sequence. Plan view (a) and cross-section (b) (after Beukes, 1983).*

These grade upwards into chloritic mudstone, siltstone, quartz-wacke and iron formation of the Koegas Subgroup, which are regarded as deltaic sediments deposited within a lacustrine setting (Beukes, 1984).

Clendenin (1989) and Clendenin *et al.* (1986) postulated that the Ghaap/Chuniespoort Groups were deposited on a gentle south-west dipping ramp, which did not have a prominent break in slope as proposed in the Beukes model (Fig. 4.2). The ramp is thought to have been bounded by a shallow basin to the west. Periods of non-deposition and erosion were followed by transgressions marked by mixed carbonate-thrombolitic mud facies covering the basin, or by an onlap of distal iron formation.

Altermann and Hälbich (1991) and Hälbich *et al.* (1993) dispute the hypothesis that the carbonate basin became deeper towards the western and southwestern margin of the Kaapvaal Craton and provide evidence of supratidal to intertidal flats in the carbonate rocks in the south western portions of the Griqualand West region, analogous to the shallow water carbonate platform of Beukes (1983) to the east. They envisage the deepest portion of the basin to have lain between the two shallow tidal platforms, coincident with the Griquatown fault zone. Hälbich *et al.* (1992) used trace element data, REE patterns and the distribution of organic carbon to show that shallow and fresh water contamination conditions prevailed during the genesis of the iron formations in this south-western region. They envisage that two contemporaneous separate sub-basins developed on the craton, one in the Transvaal and the other in Griqualand West.

Geophysical modelling of the regional government survey and gravity data by Geerthsen *et al.* (1991) suggest the presence of thick shelf sediments towards the west, which supports the Beukes (1978) model (Fig. 4.5). Altermann and Halbich (1990 and 1991), however, recognised an early fold and thrust event (pre-Makganyene) within the Transvaal Supergroup along the southwestern margin of the craton. They challenged the great thickness proposed by Beukes (1983 and 1987) for his "deep basin" facies as well as his stratigraphic correlations.

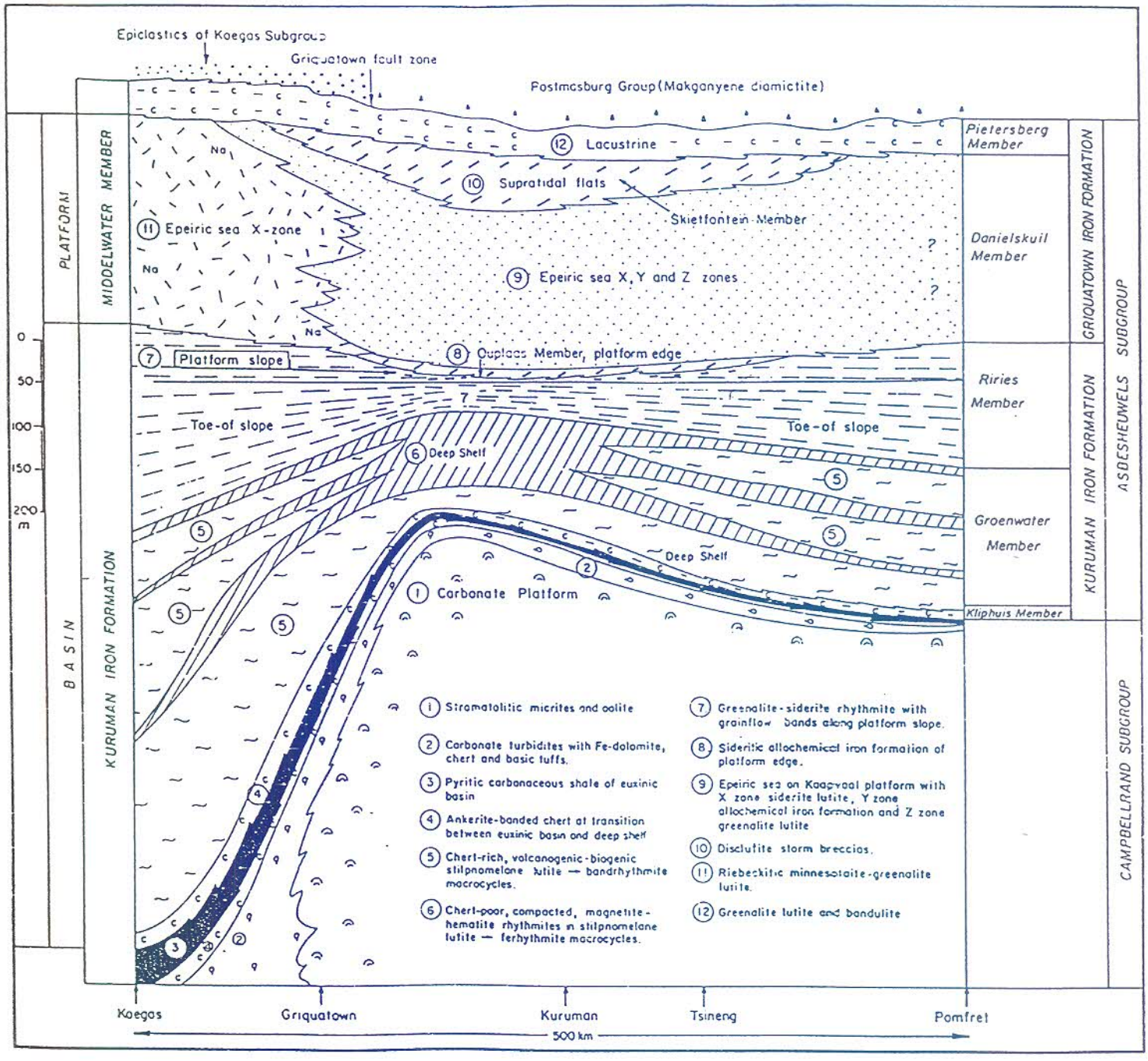

Fig. 4.4 *South-north section illustrating stratigraphic relationships and inferred palaeodepositional environments of the Asbesheuwels Subgroup in Griqualand West (from Beukes, 1983).*

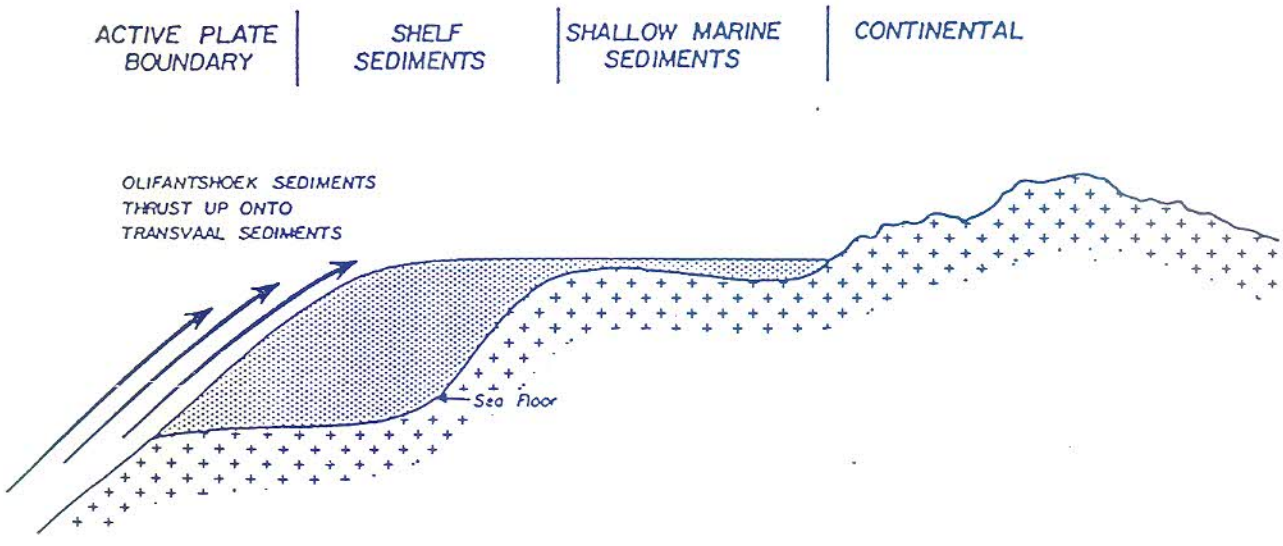

Fig. 4.5 *Conceptual model of the depositional environment of the Asbesheuwels Subgroup (after Geerthsen et al., 1991). Thickening may also be the result of tectonic duplication (Altermann and Halbich, 1990 and 1991).*

4.3 **The Postmasburg Group**

4.3.1 *Introduction*

The Postmasburg Group overlies the Ghaap Group unconformably. That the Griqualand West, Transvaal and the Kanye basins developed, from this stage on, as separate basins now seems to be fairly well established, but is by no means proven:

(i) Correlation of the Pretoria Group in the Transvaal basin with the upper portion of the Griqualand West sequence and the sedimentary rocks of the Kanye basin is poor, with only the Hekpoort-Ditlhojana-Tsatsu-Ongeluk andesites appearing to be a convincing marker unit (Eriksson *et al.*, 1993).

The Hekpoort volcanics were extruded subaerially in contrast to the largely subaqueous Ongeluk volcanics (Schutte, 1992).

(ii) Eriksson *et al.* (1988) and Crockett (1972) provide sedimentological as well as geophysical evidence suggesting that the present extent of the Pretoria Group in both the Transvaal and Botswana basins broadly reflects the original extent. Cheney and Winter (1995), however, dispute this hypothesis as there is a broad stratigraphic similarity between the Postmasburg and Pretoria Groups indicating that they could have been connected.

Large portions of the upper Ventersdorp strata have been eroded along, or to the west of the north-south Vryburg Arch, which separates the Griqualand West from the Transvaal basin (Hälbich *et al.*, 1993)

4.3.2 *Makganyene Formation*

The unconformity at the base of the Makganyene Formation cuts progressively down through the Ghaap Group from the Koegas Subgroup to the Griquatown Formation, as one moves from the basin onto the inferred platform (Fig. 4.2).

Two distinct facies are evident in the Makganyene Diamictite (Beukes, 1983):

(i) Interbedded massive diamictite, poorly bedded diamictite, conglomerate, pebbly sandstone, siltstone, varved shale and mudstone (Visser, 1971). Evidence of glacial action includes striated pebbles, rafted stones and remnants of an eroded glacial pavement (Visser, 1971). It is confined to the Kaapvaal platform area and the rock types are interpreted as a piedmont glacial and glaciofluvial assemblage, with the area under glaciation having being limited and probably centred over the Vryburg Arch (Visser, 1971; Beukes, 1983). Nearly all the sediments were derived intrabasinally, by glacial erosion of the underlying formations of the Transvaal Supergroup.

(ii) Rhythmic alternations of arenaceous and argillaceous diamictite, conglomerate, clayey sandstone, subgreywacke, cherty iron carbonate, dolomitic limestone and banded jaspilite (De Villiers and Visser, 1977). Broadly speaking, this facies comprises stacked cycles of graded diamictite, greywacke and siderite-bandlutite (Beukes, 1983). The association of diamictite with immature sandstones and non-clastic beds in a cyclic fashion as well as the presence of rafted pebbles suggest that the material was deposited under water, largely from a floating ice mass (De Villiers and Visser, 1977). These represent glaciomarine deposits which formed from the transportation of debris in a southerly direction into a water body which lay to the south and south-west of the Vryburg Arch. Some of the diamictite beds, especially those interbedded with carbonates, probably represent slumped till derived from the basin margin. Clayey sandstone/subgreywacke, siltstone and conglomerate assemblages are interbedded at regular intervals within the diamictite. The presence of graded bedding and slump structures in these beds as well as the intrabasinally derived fragments in the conglomerate suggest that these sediments were deposited under the influence of gravity, as slumps and turbidity flows during periodic retreats of the ice (De Villiers and Visser, 1977). Chemical sediments (carbonate and iron-formation) were deposited during quiet interglacial periods. This sedimentation was frequently disturbed by turbidity currents resulting in erosion and re-transportation by the flows. The fact that most of the pebbles in the diamictite comprise chert is explained by a rather homogeneous source area which consisted of the underlying iron formation and carbonate sequences (De Villiers and Visser, 1977).

The thickness of the Makganyene Formation is highly variable. Visser (1977) postulated a southward decrease in thickness, whilst De Villiers and Visser (1971) observed an increase in thickness from 68m near Sishen to 552m to the west of Postmasburg. In places however, the Makganyene is entirely missing.

4.3.3 *Ongeluk Formation*

The Makganyene diamictites are conformably overlain by the Ongeluk lava in the Kuruman area, a laterally extensive sequence of tholeiitic basaltic andesites which were extruded under water in a marginal basin within the continental setting of the Kaapvaal Craton (Schutte, 1992). Volcanic ash and fragments are present in the upper part of the Makganyene diamictite sequence indicating that the initial stages of Ongeluk volcanism were contemporaneous with the last stages of glacial and/or debris flow sedimentation (De Villiers and Visser, 1977). This material is not identical in composition to that of the Ongeluk lava (Beukes and Klein, 1990). The occurrence of platy and y-shaped shards points to plinian eruptions which are normally associated with acid volcanism (Schutte, 1992).

The Ongeluk Formation is subdivided into two distinct lava types (Schutte, 1992): The first type is the **Regional Ongeluk lava** which is grey-green to bluish-grey in colour and covers almost the entire outcrop region. The second type, termed the **Kalahari Ongeluk lava**, is normally of a bright-maroon colour and occurs towards the edge of the Kalahari Basin (Hotazel-Black Rock area) and near the top of the volcanic pile. The volcanic characteristics of the Kalahari Ongeluk lava, which lies at the top of the pile in the Kalahari Basin, are similar to that of the Regional Ongeluk lava but disseminated goethite and hematite impart a characteristic reddish to purple colour to the latter.

Schutte(1992) tentatively estimated the thickness of the Ongeluk lava at 500m. Recent deep stratigraphic drilling and seismic profiling in the Kalahari Basin by Samancor has shown that the lavas are between 1 000m and 1 200m thick.

The Ongeluk Formation is composed of massive lavas, pillow lavas and hyaloclastite beds in close association. Massive lavas are the dominant rock-type which extruded from long fissures or multiple vents on a broad, flat, slowly subsiding plain similar to that inferred for other continental flood basalt provinces (Schutte, 1992). The general absence of sedimentary intercalations between flow units suggests short time intervals between eruptions.

4.3.4 *Hotazel Formation*

The Ongeluk lava is conformably overlain by jaspilite, iron-formation and bedded manganese deposits of the Hotazel Formation of the Voëlwater Subgroup (Fig. 4.6), which may attain a thickness of 200m. Virtually the entire manganese field, save for the outcrop at Black Rock, is covered by younger rocks of the Olifantshoek Group and/or the Phanerozoic Dwyka tillite, as well as Cretaceous to Tertiary Kalahari Group sediments.

Three manganese units are interbedded within the banded iron-formation of the Hotazel Formation (Fig. 4.6). The lowermost manganese bed is the main source of ore and varies in thickness from 5m to 45m. The middle manganese unit is of uneconomic grade and only 1 to 2m thick, whilst the upper unit is about 5m thick on average and is only mined on a limited scale. The manganese layers are rimmed by hematite-lutite units.

Two major types of ore occur within the main Kalahari Basin i.e.; a lower grade (36% Mn) Mamatwan-type and a higher grade (48% Mn) Wessels-type. The former is considered to represent a primary or diagenetic phase of mineralisation. It is essential braunitic in composition and is dull, compact and finely laminated or banded. Ellipsoidal carbonate ovoids up to 2mm in diameter are conspicuous and carbonate lamellae/bands invariably accentuate the layering within the ore. The Wessels-type ore on the other hand, is coarse-grained, shiny, massive or vuggy and may have a brecciated appearance. The principal ore minerals are hausmannite and braunite II.

The Beaumont facies of this formation which comprises jaspilite interbedded with mafic lava, tuffs and ferruginous dolomite occurs in a north-south trending belt west and south-west of Postmasburg, is regarded by Beukes (1983 and 1985) as a proximal volcanogenic-sedimentary facies equivalent to the distal, interbedded iron formation and manganolutite of the Hotazel Formation. Iron formations in the Korannaberg have been correlated by Beukes with the Hotazel Formation

(Beukes, 1983 and 1985). Exploration by SAMANCOR indicates that these rocks can be correlated with the Hartley Hill volcanics. The Hotazel Formation is conformably overlain by a shallowing-upward platformal carbonate sequence known as the Mooidraai dolomite (Fig. 4.6).

4.3.5 *Mooidraai Formation*

The Mooidraai Formation comprises dark grey cryptalgal laminated carbonates, domal stromatolites, breccias and planar laminated rhythmites deposited in the following different settings i.e.:

(i) Carbonate platform sediments that prograded basinward progressively over the Ongeluk lava and the Hotazel Iron Formation. Cryptalgal laminations at the base may indicate deposition in fairly shallow water (Beukes, 1983).

(ii) Gravity-flow deposits comprising massive breccias, laminated and graded carbonates, deposited in front of a shallow water platform (Beukes, 1983).

4.4 **The Olifantshoek Group**

4.4.1 *Introduction*

These sediments represent the first major clastic deposits within the Kalahari Manganese Basin and are only preserved along the northern and western boundaries of the Kalahari basin. The absence of the Olifantshoek stratigraphy in the rest of the basin might be attributed to erosion during Permo-Carboniferous Dwyka glaciation, but could also reflect a primary depositional pattern.

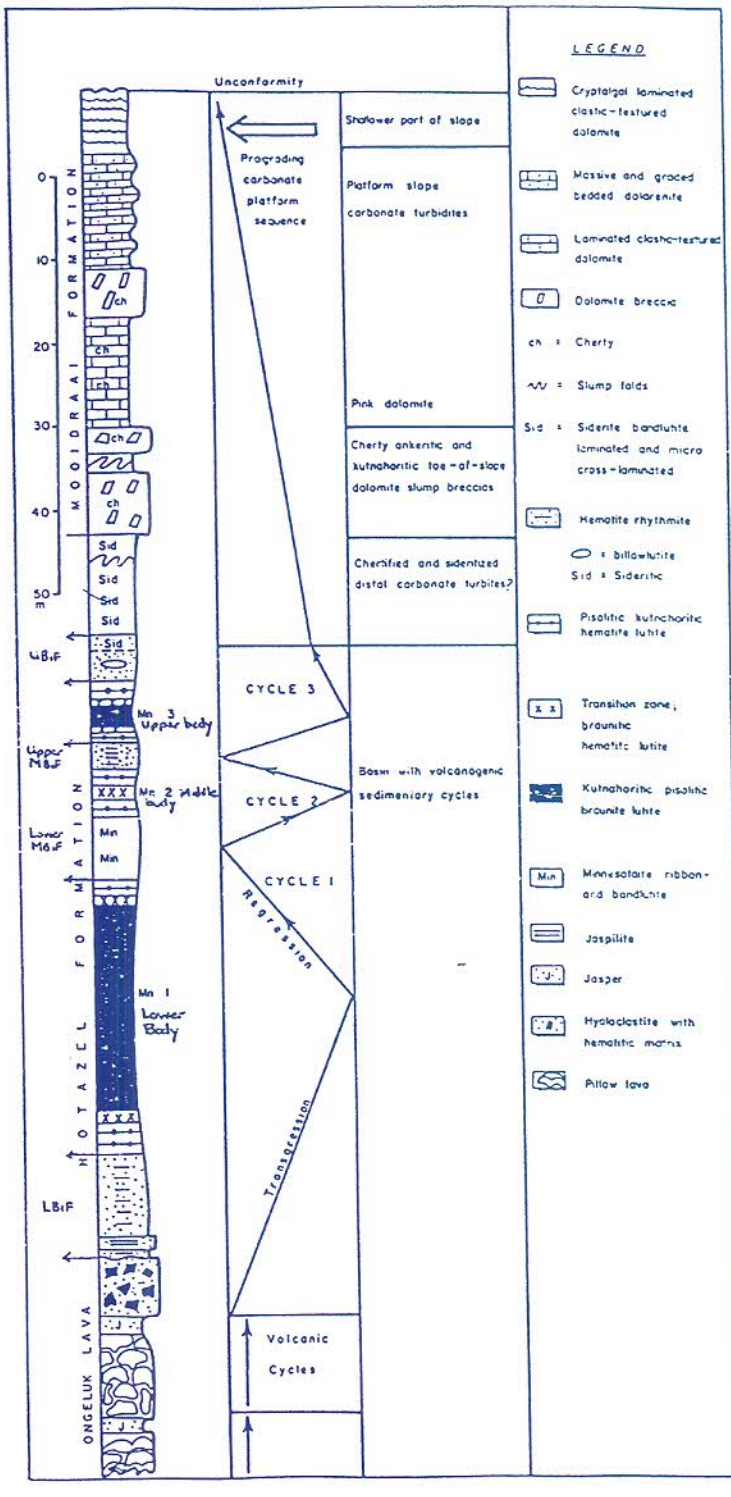

Fig. 4.6 *Stratigraphic profile of the Hotazel - and Mooidraai Formations in the Kalahari Manganese field with an interpretation of their environments of deposition (after Beukes, 1983).*

4.4.2 *Mapedi Formation*

The Mapedi Formation forms the basal part of the Olifantshoek sequence and is also known as the Gamagara Formation around the Maremane Dome. It lies with a distinct unconformity on the older rocks (Table 4.1). The unconformity progressively cuts down through the Hotazel Iron Formation, Ongeluk Lavas, Asbesheuwels Subgroup into the Cambellrand dolomite. The unconformity is marked by a hematite-pebble conglomerate and shale unit which fills depressions along the undulating unconformity surface and is thought to represent a braided alluvial fan complex (Van Schalkwyk and Beukes, 1986). In the Kalahari Basin the basal unit comprises an irregular thickness of Hotazel Formation breccia, ferruginous shales and thin quartzite horizons. The bulk of the Mapedi consists of interbedded light green to greyish-green and maroon shales with subordinate graphitic shales and thin ferruginous or pale quartzite layers. These form two distinct upward coarsening cycles in the Sishen area which Van Schalkwyk and Beukes (1986) interpreted as having formed in a deltaic environment. A thick (385m) succession of highly amygdaloidal mafic lava, pyroclastics and red to green tuffaceous shale occur within the Mapedi Formation.

4.4.3 *Lucknow Formation*

The overlying Lucknow Formation consists of fine-grained white massive orthoquartzite which grades upward into pebbly or coarse-grained maroon/greyish-green sandstone. Herringbone cross-stratification is visible within the quartzites in cuttings on the main national road just south of Olifantshoek. The Lucknow Formation probably represents a fluvially-dominated, high-energy, beach deposit. A conspicuous off-white dolomite horizon is intercalated within the Lucknow Formation on the farm Droëkloof 293 in the Korannaberg.

4.4.4 *Hartley Formation*

In the Langeberg and Korannaberg mountains a number of explosive subaerial mafic volcanic centres existed, which formed the Hartly basalt, separating the Lucknow quartzite and overlying Fuller quartzite (Cornell, 1987); (Table 4.1).

4.4.5 *Volop Subgroup*

The overlying Volop Subgroup comprises four formations, characterised mainly by two upward-fining cycles of braided fluvial quartz sandstones (Jansen, 1983). The contact between the Volop and underlying Mapedi-Lucknow-Hartley basalt is regarded as an unconformity by Cheney and Winter (1995).

4.5 **Karoo Supergroup**

4.5.1 *Dwyka Formation*

The Dwyka tillite forms a prominent north-south trending palaeo-glacial valley-fill along the western margin of the Kalahari Basin and is in places up to 600m deep. Subsidiary Dwyka valley-fills are known elsewhere in the environments of the Kalahari Basin but are not nearly as deep.

Dolerite dykes and sills occur throughout the area and represent several episodes of intrusion from Ongeluk to Karoo times (Schutte, 1992). These dykes are orientated approximately NNE-SSW near Olifantshoek but follow a N-S trend towards the east.

4.6 **Structural Geology**

Structurally, the area may be divided into two distinct domains, separated by a major post-Olifantshoek thrust fault, the Blackridge thrust (Fig. 4.7):

(i) The area to the east of, and in the footwall of the thrust is characterised by gently plunging north-south trending open dome and basin structures. Dips are gentle, normally less than 20° . Faulting is dominated by N-S and ENE-WSW trending high-angle extensional structures which may have had a scissors type of movement.

(ii) The area to the west of the thrust is characterised by an imbricated fold and thrust belt with tight, double-plunging, eastward verging, north-south trending folds. The overall ramp-like shape of the carbonate platform at the margin of the Kaapvaal Craton in this area obviously facilitated and accentuated this structural event. This deformation post-dates that outlined in (i) and must have taken place prior to 1780 Ma.

Altermann and Halbich (1990 and 1991) recognised an early phase of thrusting within the Asbesheuwels Subgroup, pre-dating the deposition of the Makganyene diamictite in the area south of the Griquatown fault zone. This deformation as well as the later thrusting event described in (ii) above, resulted in tectonic transport to the east, north-east and south-east in this area. Both deformational episodes become more intense towards the present rim of the craton.

An additional deformational phase, which resulted in gentle folding and high-angle faulting of the Transvaal Supergroup and theOlifantshoek Group as well as two earlier sets of thrusts, complicates matters especially towards the craton margin, but its effects decrease northwards and eastwards onto the craton. This event, because the fold axes are parallel to the general strike of structures in the Namaqua Metamorphic Belt, is assumed to be of Namaquan age (1100 Ma).

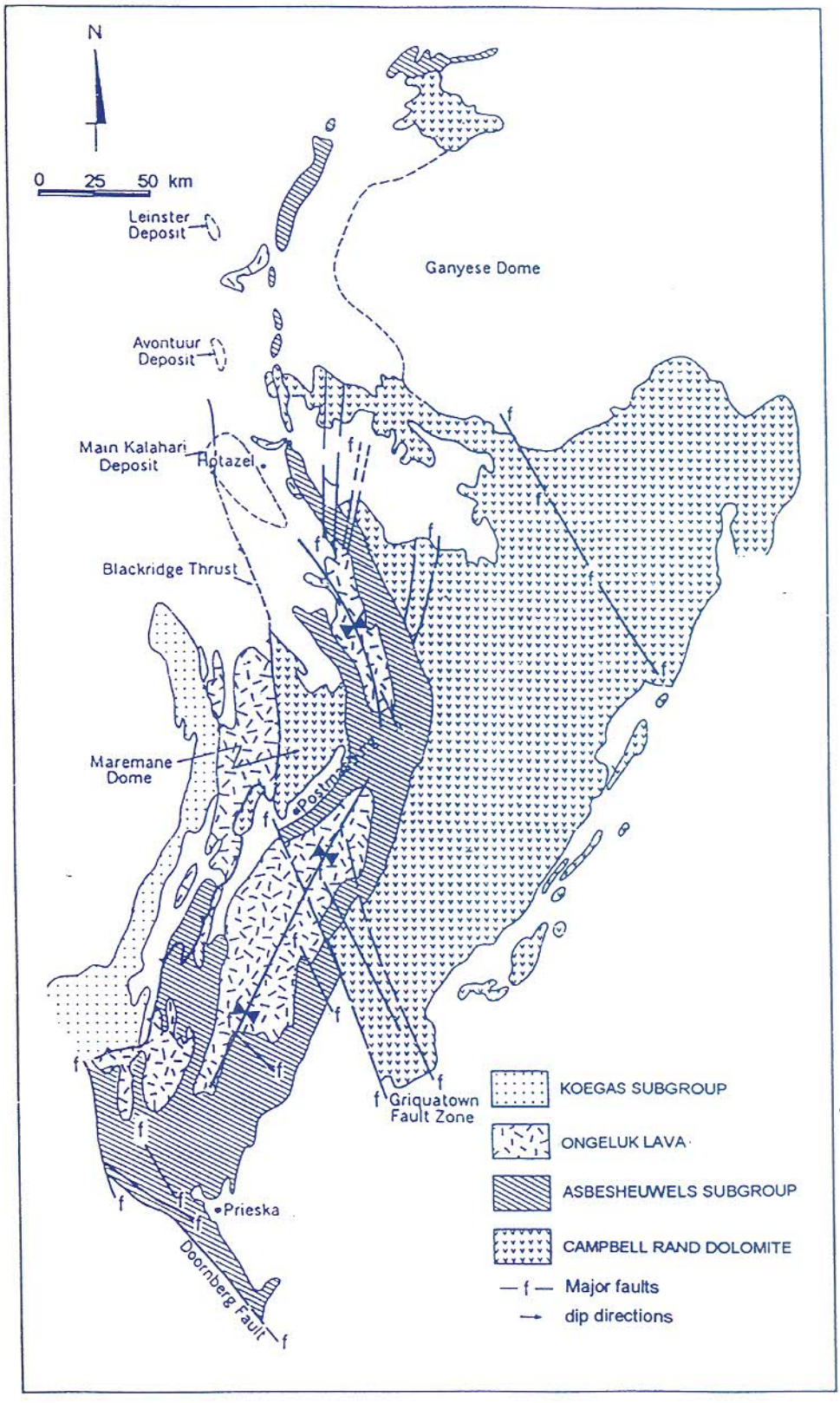

Fig. 4.7 *Major structural features affecting the Griqualand West Sequence of the Transvaal Supergroup.*

5. APPROACH OF THIS STUDY

5.1 A Basin Analysis Concept

A basin analysis approach was employed to help in understanding the distribution of and controls on the manganese mineralisation in the Kalahari field.

Major oil companies have been utilising techniques of quantitative basin analysis in exploration for a decade and a half or more (Eidel, 1991). Ore-forming processes in stratiform, sediment-hosted ore deposits commonly involve sedimentary processes, diagenesis, basinal brines and palaeohydrology.

Basin analysis involves the following (De Vries Klein, 1991; Miall, 1990):

(i) The regional synthesis of stratigraphy and sedimentation in terms of the tectonic framework. This primarily involves the recognition of unconformity-bound (time-bound) stratigraphic sequences, which are ideally established through seismic methods, or through the recognition of unconformities in drill core, as well as by detailed lithostratigraphic correlation and application of biostratigraphic zonation.

(ii) Each sequence so established must then be interpreted in terms of its component depositional systems using sedimentological data, the principles of facies analysis and basin mapping techniques (e.g. isopach maps, structural contour maps and various ratio maps).

5.2 Techniques employed

The present is based on three transects through the Kalahari basin. Reference, where applicable, has been made to other areas examined outside the confines of these transects. The three transects include: (Fig. 5.1; folder at back)

(i) An east-west transect in the central part of the basin from the farm Epsom 285 to the Hotazel Mine.

(ii) An east-west transect across the southern part of the basin from the farm Smuts 364 through to the Mamatwan Mine.

(iii) A northwest-southeast transect from Mamatwan Mine to the farm Olivepan 282.

The study involved relogging of all available diamond drill core. Special attention was paid to the nature of the underlying Ongeluk volcanics, sedimentary structures, rock alteration, the characteristics of any mineralisation present and factors which may control its grade, as well as the identification of key marker beds and unconformity-bound sequences critical in tectonostratigraphic correlation.

A total of 30 samples were investigated by XRD techniques. Twenty samples of hematite-lutite which are the dominant host for the Mn mineralization were also examined petrographically.

Thirty samples were analysed by XRF techniques for major and trace element concentrations. The XRF analysis were performed according to the technique of Norrish and Hutton (1969). Both XRD and XRF analysis were executed at the Geology Department of the University of the Orange Free State.

Subsurface basin mapping techniques were employed to establish the overall palaeogeographic setting, and included:

(i) Facies analysis maps/diagrams of the Hotazel iron formation and the Mooidraai dolomite.

(ii) A basin configuration map using unconformity surfaces as datum lines.

(iii) Isopach maps of the above-mentioned facies.

5.3 Classification and Nomenclature of Iron Formation

An iron formation is defined as an iron-rich sedimentary rock consisting of microcrystalline iron minerals (femicrite) and chert (Beukes, 1983). The chert occurs either as chert mesobands and microbands or as microcrystalline interstitial grains. The iron formations display textural and structural features analogous to those in carbonate rocks (Dimroth, 1976 and 1979). The complex nomenclature and classification of iron formation, based on carbonate terminology by Beukes (1980b and 1983) is given in Fig. 5.2 and Table 5.1. According to this classification, allochemical iron formation is composed of allochems (grains) such as pebbles and grains whereas orthochemical iron formation consists of massive Felutite. Microbanded iron-formations are referred to as ferhythmites which for the most part represent autochthonous iron-formations. An adjective is used to describe the mineralogical composition of the iron-formation and the dominant mineral phase is placed first (Fig. 5.2).

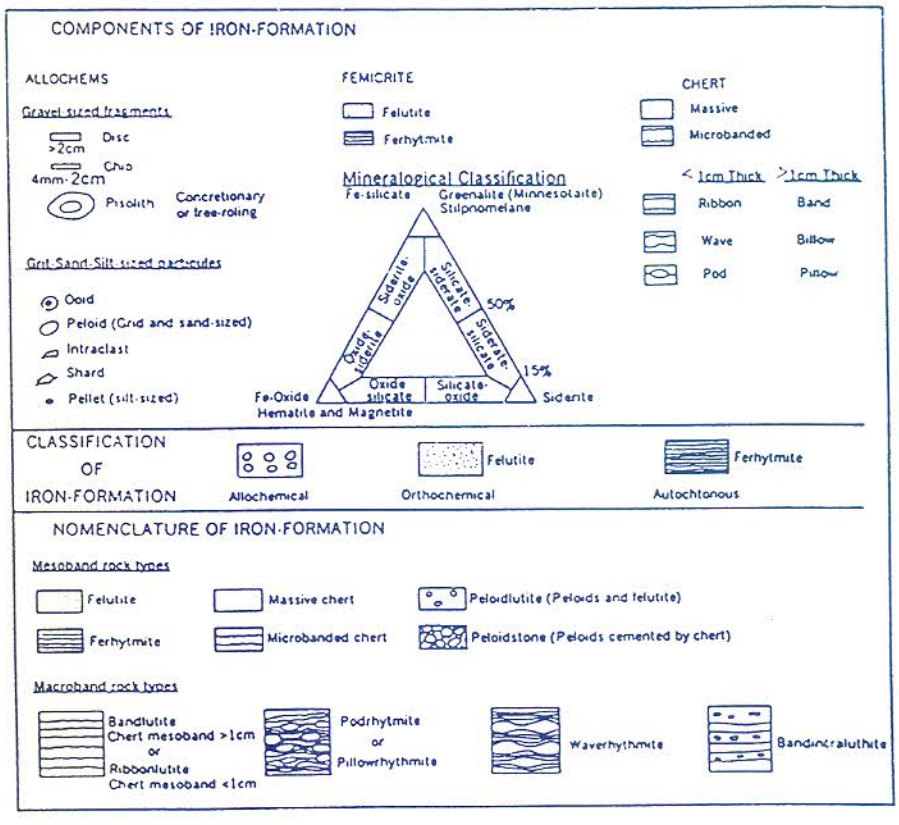

Fig. 5.2 *The components, classification and nomenclature of iron formations (after Beukes, 1983).*

TABLE 5.1 PROPOSED CLASSIFICATION OF AND NOMENCLATURE FOR IRON FORMATION (after Beukes, 1978, 1980 and 1983).

CLASSIFICATION

I. Allochemical iron-formation (Contain allochems) } Endoclastic iron-formation
II. Orthochemical iron-formation (Felutite dominates) }
III. Autochthonous iron-formation (Ferhythmite dominates) Chemical/Biochemical iron-formation
Metamorphic equivalent : Iron-formation → itabirite

NOMENCLATURE

Extraordinary features	Mineralogy	Main rock name				
1. Mineralogical, textural, structural, etc.	2. Composition femicrite	3. Chert mesoband ("stone") 3.1 Texture	3.2 Structure		4. Femicrite mesoband 4.1 Texture	4.2 Structure
Ankeritic	Hematite	*Allochems*	Ribbon		*Allochems*	
Riebeckitic	Magnetite	Discs	Wave	Thickness	Discs	Felutite
Pyritic	Stilpnomelane	Chips	Pod	≤ 10 mm	Chips	(Massive)
Cherty	Greenalite	Pisolites	———	———	Pisolites	
	Minnesotaite	Oncolites	Band	Thickness	Oncolites	Ferhythmite
	Silicate + siderite	Intraclasts	Billow	> 10 mm	Intraclasts	(Micro-
	= Coloursiderite	Peloids	Pillow		Peloids	laminated)
	Siderite	Ooids	*Metamorphic*		Ooids	*Metamorphic*
	Metamorphic	Pellets	Similar structures but		Pellets	lutite → fels
	Stilpnomelane → Biotite		chert → macroquartz			rhythmite →
	Minnesotaite → Grunerite	*Stromatolitic*			*Ripplets*	birite
	Also various other types of metamorphic minerals may be present					
		Ferruginous cherts			Iron-formations	
		Chert mesobands alternating with femicrite mesobands = banded iron-formations				

EXAMPLES OF ROCK NAMES

A. 2 as 4.2 : siderite lutite, greenalite-siderite rhythmite, etc. } Iron-formations } Mesoband rock types
B. 4.1 in 4.2: disclutite, pelletlutite, etc.
C. 3.1 in 3.2: ooidstone, peloidstone, stromatolitic chert, etc. } Ferruginous cherts
D. 3.2 alternating with 4.2: ribbonlutite, podrhythmite, pillowlutite, etc.
E. 3.1 in 3.2 alternating with 4.2: ooidbandlutite, pelletribbonlutite, etc. } Banded iron-formations (macroband rock types)
F. 3.2 alternating with 4.1 in 4.2: bandintralutite, billowpelletlutite, etc.
G. 3 alternating with 4: "ooidbandpeloidlutite" etc. (prefer descriptions)
H. Mineralogical adjective.

Dominant mineral placed first. Mineral constituting allochem or mineral which is present in chert mesoband is italicised as in greenalite-*siderite* oolutite (oolites of siderite in a matrix of greenalite lutite).

28

5.3.1 *Facies description*

Iron formation must be viewed in terms of two models (Dimroth, 1979):

(i) A chemical model that relates the present mineralogy of the rock to its original depositional environment and to later diagenic (and metamorphic) processes.

(ii) A model of physical sedimentation relating sedimentary structures and textures of the rock to hydrodynamic processes during deposition.

5.3.1.1 Mineralogical approach

Chemically precipitated sediments, by their composition, mineralogy and the oxidation state of their various elements, may reveal much about the chemistry of the environment in which they were deposited (Gross, 1965; Dimroth, 1979). Eh and pH conditions are the controlling factors which determine the iron mineral phase in the depositional environment (Eichler, 1976). Concentrations as well as changes in P/T conditions have no significant influence on which iron phase is precipitated.

James (1954) distinguished four facies-types of iron formation i.e.; oxide, silicate, carbonate and sulphide facies. These facies are deposited in that order from shallow to deep water within the basin, with relatively high Eh conditions in the oxide facies, intermediate Eh conditions in the carbonate and silicate facies, at low Eh values in the sulphide facies. The relative position of the iron formation facies in a hypothetical restricted sedimentary basin is shown in Fig. 5.3 and the characteristic features of the different mineralogical facies is summarised in Table 5.2. Three points are worth mentioning as regards the definition of the facies:

(i) The facies are defined by the predominant iron mineral present, although other iron minerals are also invariably present.

TABLE 5.2 *SPECIAL FEATURES OF SEDIMENTARY FACIES OF IRON-FORMATION (slightly modified after James, 1954 in Eichler, 1976).*

	Oxide-facies		Silicate-facies	Carbonate-facies	Sulfide facies
	hematitic	magnetitic			
Lithology	evenly to maculate banded; alternating layers of hematite and quartz (chert)	evenly to maculate banded; layers of magnetite and silicate–carbonate-chert	± well banded granular green silicates, interlayered with quartz (chert) and magnetite	± well banded layers of carbonates and quartz (chert)	finely banded pyritic and carbonaceous slate with chert
Iron minerals	hematite (martite)	magnetite	hydrous iron silicates; greenalite; stilpnomelane; minnesotaite: (carbonates, iron oxides)	iron carbonates siderite, ankerite (magnetite, pyrite, iron silicates)	pyrite (iron silicates, carbonates)
Iron content (average % Fe)	30–42 (ø38)	25–35	20–30	20–35 (ø21)	15–25
Special features	no detrital dilution; (oolites)	granules, oolites	transitional to magnetite-oxide and carbonate-facies	stylolites, graphitic	commonly graphitic
Chemical environment	strongly oxidizing	weakly oxidizing to weakly reducing	weakly reducing	reducing	strongly reducing

(ii) The facies are commonly intergradational.

(iii) Sulphide facies are practically absent from all iron formations except those developed in Archaean greenstone belts.

The theoretical Eh and pH conditions governing the stability of the various iron minerals have been calculated by Garrels and Christ (1965).

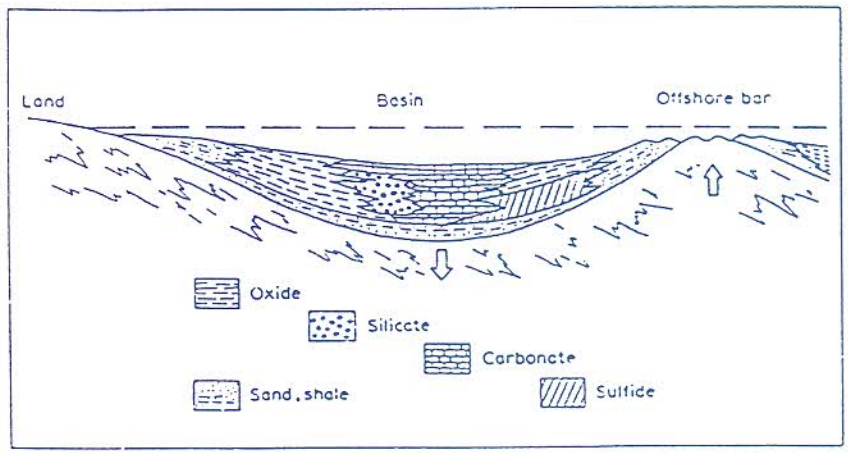

Fig. 5.3 *Schematic section showing the lateral and vertical distribution of different facies of iron-formation in a barred depositional basin (after James, 1954) as slightly modified by Eichler (1976).*

5.3.1.2 Textural Approach

Iron formations display textural and structural features analogous to those in carbonate rocks which allows the following important conclusions to be made (Dimroth, 1976 and 1979):

(i) Particles come in various sizes (clay-size, sand-size and gravel-size).

(ii) The particles were relatively hard and were non-cohesive

(iii) The fresh sediment had mechanical properties similar to those of lime muds, sands and gravels.

5.3.2 *Types of Iron Formation*

Four distinct types of iron formation have been recognised in the geological record (Maynard, 1991):

(i) Algoma Type:

This type is best developed in the Archaean greenstone belts but occurs in rocks of a variety of ages. The associated strata are volcanic with subordinate sandstones of the greywacke-type, a combination of lithologies that suggests deposition on the flanks of volcanic belts with little sediment supplied by continental sources. Commonly, the iron formation follows a basin to shelf transition from sulphide facies through carbonate or silicate facies to oxide facies.

(ii) Lake Superior Type:

Lake Superior-type embraces the giant banded iron formations of the lower Proterozoic (between 2,5 and 1.8 Ga). Significant examples include the Animikie Basin of the United States, the Hamersley Basin of Australia, the Transvaal Basin of South Africa and the Labrador Trough of eastern Canada. These are distinguished by a stable continental shelf association of enormous lateral extent. The environment of deposition ranges from deep shelf to intertidal. Lake Superior-type iron formations may show similar mineralogical facies changes to the Algoma-type as one proceeds from deep to shallow water.

(iii) Rapitan Type:

This type is associated with glacial strata in the Upper Proterozoic and is particularly well developed in the Mackenzie Mountains of Western Canada and the Damaran Orogen of Namibia. The iron formation occurs in a thick, dominantly clastic sedimentary sequence with minor volcanics. The

immediate host of the iron formation is a diamictite in most cases, but may also be metamorphosed mafic volcanics. These deposits, although consisting of bands of alternating chert and iron minerals, differ from the older BIF-types in being only oxide facies, usually hematite. Clastic-textured iron formation that makes up the shallower water portions of some Lake Superior-type iron formations is not developed in the Rapitan-type.

The Rapitan-type iron deposits are thought to have formed in shallow water cratonic rifts (Maynard, 1991). The thermal gradient between the cold ice front and hot hydrothermal discharge from the small spreading centres produces a vigorous circulation that brings Fe and Mn laden waters into the nearshore glacial-marine environment. Precipitation of the metal oxides is facilitated by the sinking of dense, oxygen-rich surface water at the front of the ice.

(iv) Clinton or Minette Type:

These deposits are confined to the Phanerozoic and are distinguished by an absence of chert and by the dominance of oolite structures, hence the synonymous name, oolite ironstones. Mineralogically, Clinton-type deposits may constitute iron oxides, iron silicates, or both. Siderite, if present, is a diagenetic product, and sulphides are rare. The classic mineralogical facies of iron formation (James, 1954) do not appear in these sequences. Another difference is that the silicates, chamosite and berthierine, are Al-rich, whereas Al-poor silicates such as greenalite dominate in other types of iron formation. Clinton-type deposits are hosted by shallow water (intertidal) clastics and are usually found in a definite vertical succession at the top of regressive cycles.

6. GENETIC CONCEPTS OF IRON FORMATIONS

6.1 Introduction

Possibly the two most significant factors that stimulated interest in iron formations are the vast accumulations of this rock-type during the Precambrian era as well as their economic significance. Iron formations of the early Proterozoic represent 90% of the total mass (10^{15}tons) deposited throughout the geological history (Gross, 1991). Gross (op. cit) further stated that not only is more than 95% of the world's iron ore production accounted for by this rock-type, but also that most of the large stratiform deposits of manganese, copper, zinc, lead, gold, silver, tin, tungsten and rare earth elements are associated with facies of this rock-type.

Many divergent hypotheses have been formulated to account for the large accumulations of iron formation during the early Proterozoic. Considerable uncertainty still exists as to the origin of these enormous concentrations as well as the mechanisms and methods involved in element concentration, transport, deposition and segregation.

It is now generally accepted that most iron formations formed by chemical precipitation. Obviously the elements must have been derived from somewhere and have been contributed to the depository by some system. Concentration levels had to be kept fairly high over a continuous time span to allow for the sheer size of these deposits.

6.2 Source of the Iron and Silica

6.2.1 *Terrigenous sources*

During the first part of the century most researchers accepted a continental source for the mineral components making up banded iron formation . Table 6-1 summarises some of these ideas

TABLE 6.1 TRADITIONAL IDEAS ON THE ORIGIN OF MINERAL CONTENT IN BANDED IRON FORMATION.

CONCEPT	REFERENCE
Leaching of iron and silica from mafic lavas by organic solutions and carbonated waters (humid climate)	Gruner (1992) Moore and Mynard (1929)
Lateritic continental weathering. CO_2-rich atmosphere and transportation of Fe^2 in surface waters	MacGregor (1927) Lepp and Goldish (1964)
Lateritic weathering of Archaean granites, gneisses and greenstones. Swamp conditions developed - colloidal solutions	Svitalski (1937)
Monsoon-type climate. Ferrous iron transported to a lacustrine-type environment during wet season, dry season influx minimal, but alkaline, and transported silica	Sakamoto (1950)

Van Hise and Leith (1911) disputed that weathering of a landmass was a realistic source for the iron and silica. They objected to the fact that iron formations of comparable size are lacking in the Phanerozoic and that residual rocks deficient in iron and silica are not observed in associated rock sequences.

Holland (1973) and Eichler (1976) are also sceptical of continental weathering and river transport as mechanisms for element supply. The immense quantity of

iron locked up in single iron formations (10^{14} tons for the Hamersley Basin alone; Trendall and Blockley, 1970) seems unacceptable. Holland (1973) found it difficult to imagine the chemical separation of the elements from a clastic sediment load to account for the terrigenous detritus-free banded iron formations and, in addition, the atmosphere during the early Proterozoic appears to have been at least mildly oxidising which would limit the transport of Fe^{2+} in surface waters.

6.2.2 *A Volcanogenic-Hydrothermal source*

A volcanogenic origin for the development of the Algoma-type iron formation has generally always been accepted. However, researchers have been hesitant to relate the large accumulations of Lake Superior-type iron formations to a volcanic source.

Volcanogenic deposition of iron was recorded as early as 1650 at Santorini Island in the Aegean Sea (Behrend, 1936). In addition, chemical data by Zelenov (1958) have shown that between 35 to 50 metric tons of iron and silica are contributed at present to the mouth of the Lur'eva River per year from the thermal springs flanking the Ebeko volcano on the Sea of Okhotsk.

Collins *et al.* (1926) suggested that iron formation was precipitated from ascending heated mineralised waters. Carbon dioxide, iron, silica and sulphur would be dissolved in these heated waters and permeate the volcanic rocks, altering them to carbonates and sulphides at depth. Fluids reaching the surface would spread out and accumulate in depressions. Concentrations of carbonate and silica increased upon evaporation and cooling of the heated waters, initiating precipitation.

Castro (1994) proposed subduction associated with active margins as the mechanism whereby iron and silica are supplied. During subduction, seawater

would penetrate the oceanic lithosphere through joints and faults and hydrothermally leach iron and silica.

Kimberley (1989a) remarked that rift failure and plate separation during the Precambrian was probably much more rapid than that observed in more recent settings. Abrupt rifting would result in the development of a closed or restricted basin exposing fresh crust. Seismic pumping along the sheared rifted margin would then facilitate the circulation of heated sea water through fresh crust.

Iron deposits are currently forming along many of the earth's mid-oceanic ridges and these are clearly hydrothermal or volcanic in origin (Rona and Scott, 1993). These submarine hydrothermal systems can release sufficient amounts of dissolved iron to satisfy the reaction with sulphate close to the vent and allow for the precipitation of iron more distal to the hydrothermal feeder (Carrigan and Cameron, 1991). In an extensive overview regarding genetic concepts for the origin of iron formations, Gross (1991) concluded that most current researchers favour volcanic emanations and hydrothermal effusive sources as the main contributors of iron and silica.

6.2.3 *The oceans as a source*

Holland (1973 and 1984) made some quantitative estimates regarding the amount of iron and silica needed in the formation of the Hamersley Group. He estimated that one layer contains more iron than the total estimated yearly input into the oceans and therefore rejected weathering of a landmass, or the contributions of volcanic sources as realistic contributors.

Holland (1973) suggested the oceans themselves as a source for the mineral constituents. The iron was either leached and dissolved from the sea-floor rocks, transported by upwelling currents, oxidised and precipitated in a near-surface

environment, or the iron was supplied by the reduction of detrital ferric iron minerals to soluble ferrous iron in the deep anoxic environment.

6.3 Replacement Origin of Banded Iron Formation

Dimroth and Chauvel (1973) observed oolitic textures in the Sokoman Iron Formation in the Central Labrador Trough, which were almost identical to those displayed in marine limestones, and proposed a replacement origin for the iron formation. Similarly, Kimberley (1974 and 1978) advocated that iron-rich sediments were developed as the result of the replacement of a carbonate precursor.

Eugster (1969), from his work on the Lake Magadi sediments in Kenya, concluded that magadiite (sodium-silicate gel) acted as a precursor to bedded chert sequences. Eugster and Ming Chou (1973) proposed a playa lake environment for the deposition of iron formations. Subsurface groundwater is charged with Ca^{++}, Mg^{++}, SiO_2 and HCO_{3-} and emerges through springs on the playa flat fringing an alkaline lake. Through evaporative concentration and carbonate precipitation, alkaline brines are formed and magadiite precipitates from the alkaline solutions in the lake. During diagenesis some magadiite is converted to chert while some reacts with iron minerals to form riebeckite.

Lepp and Goldish (1964) showed that by starting with a mixture of $1CaCO_3$: $1FeCO_3$ and replacing $CaCO_3$ by SiO_2, the resulting chert and siderite precipitate would contain about 45% SiO_2. This figure is similar to the silica content of many iron formations. They also showed that siderite containing 25% iron would, on alteration to hematite, contain 31,2% iron. They therefore, favoured the idea that iron formations were initially deposited as carbonate iron

formations. During diagenesis, siderite was altered to hematite, magnetite and silicate facies.

6.4 **Palaeoenvironmental Setting**

Gross (1970, 1980 and 1983) distinguished between the differing tectonic settings in which the Algoma-type and Superior-type iron formations form. These are shown schematically in Figure 6.1.

Gross (1970) noted that many of the large Precambrian iron formations occur close to present continental margins. He suggested that they were deposited in close proximity to or formed part of a single depositional environment, on a Precambrian land mass that separated at a latter stage along deep seated faults and tectonic systems of global dimensions.

It is widely accepted that the voluminous blanket-like Superior-type banded iron formations were deposited in relatively shallow-water marine settings, probably in clastic-free continental shelf basins, often of enormous dimensions (James, 1954). In some cases the proposed depositional basins are regarded as open environments (frequently referred to as oceans) even- though they were restricted from terrestrial input (Gross, 1980; Button *et al.*, 1982; Beukes, 1983; Morris and Horwitz, 1983; Holland, 1984; Simonson, 1985). Deposition took place under stable tectonic conditions over extended time periods. Many workers favour barred or partly barred settings, as Trendall and Blockey (1970) interpreted for the Dale Gorge Member of the Hamersley basin. Many banded iron formation depositional basins have been depicted as barred

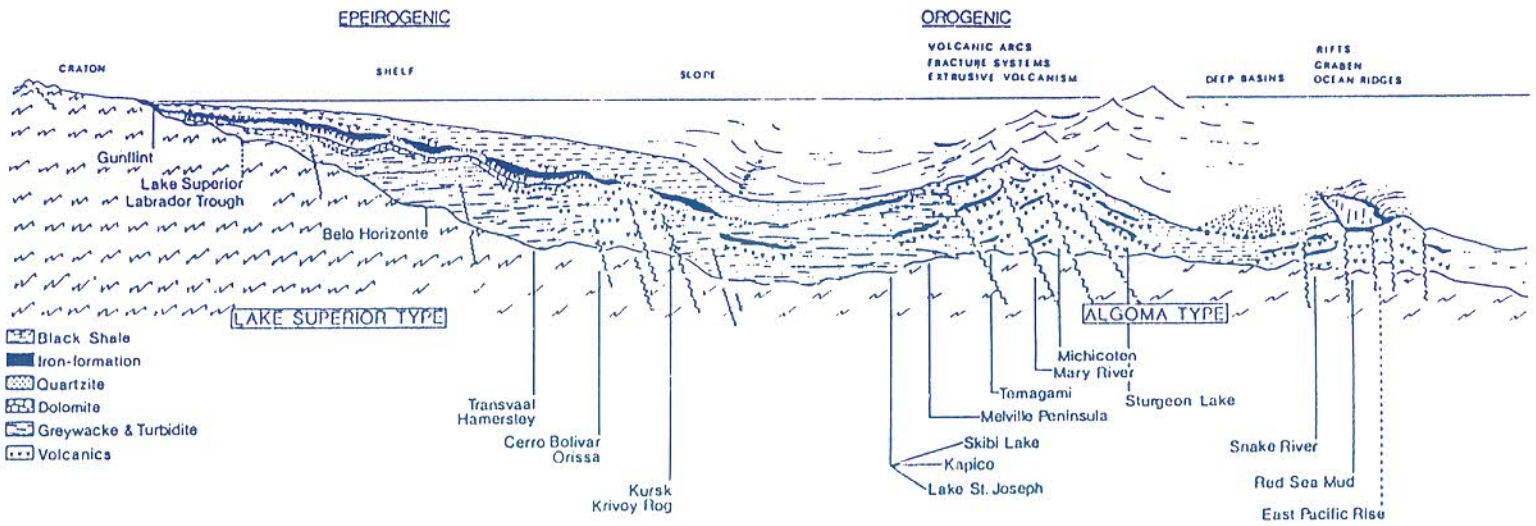

Fig. 6.1 *Tectonic environments for deposition of iron formation (from Gross, 1980).*

lagoons starved of terrestrial detritus, which permitted sedimentation in a quiet shallow water environment (Dimroth, 1976; Button, 1976).

Fresh water lakes (Hough, 1958; Govett, 1966) or playa-lake complexes have also been proposed as possible environmental settings (Eugster and Chou, 1973). Evaporitic settings were also favoured by Trendall (1973 and 1973a), Kimberley (1974), Dimroth (1976) and Garrels (1987).

Algoma-type iron formations formed at, or relatively close to volcanic centres, in marine rift basins, along fault scarps in grabens and along oceanic ridge systems. They range in age from early Precambrian to metalliferous deposits along modern spreading centres. The palaeographic interpretation of Algoma-type iron formation is fraught with difficulties (Dimroth, 1976). Parallel laminations are generally the dominant structure and indicate deposition in a low-energy environment. However, low-energy environments range from the subaerial domain to the deepest ocean basins. Volcanogenic iron formations are commonly, but not always, intercalated in terrigenous volcanogenic sediments. It is reasonable, in this case, to assume that they were deposited in the same environment as the associated terrigenous sediments, which are often interpreted as pelagic.

6.5 Chemical Factors Controlling the Solubility of Iron, Manganese and Silica

The formation of an economically significant manganese deposit requires that two general conditions be met (Force and Cannon, 1988).

(i) Manganese must be concentrated to at least 200 times its average crustal abundance.

i) Iron cannot be concentrated to any appreciable degree above its average crustal abundance of about 5%.

The oxidation stage of iron in solution is highly dependent on the pH and redox potential of the iron-water system. Figure 6.2 shows iron in the expected different oxidation state domains depending on Eh and pH of the iron-water system. Seven solute species are expected to form. Three ferric species, of which two are hydroxy complexes occur. Three ferrous species also occur, including two hydroxy complexes of which one is anionic and one a ferrate complex (FeO_4^{2}) where iron is in the +6 oxidation state. Since the anionic complexes only attain dominance under high pH conditions, unusual in natural systems, their geochemical significance is small.

The pH-Eh diagram (Fig. 6.3) shows iron in specific dissolved concentrations, and also the stability regions for the different solids. The effect of fairly high concentrations of carbon dioxide, fluoride, chloride and sulphur on the behaviour of iron is shown in Fig. 6.4. Although these concentrations might be considered as unsatisfactory for potable water, many natural waters have concentration levels as high or greater (Hem, 1972). Pyrite is stable over a large field, siderite ($FeCO_3$) over a limited Eh-pH range, while only a small stability region for $Fe(OH)_2$ remains. The dominant solute-types bordering the $Fe(OH)_3$ and $FeCO_3$ stability fields, are the ferric fluoride complex FeF_2^{+} and the ferrous sulphate complex $FeSO_{4aq}$.

Figure 6.4 also indicates that iron is soluble in highly oxidising conditions at a low pH. Hem (1972) discussed five different mechanisms that will affect the solubility of iron:

(i) Change in pH.

(ii) Change in Eh.

(iii) Assuming other factors to remain constant, the solubility of iron will be affected by the increase or decrease in anion activity. Thus, addition of

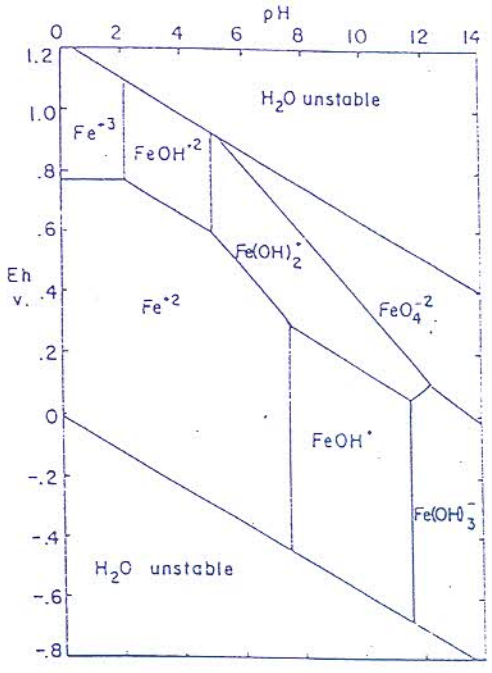

Fig. 6.2 *Areas of dominance for solute species as a function of pH and redox potential in the system Fe-H_2O at 25°C and 1 atm (after Hem, 1972).*

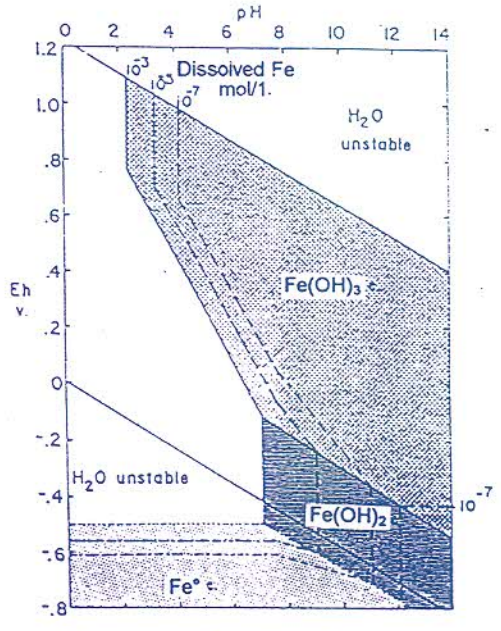

Fig. 6.3 *Stability fields for solids as a function of pH and redox potential in the system Fe-H_2O at 25°C and 1 atm. Activity of dissolved iron 10^{-3} mol/l (56 mg/l Fe). Positions of stability-field boundaries for (Fe) = 10^{-5} and 10^{-7} mol/l are indicated by dashed lines (after Hem, 1972).*

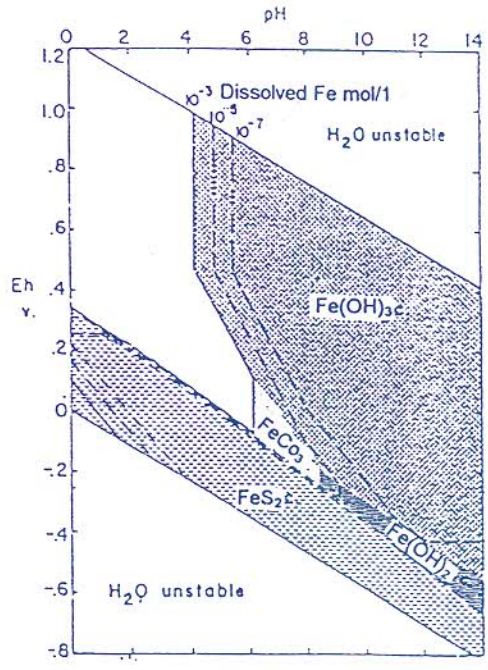

Fig. 6.4 *Stability fields for solids as a function of pH and redox potential in the system Fe-F-Cl-S-CO_2-H_2O at 25°C and 1 atm. Total dissolved activities specified 10^{-3} mol/l for F (19 mg/l) and CO_2 (equivalent to 61 mg/l HCO_3-) and 10^{-2} mol/l for Cl (355 mg/l) and S (equivalent to 960 mg/l SO_4^{-2}). Shaded areas represent stability boundaries for dissolved Fe activity, equal to 10^{-3} mol/l (56 mg/l). Dashed lines show positions of boundaries at Fe activity of 10^{-5} and 10^{-7} mol/l (after Hem, 1972).*

bicarbonate to the iron-water system will increase the siderite stability field. If bicarbonate activity is decreased, the solubility of ferrous iron will increase, also possibly affecting the pH.

(iv) The solubility of metal generally increases in the presence of complex ions. Iron in both the ferrous and ferric state can form strong complexes with organic ligands. The solubility of iron in soils is greatly affected by the concentration of organic solute.

(v) A change in temperature and pressure. Hem (1972) investigated the manganese stability fields as solids and solutes, and the solubility of Mn as

a function of pH and redox potential at standard conditions of temperature and pressure (Figure 6.5) Figure 6.5 shows the manganese oxides occurring in different Eh-pH domains and displaying three oxidation states, the +2 ($Mn(OH)_2$), +3 (Mn_3O_4) and the +4 (MnO_2). The solute complexes involved include $MnOH^+$ and $HMnO_2$.

With the addition of other anions to the manganese-water system, new solids and solute complexes will be produced. Similar to iron (siderite), the addition of bicarbonate to the manganese-water system will increase the stability field of $MnCO_3$ and also produce an additional solute complex $MnHCO_3$ (Figure 6.6). The bicarbonate complexing effect is to slightly increase the MnO_2 stability boundary. The effect of a sulphur addition to the Mn-water system is shown in Fig. 6.7. Overall however, anion concentration at normal levels in a manganese-water system seems to have a rather limited effect on the behaviour of Mn as compared to Fe. Effects on an Eh-pH diagram will only be influenced in the presence of a high concentration of ligands. Manganese complexes with chloride and fluoride are almost non existent. The solubilities of iron and manganese, compared in Fig. 6.8, exhibit the following characteristics:

(i) Both Mn and Fe form virtually insoluble oxides or carbonates in high pH conditions, regardless of Eh.

(ii) Both metals have substantially increased solubilities (up to 3 orders of magnitude) at lower Eh and pH conditions and are therefore particularly soluble in anoxic reducing conditions.

(iii) The dashed line showing the solubility of iron indicates that for any Eh and pH within the water stability field and taking into consideration both the CO_2 and sulphur species activity in a purely inorganic system, more manganese will be in solution than iron. If the alkalinity is gradually increased throughout the pH range 5 to 8, manganese will stay in solution and will precipitate only at a higher pH (Krauskopf, 1956). The manganese may precipitate as an oxide, carbonate or silicate depending on the Eh and the concentration of carbonate and silicate ions.

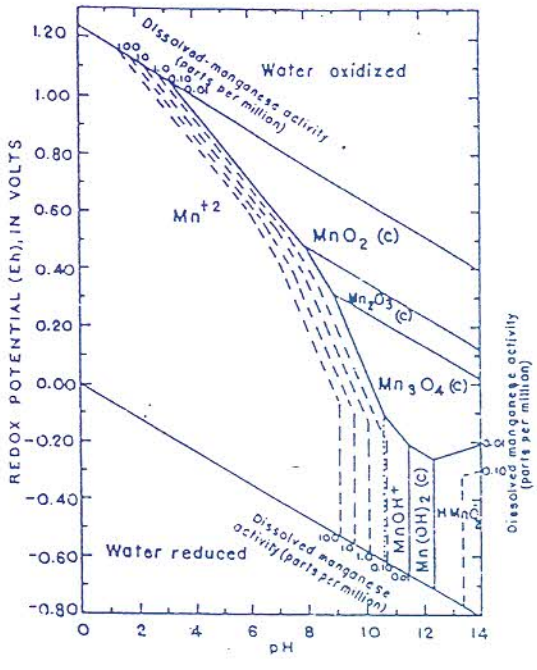

Fig. 6.5 *Fields of stability of solids and solutes, and solubility of manganese as functions of pH and redox potential at 25°C and one atm. in the system Mn-H_2O (after Hem., 1972).*

Under certain chemical conditions within the supergene environment it is therefore possible to effectively separate iron from manganese. However, it is also possible that both Fe and Mn may co-precipitate from a natural solution containing both the elements where rather strong oxidising agents are present or where the pH is very high (Roy, 1981).

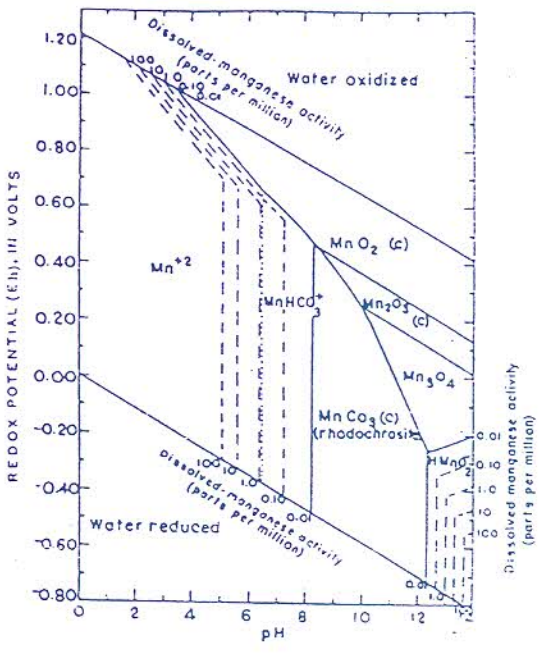

Fig. 6.6 *Field of stability of solids and solutes, and solubility of manganese as functions of pH and redox potential at 25°C and one atm. in the system Mn-CO_2-H_2O. Bicarbonate species activity 2000 mg/l as HCO_3. (after Hem, 1972).*

The solubility of amorphous silica as $Si(OH)_4$ in natural waters is little affected over the pH range 4 to 8.5, or by salinity up to the composition of modern sea water. Silica however, becomes progressively more soluble with increasing alkalinity (Siever, 1971; Figure 6.9). This is further substantiated by Krupp *et al.* (1994) who present evidence that highly acidic water (pH 3.9) would aggressively dissolve most minerals in an igneous rock with the exception of quartz. Sedimentologists have often advocated that chert precipitation is favoured in a more acidic environment (Beukes, 1973; Nel *et al.*, 1986).

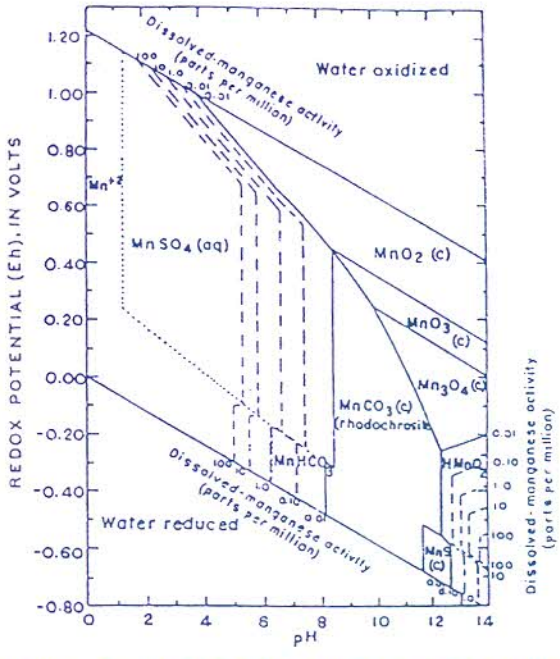

Fig. 6.7 *Fields of stability of solids and solutes and solubility of manganese as functions of pH and redox potential at 25°C and one atm. in the system Mn-S-CO_2-H_2O. Total CO_2 species activity 2000 mg/l as HCO_3^-, total sulphur species activity 2000 mg/l as SO_4^{-2} (after Hem, 1972).*

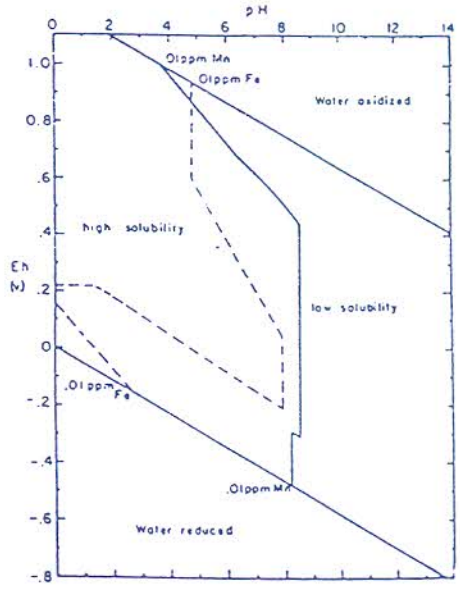

Fig. 6.8 *Comparative solubility of manganese and iron in the system H_2-S-H_2O at 25°C and one atm. Total CO_2 species activity 2000 mg/l as HCO_3^-, total sulphur species activity 2000 mg/l as $SO4^{-2}$. (after Hem, 1972).*

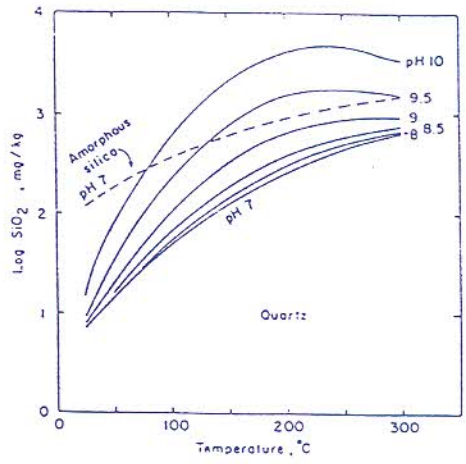

Fig. 6.9 *Solubility of quartz from 25° to 300°C at pH values ranging from 7 to 10 (solid lines). The dashed line shows the solubility of amorphous silica at neutral pH (after Fournier, 1985).*

Most authors agree that the Precambrian seas were saturated with respect to amorphous silica. Silica secreting organisms were apparently absent and concentration and precipitation of silica was controlled by evaporation and cooling.

The high silica concentrations in Cretaceous ophiolite complexes and at present day deep sea hydrothermal metalliferous sites are regarded as evidence for higher silica solubility under elevated temperatures in aqueous systems (Crerar and Anderson, 1971; Walther and Helgeson, 1977).

Thick accumulations of siliceous sinter are commonly observed around many presently active hot springs (Fournier, 1985). These waters are neutral to slightly acid in the reservoirs at depth and commonly become alkaline after upward movement owing to a loss of CO_2 during boiling and evaporation. In contrast, highly acidic waters (pH=3) tend not to form thick siliceous deposits because hydrogen ions appear to inhibit the polymerisation of dissolved silica. It can therefore generally be concluded that thick siliceous sinter deposits imply neutral to slightly alkaline waters that have risen quickly from underground reservoirs where waters were in equilibrium with quartz at temperatures in excess of 210°C.

6.6 Genetic Modelling of Banded Iron Formation and Associated Manganese Deposits

A survey of the relevant literature indicates that there are essentially two models which can be invoked for the genesis of banded iron formation and associated manganese mineralisation:

(i) a volcanogenic exhalative model.

(ii) a non-volcanogenic sedimentary model encompassing upwelling anoxic waters.

6.6.1 *Volcanogenic exhalative model*

Much has been learned from iron and associated manganese deposits currently forming along the ocean floor. The deposits are typically located in block faulted topographic highs adjacent to the medial rift of the mid-oceanic spreading centres, along fracture zones transecting these spreading centres, in basins along an axial trough on volcanic seamounts as well as within back arc basins flanking an island arc (Roy, 1981; Rona and Scott, 1993).

A number of mechanisms have been proposed for the origin of the metals (Roy, 1981):

(i) Leaching at a shallow level

Hot acidified and reduced sea water containing dissolved acidic magmatic gases can leach iron, manganese, silica and other minor elements from the extruding lava pile at a shallow depth (Krauskopf, 1956; Bonatti, 1967). The process is facilitated by lava containing a high proportion of hyaloclastites. Continuous mixing with normal seawater will cause a progressive increase in pH, resulting in the precipitation of iron first followed by manganese as the Eh levels rise.

(ii) Hydrothermal circulation of seawater

Circulation of descending seawater through highly fractured basaltic rocks in regions of high heat flow results in the leaching of metals from the wall rocks (Bonatti *et al.*, 1972 and 1976; Bischoff and Dickson, 1975; Cann *et al.*, 1977). The

metal load is precipitated on the sea floor upon re-emergence. The concentration levels of metal in solution are determined by factors such as depth of and rate of convective circulation, temperature, pH and Eh conditions. On mixing with normal seawater, the hydrothermal fluid gradually regains its original character (alkaline and oxidising) resulting in the precipitation of Fe at a lower Eh and pH while Mn, because of its higher solubility, is deposited at a later stage at a higher Eh and/or pH.

(iii) Deep-seated degassing

Metalliferous sediments adjacent to active spreading ocean ridges are exceptionally rich in Fe, Mn, Ba, V, U and As and depleted in Al, Ti and Th (Boström, 1973, 1976a and 1976). A well-defined exponential relation between the rate of ocean floor spreading (increased spreading rate leading to more intense heat flow) and the (Fe + Mn)/Al ratio in ocean floor sediments (ratio increasing with faster spreading rate) would suggest that the same basic process controls the spreading rate and the chemistry of active ridge sediments (Boström, 1973; Boström *et al.*, 1976). Therefore, active ridge sediments should be characterised by a high (Fe + Mn)/Al ratio. However, Fe and Al are not effectively fractionated in the products of hot springs in basaltic areas and experimental work done on the leaching of basalt with NaCl brines also shows that there is no fractionation between Fe and Al in the fluid (Scott and Hajash, 1976). Therefore, Boström (1973, 1976a and 1976) argued that the reaction of seawater with basalt cannot produce the characteristic Al-poor and Fe-rich signature of the sediments. He advocates that CO_2-rich emanations, possibly derived by degassing during the differentiation of primitive pyrolite to peridotite and basalt at deep levels, and which tend to be enriched in Fe, Mn, P, Ba and U and depleted in Al, Ti, Si and Th, are the most likely source of metal. Because these iron-rich sediments are characteristically depleted in Al, both Boström (1973 and 1976a) and Scott and Hajash (1976) rejected land-based chemical weathering as a means of supplying the necessary metalliferous elements.

The volcanogenic-sedimentary iron and manganese deposits can be further subdivided into two contrasting morphological types: firstly, those which form mound-like deposits on the ocean bottom either directly over, or spatially close to, the volcanic mounds in an environment characterised by open circulation with easy access to oxygenated water (Fig. 6.10) and secondly, those which accumulate in stagnant poorly oxygenated conditions in topographic lows on the sea floor (Bonatti 1972), the best known example being the Atlantis II Deep in the Red Sea.

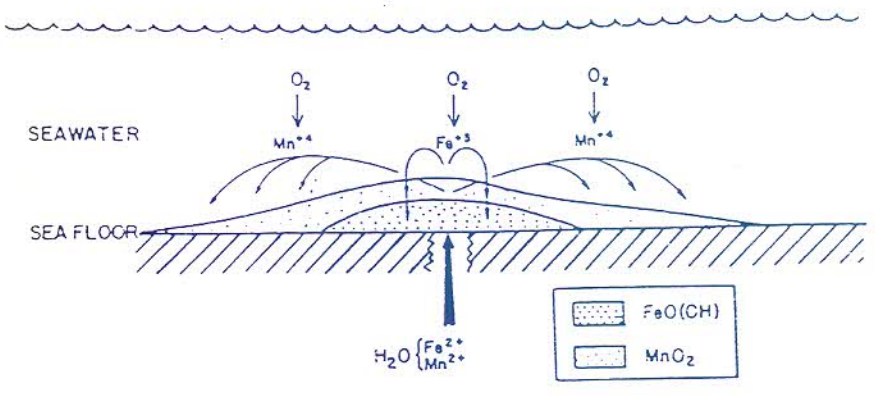

Fig. 6.10 *Formation of Fe-Mn deposits from Fe-Mn bearing hydrothermal solution on an oxygenated ocean floor (after Roy, 1981).*

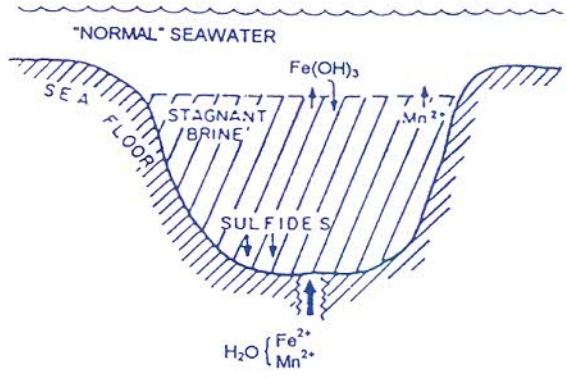

Fig. 6.11 *Formation of Fe-Mn deposits from Fe-Mn bearing hydrothermal solutions in stagnant poorly oxygenated conditions in topographic lows (After Roy, 1981).*

6.6.2 *Sedimentary models for the precipitation of banded iron formation and associated manganese deposits*

In recent years genetic models for the deposition of the extensive Superior-type banded iron formation have been approaching common ground. These models generally all centre around a common theme, namely, that banded iron formation was deposited from upwelling currents in an ocean stratified with respect to oxygen and solute content.

In the Black Sea, the seawater is well oxidised and mixed to 50m below surface (Fig. 6.12). This 0 - 50m zone is called the aerobic zone and is able to sustain life. From 50m to 150m, the oxygen level drops in what is termed the dysaerobic zone. Below this elevation, the oxygen content is virtually zero (anaerobic zone). In the Black Sea, which is a partially closed (or silled) basin, this profile extends to the sea bottom.

Drever (1974) was one of the early proponents for the deposition of iron formation in stratified shallow-water marine settings. Based on the premise that the oxygen levels were significantly lower in the Proterozoic than at present, and that biological activities were at a similar level, he concluded that the ocean waters below the thermocline would be anaerobic in contrast to the near-surface mixed zone which would be relatively oxidising (Fig. 6.13). The variation in iron mineralogy was explained as a reflection of the intensity of upwelling and the rate of organic carbon supply, with hematite being preferentially deposited when the anaerobic deep water welled up onto the shallow platform (Fig. 6.13). Slight evaporation would result in the precipitation of amorphous silica from the waters which were saturated with respect to silica because of the absence of silica-secreting organisms. Siderite was precipitated basinward of the oxides where the carbon levels were higher (Fig. 6.13).

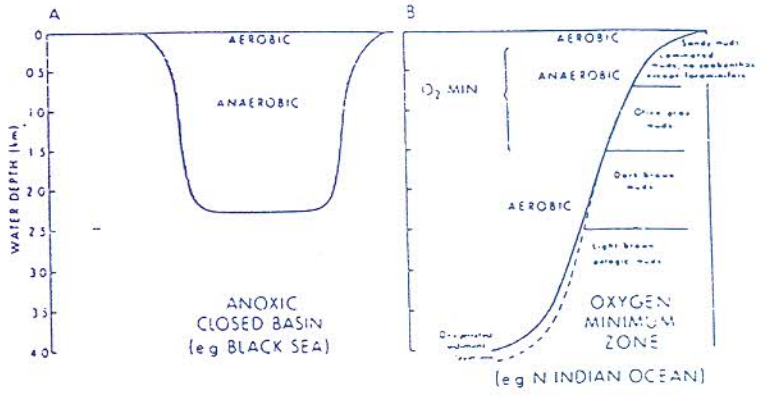

Fig. 6.12 *Circulation models for A: Anoxic closed basin, and B: Oxygen minimum zones in marine settings (after De Vries Klein, 1991).*

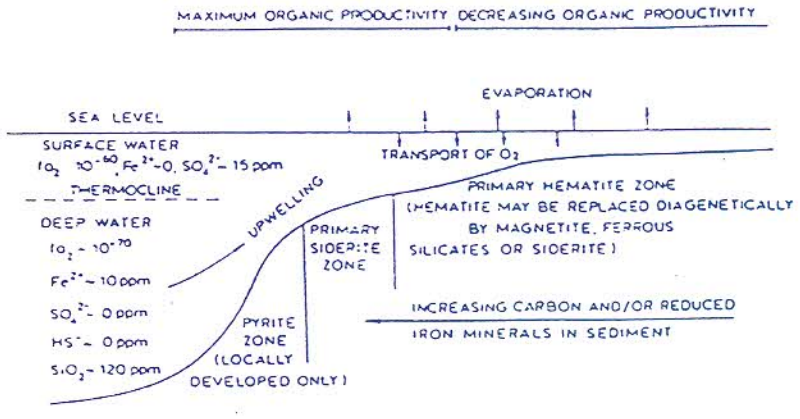

Fig. 6.13 *Idealised depositional environment of a banded iron formation. The term "hematite" includes all ferric oxides and hydroxides (after Drever, 1974).*

Even with the hematite zone in areas of high carbon supply, ferric hydroxide could be reduced diagenetically to the ferrous state to form siderite or greenalite.

The stratified ocean-continental margin model has been proposed recently for the origin of the Asbesheuwels Subgroup iron formations of the Transvaal Supergroup in South Africa by Klein and Beukes (1989), and for the Gunflint iron formation in Minnesota by Carrigan and Cameron (1991).

Major and trace element geochemistry, carbon and oxygen isotope data, as well as REE signatures across the facies transition from the Campbellrand carbonate sequence to the overlying banded iron formation of the Kuruman Formation show that the two groups of rock are chemically quite distinct. This led Klein and Beukes (1989) and Beukes *et al.* (1990) to the conclusion that the dolomite-limestone-shale lithologies originated in a water column quite distinct from that in which the iron formation was precipitated. They proposed a model with a stratified water column, in which the nearshore surface waters (during a regressive stage in the depositional basin) were the site of much organic carbon productivity and the locus of cryptalgal limestones and intraclastic limestone deposition; at somewhat

greater depth (below the chemocline), deposition of pyritic carbonaceous shale occurred (Fig. 6.14). During transgression, the deeper waters were depleted in organic carbon and enriched in dissolved ferrous iron derived from a dilute hydrothermal input.

Their sequence of iron formation facies, however, is the reverse of that advocated by Drever (1974) and James (1954). The latter workers suggest that the more reduced facies will form closer to the shelf margin because of increased organic content.

Morris (1993) believes that the necessary constituents to form the banded iron formations of the Hamersley Group were supplied by the following systems:

(i) Surface currents.
(ii) Convective upwelling as a result of mid-oceanic or hot spot activity.
(iii) Pyroclastic input (fine aluminous ash).

Sea level changes and the formation of stratified basins played a major role in the deposition of sediment-hosted manganese deposits in the past (Roy, 1992). Upwelling of anoxic deep ocean water onto the continental shelf has been postulated for the origin of many of the so-called Phanerozoic giant manganese deposits such as Nikopol, Groote Eylandt and Molango (Cannon and Force, 1983; Frakes and Bolton, 1984 and 1992; Force and Cannon, 1988). Indications are that this type of deposit formed where mixing of anoxic deep water and oxygenated shallower water intersected shallow marine strata. The oxic depositional model proposes that manganese is deposited as an oxide and/or carbonate facies on the (oxygenated) landward side of an oxic/anoxic interface intersecting the shelf of a stratified sea (Fig. 6.15a). Either or both facies of manganese deposits can form

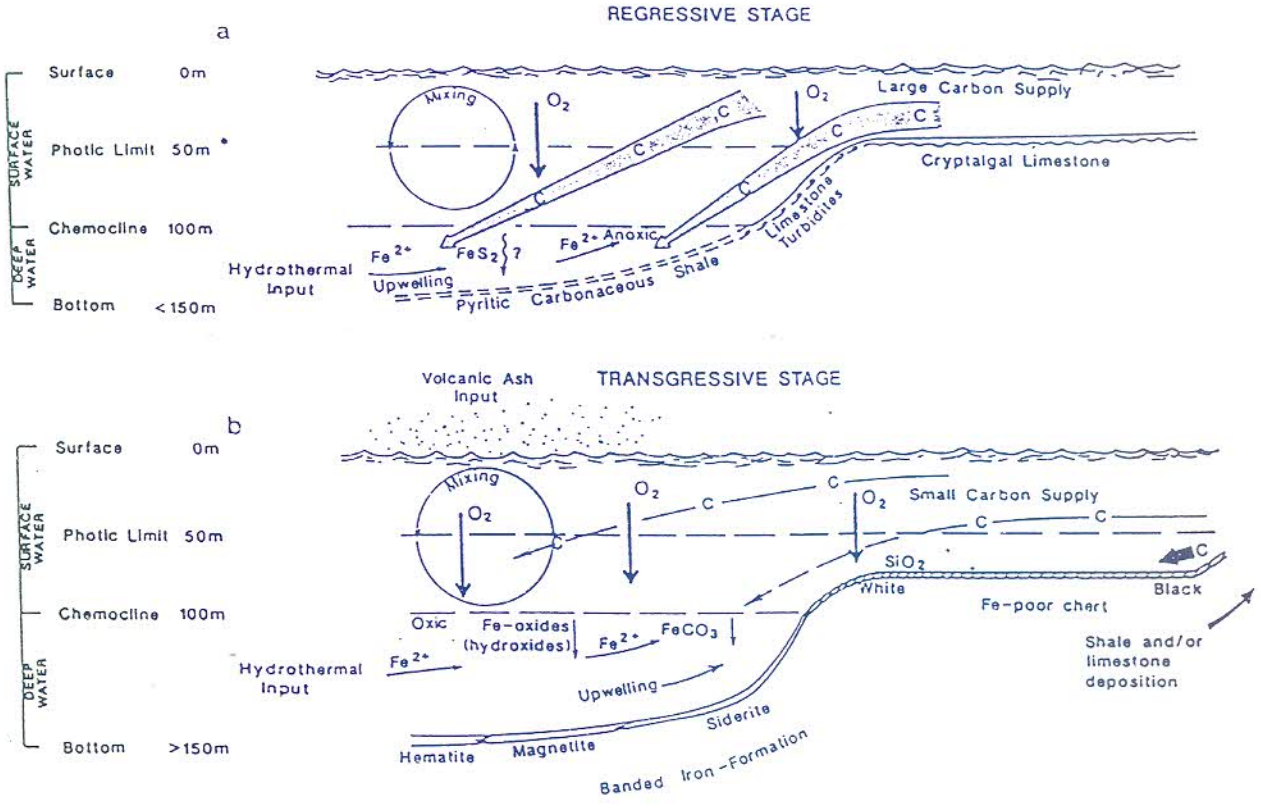

Fig. 6.14 *Schematic depositional environment for iron-formation deposition and that of associated lithofacies in a marine system with a stratified water column in (a) a regressive stage, and (b) a transgressive stage. In (a) the photic zone reaches the floor of the deep shelf, allowing for cryptalgal-laminated limestone deposition. In (b) the photic zone is considerably above the floor of the deep shelf, causing the deposition of various iron-formation facies and chert. The thick arrows labelled C (carbon) in (a) represent high carbon productivity and supply, and the narrow arrows in (b) represent much less carbon productivity and supply. The vertical depth scale is based upon the basinal reconstruction of Klein et al. (1987) (after Klein and Beukes, 1989).*

there because the oxygenated surface waters of stratified seas may be near the boundary between the manganese carbonate and oxide stability fields, where only slight changes in pH, Eh or pCO_2 can favour one of these facies.

In the model for reduced and zoned deposits, the contact between the oxide and carbonate manganese facies is thought to mark the position of the oxic-anoxic interface in the water column at the depositional site (Figure 6.15b). Manganese carbonates form as a replacement of primary carbonates in a zone just below and seaward from the redox interface.

The model of Frakes and Bolton (1984) is based on the Groote Eylandt deposit and is almost identical to that proposed by Cannon and Force (1983) but envisages deposition of the dissolved manganese in an intracratonic basin during a regressive phase immediately following a major transgressive episode (Figure 6.16). The inverse grading in the manganiferous pisolites and oolites is thought to imply precipitation during regression and oxygenation of basin water. Two processes are proposed, the veil effect (flocculent fallout from river water) in the estuarine area and the shoreward broom effect (bottom transport), to result in the concentration of manganese particulates in order to form ore deposits.

Schissel and Aro (1992) incorporated the model of Button *et al.* (1982) for the origin of Superior-type iron formations and the models of Force and Cannon (1983) and Frakes and Bolton (1984) into a single model (Fig. 6.17). The early Proterozoic seas were probably predominantly anoxic and only the upper portions were oxygenated by the newly evolving photosynthetic bacteria. In addition, these seas were probably nearly saturated with respect to silica, because silica-secreting organisms had not yet evolved. Iron and manganese may be separated in ocean water by gradually raising the Eh and pH (Figure 6.17). If deep anoxic water charged with iron, manganese and silica upwelled onto the continental shelf, iron carbonate and iron and silica oxides would precipitate first to form a banded

iron formation facies. Manganese carbonate and oxide would precipitate at a later stage once the solution reached the more oxidised shallower portions of the shelf.

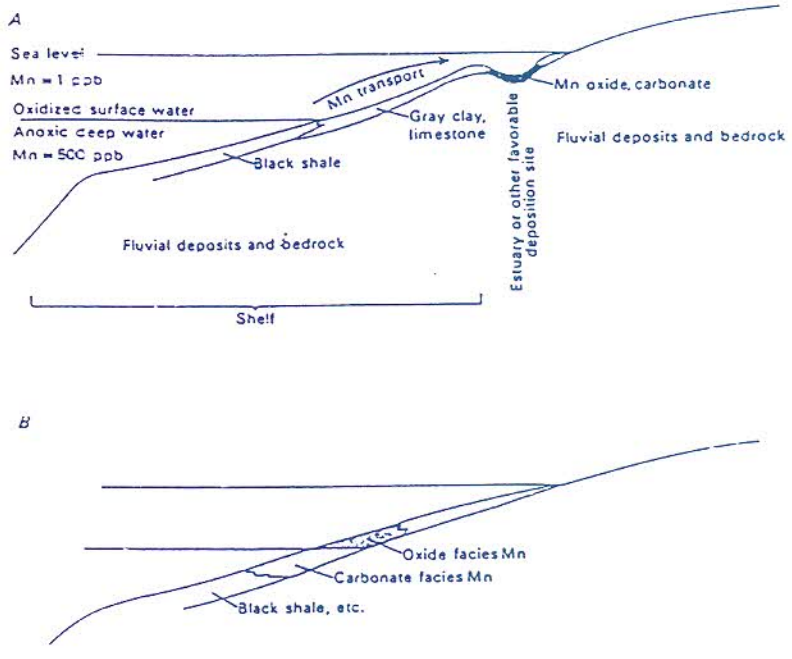

Fig. 6.15 *Depositional models for stratified basin margin manganese. A. Oxic model after Cannon and Force (1983). B. Zoned model after Force and Cannon (1988).*

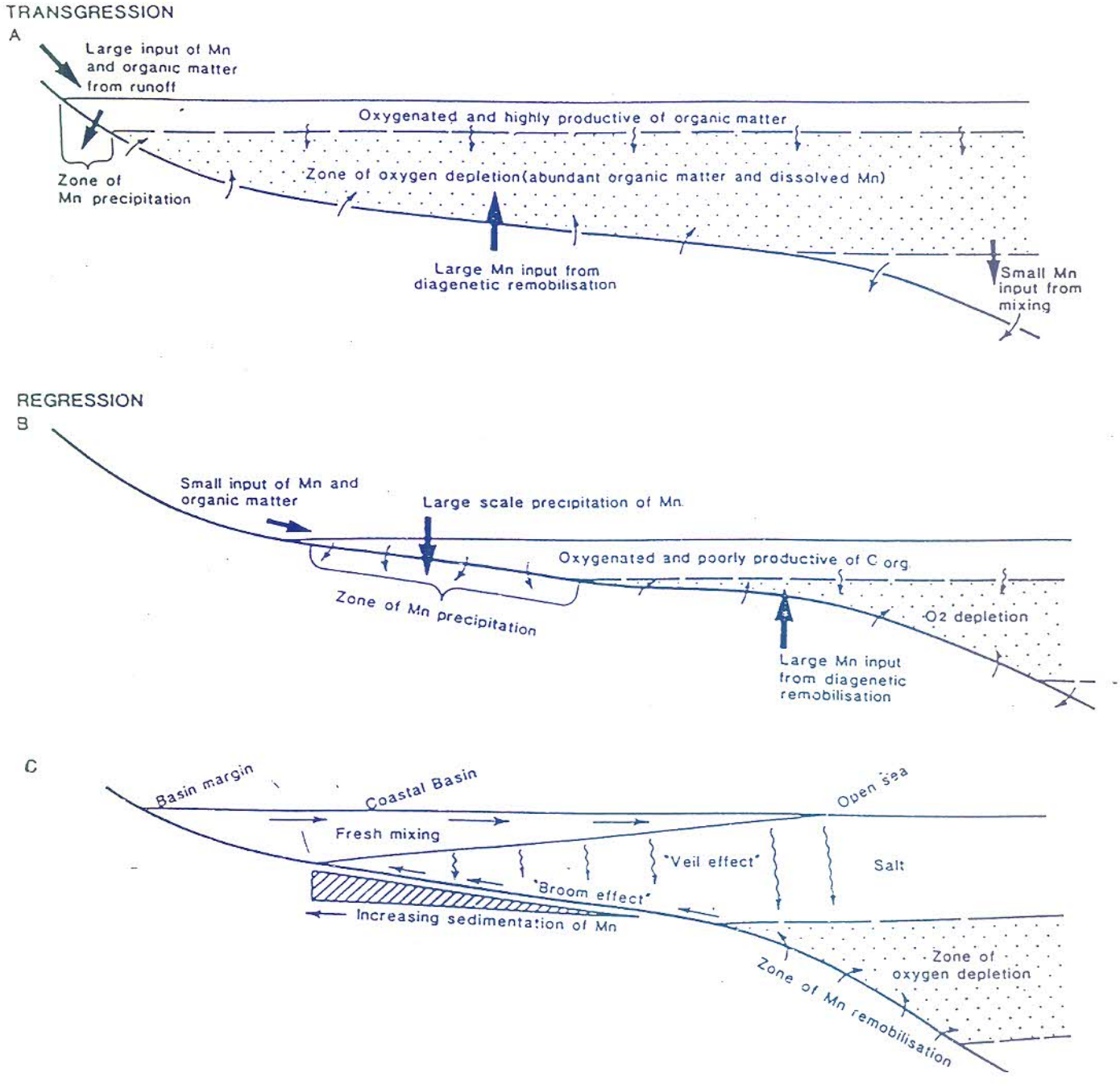

Fig. 6.16 *A: Relationships during marine transgression, showing narrow zone of Mn accumulation and concentration of dissolved Mn in a water column. B: Relationship during marine regression with abundant genetic demobilisation and wide zone of final Mn precipitation. C: Manganese sedimentation in coastal zone of intracratonic basin, showing veil effect (flocculant fallout) from saline mixing and broom effect (bottom transport and concentration) from tidal activity (after Frakes and Bolton, 1984).*

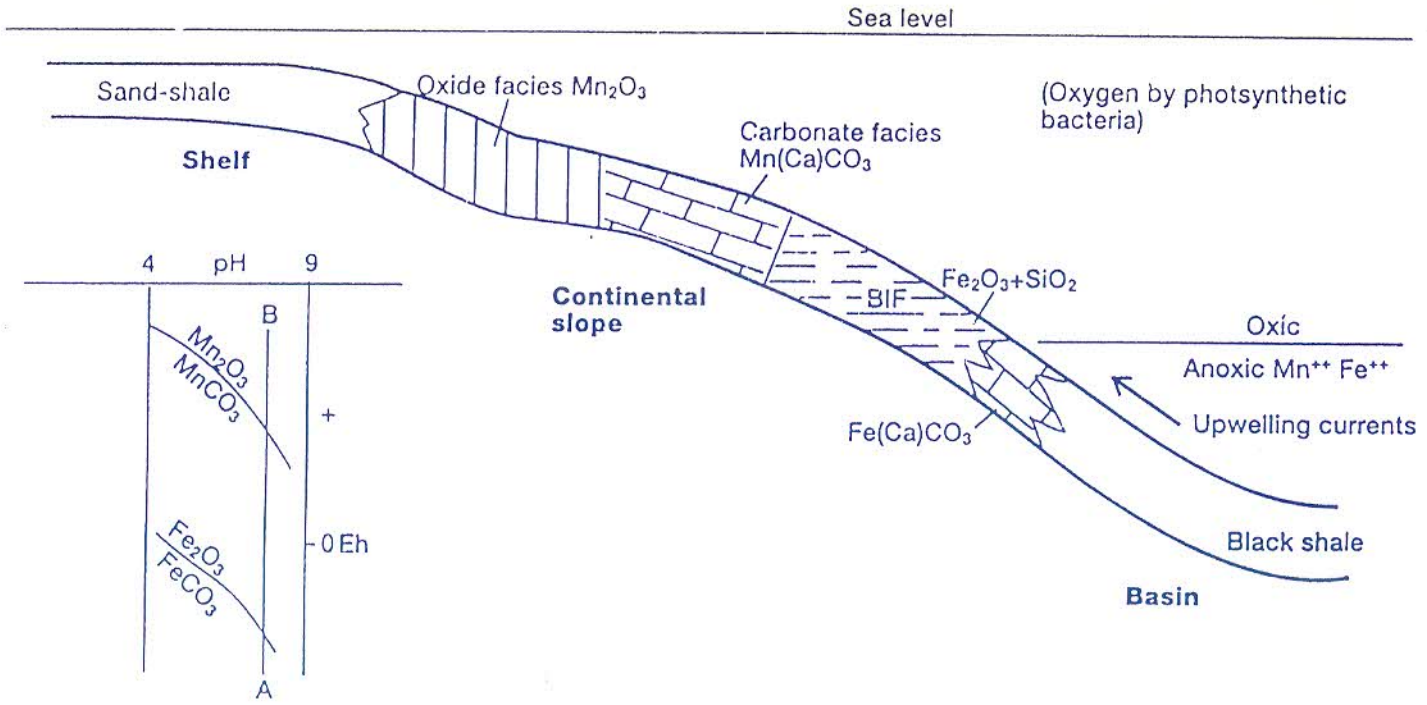

Fig. 6.17 Model of *Force and Cannon (1983) for deposition of manganese from upwelling anoxic waters, modified to include banded iron formations (after Button et al.,1982).*

61

A glaciogenic model has been proposed for certain banded iron formation-hosted manganese deposits. Beukes (1989) postulated that the manganese oxides interbedded with the banded iron formation at the Urucrum district in Brazil and the Otjisondu deposit in Namibia may have been related to periods of deglaciation following almost global freezing. Mn^{2+} was concentrated in the stagnant anoxic water below the ice, but during transgression, following interglacial warming, manganese-rich solutions were carried across the redox interface where deposition would ensue.

6.6.3 *Present-day sedimentary accumulation of iron and manganese*

Oolitic Clinton-type ironstones are forming at present within a number of East African lakes, principally Lake Malawi (Williams and Owen, 1992), and in a shallow marine setting at Cape Mala Pascua off Venezuela (Kimberley, 1989a). Iron and manganese crusts are currently forming in the stratified Baltic Sea but the only real modern analogue of the Superior-type is the Orca Basin. This basin is the most voluminous body of iron-rich seawater known and is a deep water intraslope depression in the Gulf of Mexico (Sheu and Presley, 1986; Rossignol-Strick 1987; Sheu *et al*, 1988). Cores taken from the Orca sediments indicate that they comprise intricately interlaminated red hematite layers with well laminated organic-rich and sulphide-rich black and grey muds.

7 FACIES VARIATION WITHIN THE HOTAZEL FORMATION OF THE VOëLWATER SUBGROUP AND CHARACTERISTICS OF THE ONGELUK LAVA

7.1 Introduction

Facies variation in the Hotazel Formation will be discussed focusing on facies variation within the BIF-units along three transects. Characteristics of the hematite-lutites, manganese units and underlying Ongeluk lava are discussed separately.

7.2 Banded iron formation

7.2.1 *The Epsom-Olivewood-Olivepan- Hotazel transect*

7.2.1.1 Introduction

This transect covers the central part of the Kalahari Manganese Basin (KMB) extending some 20 km from Epsom in the west to Hotazel in the east (Fig. 7.1 and Fig. 5.1). A high-grade (Wessels-type) manganese deposit is located midway along the Epsom-Olivewood farm boundary (Fig. 7.6), close to the western edge of the KMB.

A total of 31 boreholes were studied for the iron formation facies analysis. These include 24 boreholes on and around the Epsom deposit and 7 boreholes towards the eastern boundary of the basin. Facies descriptions of the Hotazel outlier are based on iron formation exposures in the Hotazel quarry and core from two boreholes, H089 and H090 (Fig. 7.1).

The Hotazel iron formation can be divided into three lithological units (Figs. 4.6) i.e.:

(i) The Lower BIF Unit conformably overlying the Ongeluk lava formation and developed at the base of the lower manganese body.
(ii) The Middle BIF Unit developed between the lower and upper manganese bodies.
(iii) The Upper BIF Unit above the upper Mn-body.

Each manganese horizon is enveloped by a distinctive red to silvery grey-coloured hematite-lutite (chapter 4)(Figs. 7.1, 7.18 and 7.22). The hematite-lutite is excluded from the facies descriptions of the banded iron formations. Some characteristics of the hematite-lutite will be discussed in a later chapter.

Five main facies-types were identified (figs. 7.1, 7.4 and 7.8):

(i) Hematite-chert facies
(ii) Hematite-chert-carbonate facies
(iii) Magnetite/hematite-chert-carbonate facies
(iv) - Greenalite-magnetite-carbonate facies.
(v) Riebeckite-amphibole facies.

Contours of the top of the lava indicate a north-south trending domal structure underlying the high-grade Mn deposit on Epsom-Olivewood (Fig. 7.3). Isopach maps show distinct thinning of the Lower and Middle BIF Units over this domal structure, suggesting the presence of a lava-palaeohigh during precipitation (Figs. 7.3, 7.7 and 7.10). Thinning of the Upper BIF Unit towards the north-west, south-west and south suggests down-cutting of the basal Olifantshoek Subgroup unconformity down the slopes of the same palaeohigh.

7.2.1.2 Lateral Facies Variation

(a) Hematite-chert facies (Oxide facies)

This facies is confined to the Epsom palaeohigh and to the Hotazel deposit along this transect (Figs. 7.1, 7.4, 7.5, 7.8 and 7.9.). It comprises microbanded and mesobanded, cryptocrystalline hematite-chert rhythmites. Indications of shallow water deposition such as wavy chert bedding, chert lenses, billows and pillows (Figs. 7.11 and 7.12) are present in the basal parts of both the Lower and Middle BIF Units. Evenly and regularly bedded hematite-chert micro - and mesobanded rhythmites (Fig. 7.13 and 7.14) dominate in the upper parts of the Middle and Upper BIF Units. The hematite-chert contacts are sharp. White coloured crystalline chert alternates with brownish to silvery-grey fine-grained hematite dust bands. Coarse-grained shiny hematite/specularite often overprints the hematite dust layers and are also present as disseminations in chert rendering a reddish colour to the chert bands.

The top of the Upper BIF Unit on the farm Epsom (285) is marked by the presence of coarse-grained sandy-textured hematite-bandlutites alternating with the hematite-chert microbanded rhythmites (Fig. 7.14). The bandlutites display a sandy peloidal texture with disrupted siliceous stringers and pods. Only the top part of the Upper BIF Unit is preserved underneath the Olifantshoek unconformity in borehole intersections on the farms Simondium (308) and Constantia (309), suggesting the proximity of a palaeo-shoreline. These farms are located close to the present western boundary of the basin. The banding of the Upper BIF Unit at Hotazel is generally thicker (± 3cm). The lower 2m is characterised by wavy and podded chert bedding.

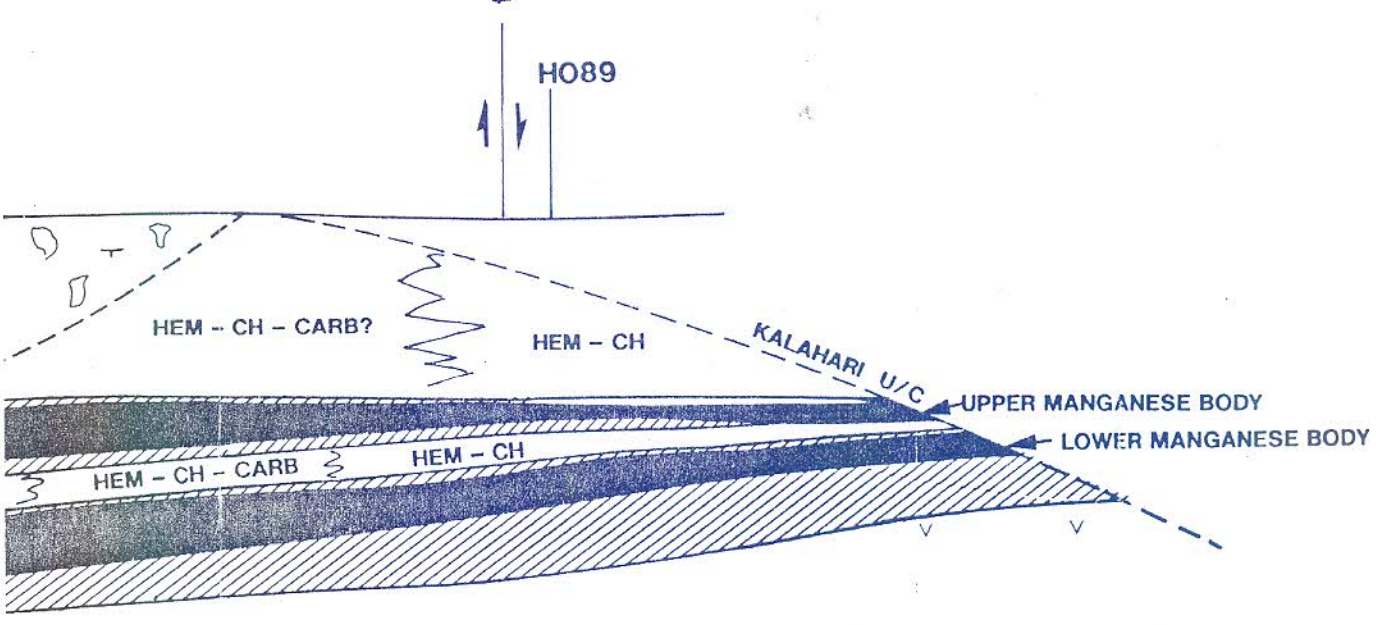

VERITICAL SCALE

0
10
20
30
40
50
METRES

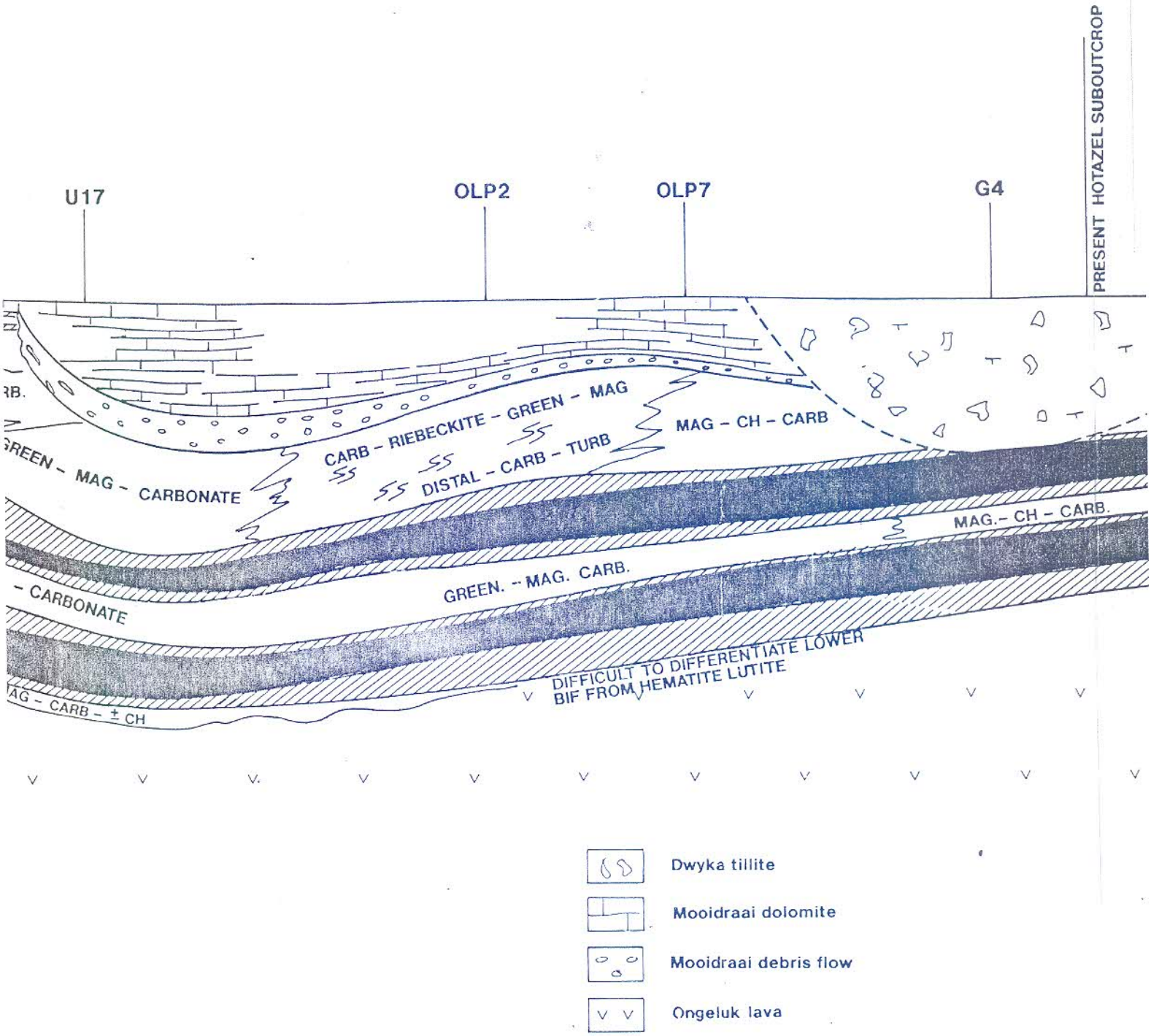

Fig. 7-1 Epsom - Hotazel Transect.

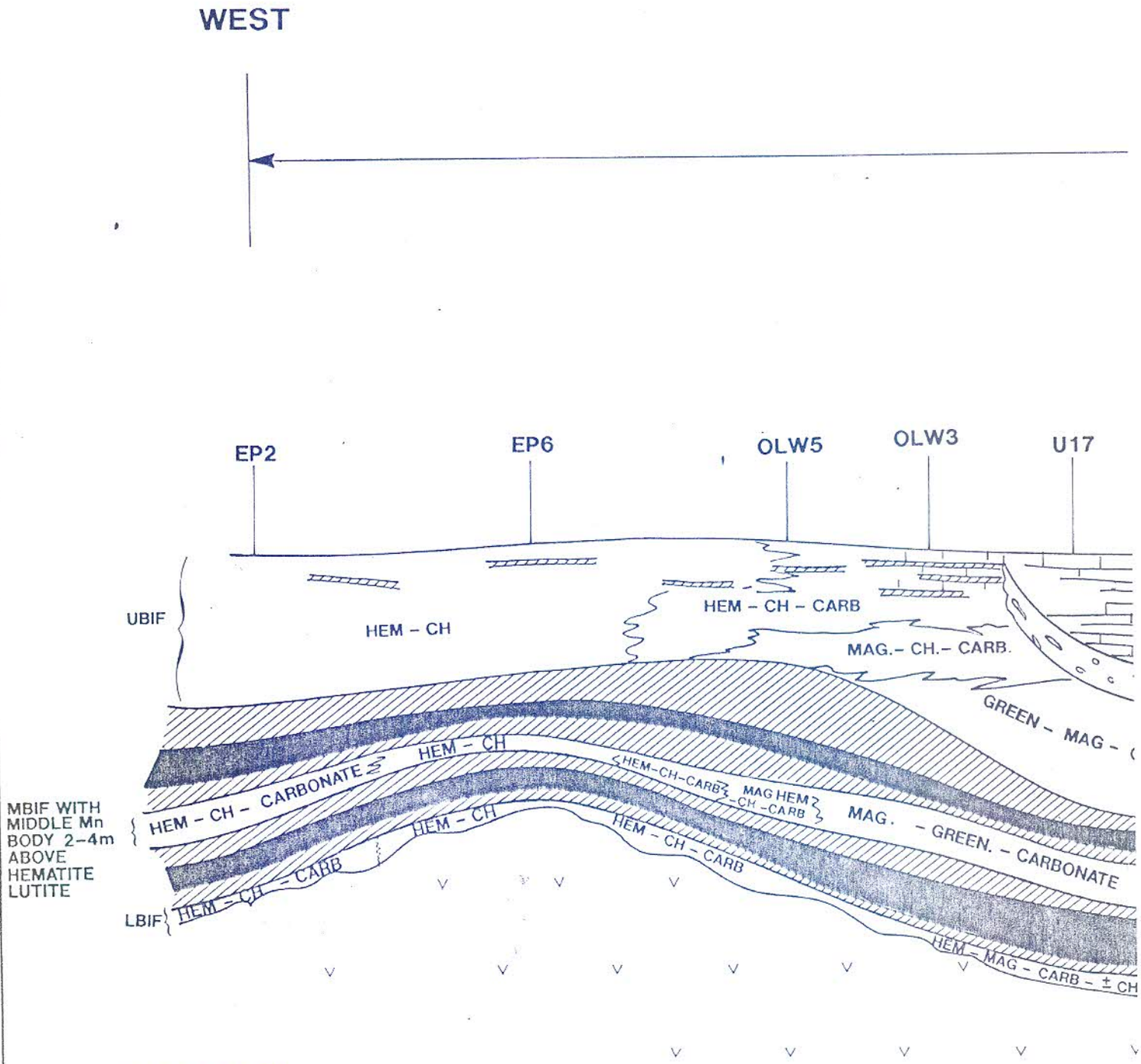

REFERENCE

HEM	=	HEMATITE
MAG	=	MAGNETITE
GREEN	=	GREENALITE
CARB	=	CARBONATE
CH	=	CHERT

HEMATITE LUTITE

Mn ORE

SSS SLUMPED LAYERS

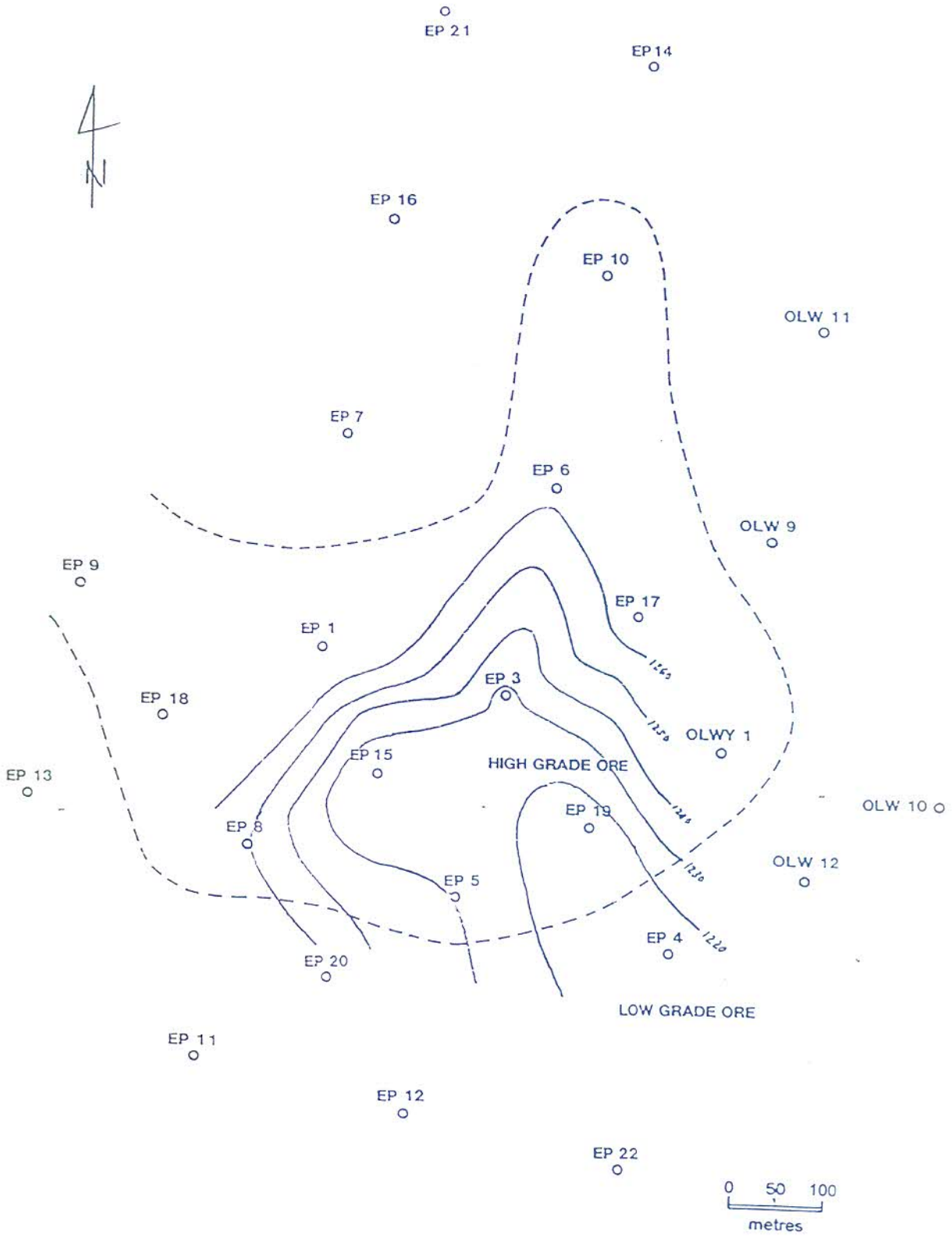

Fig. 7-2 Location of boreholes drilled by Gefco. Boundary separating high from low grade Mn ore also shown plus depth to top of lava, contours showing a domal structure.

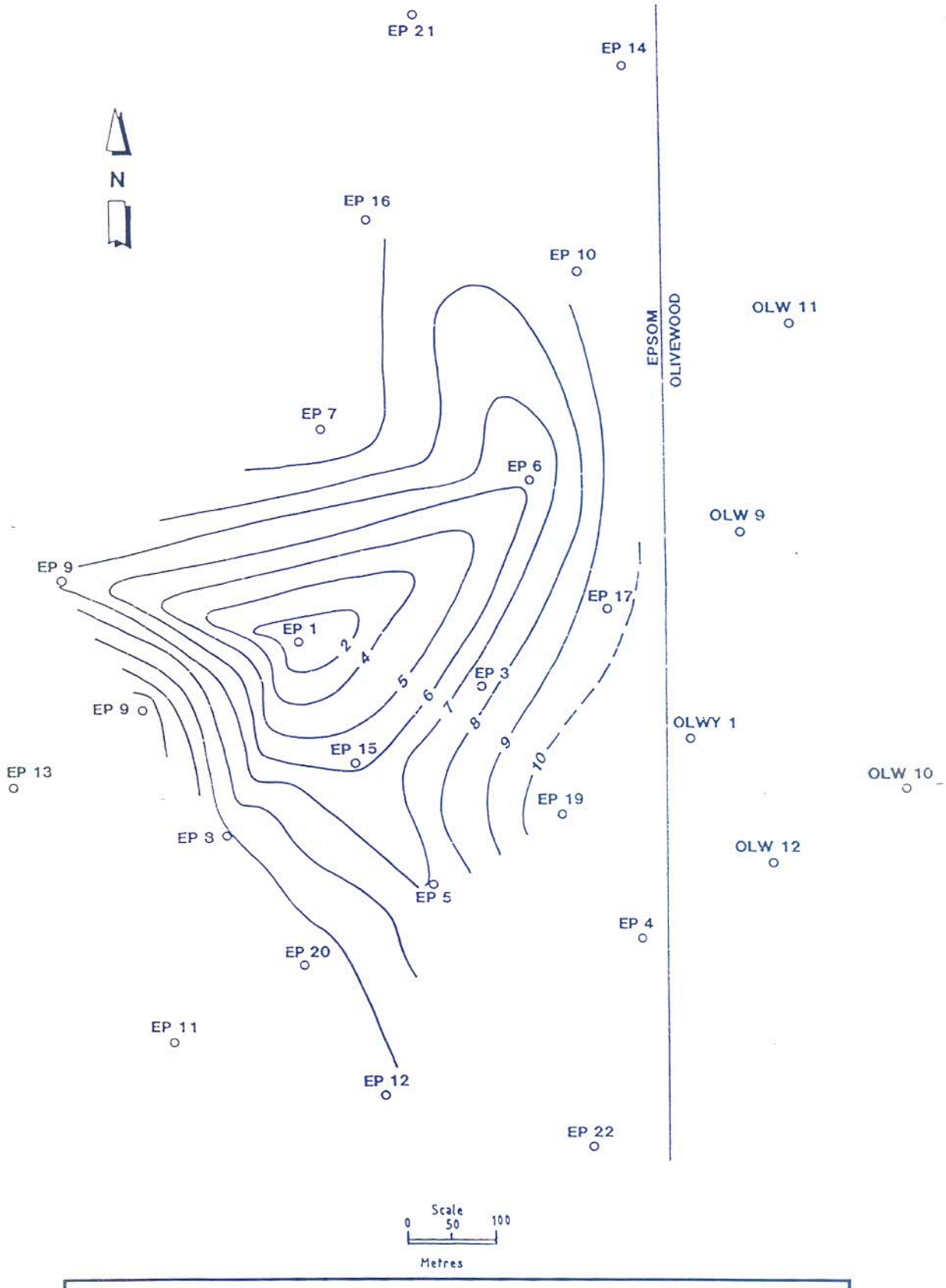

Fig. 7-3 Isopachs of the lower BIF unit, indicating the shape of the Epsom palaeohigh (thickness in metres).

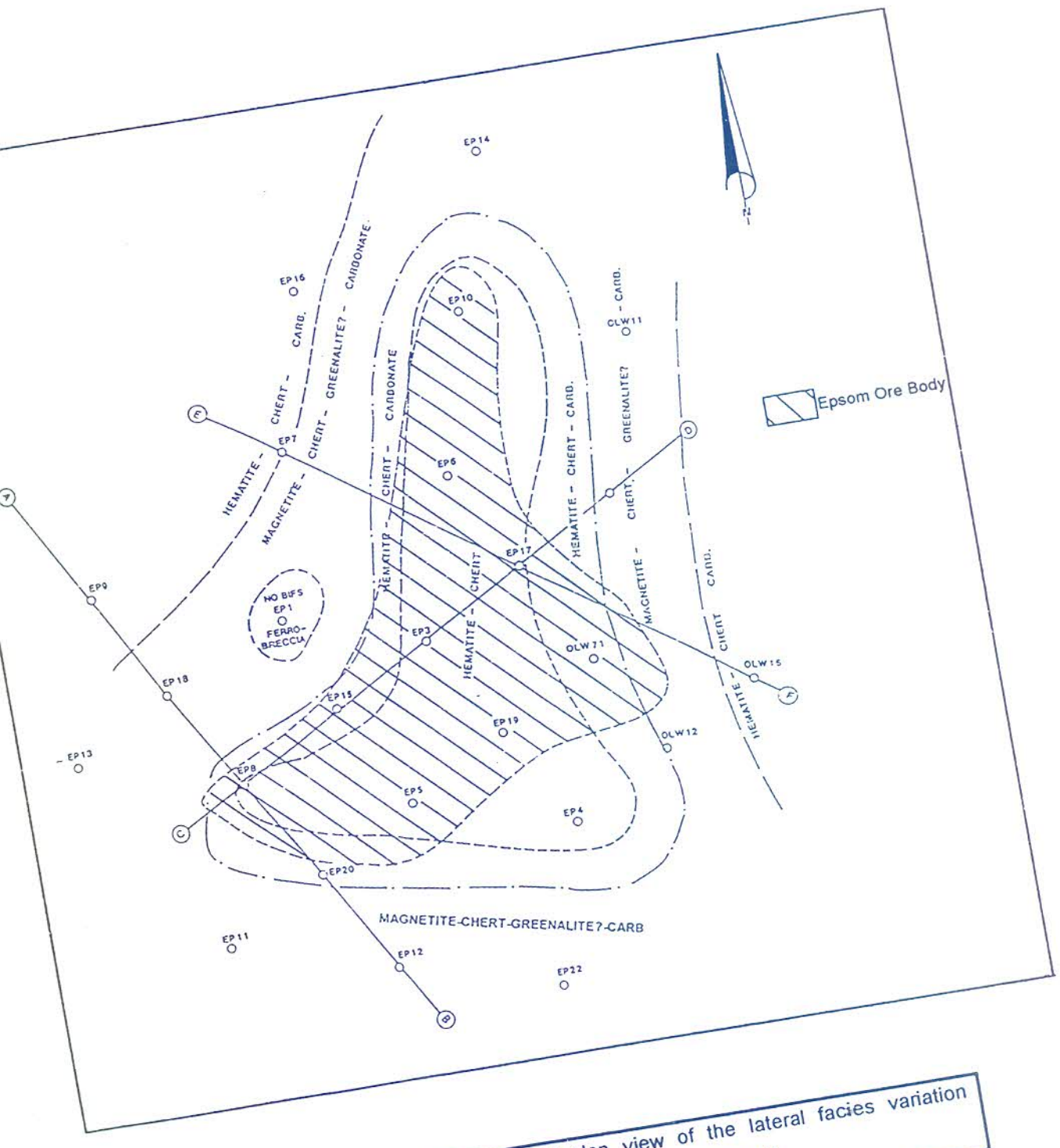

Fig. 7-4 Profile directions and plan view of the lateral facies variation across the Epsom palaeohigh (Lower BIF unit).

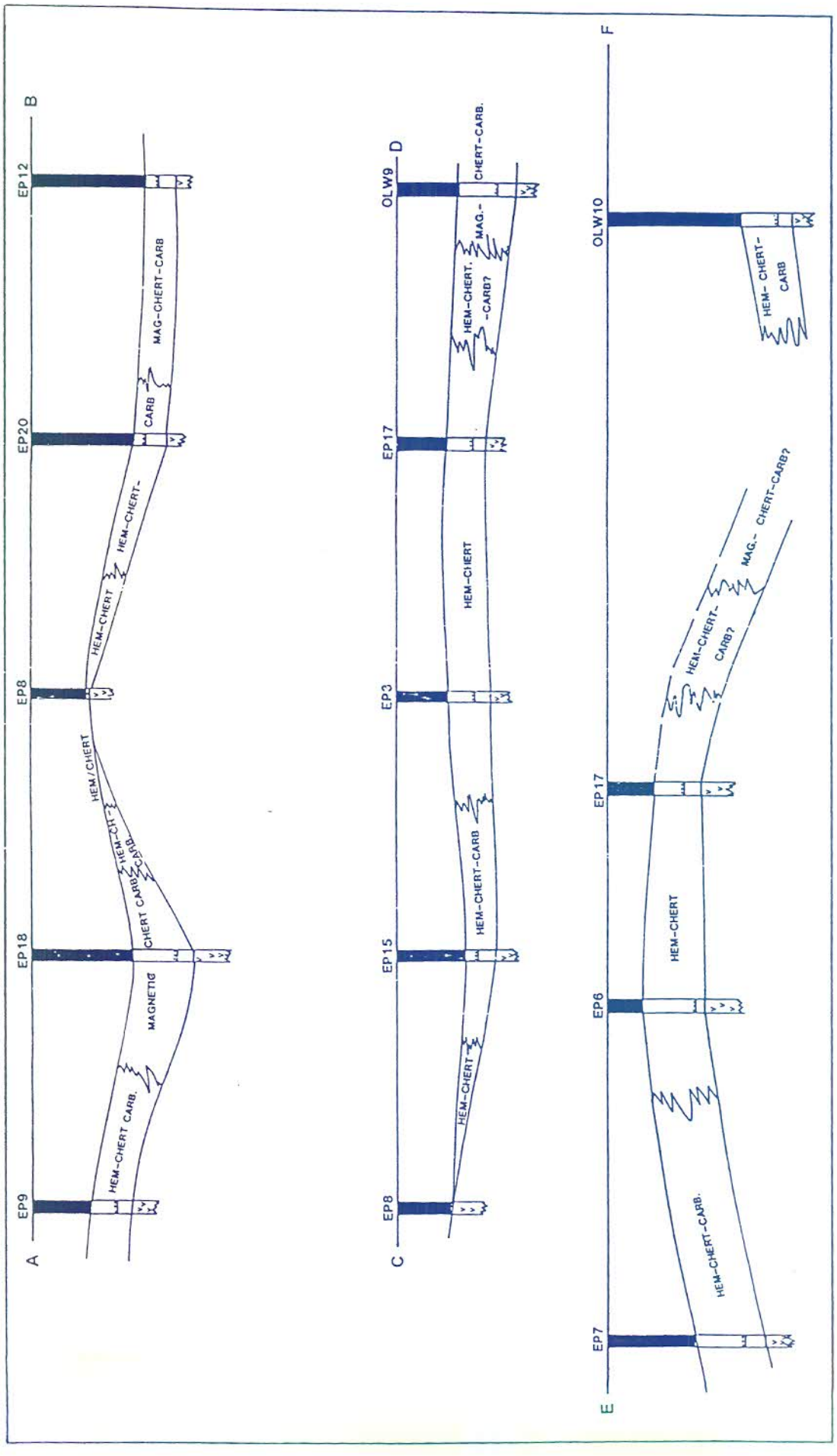

Fig. 7-5 Lower BIF facies variation across the Epsom palaeohigh.

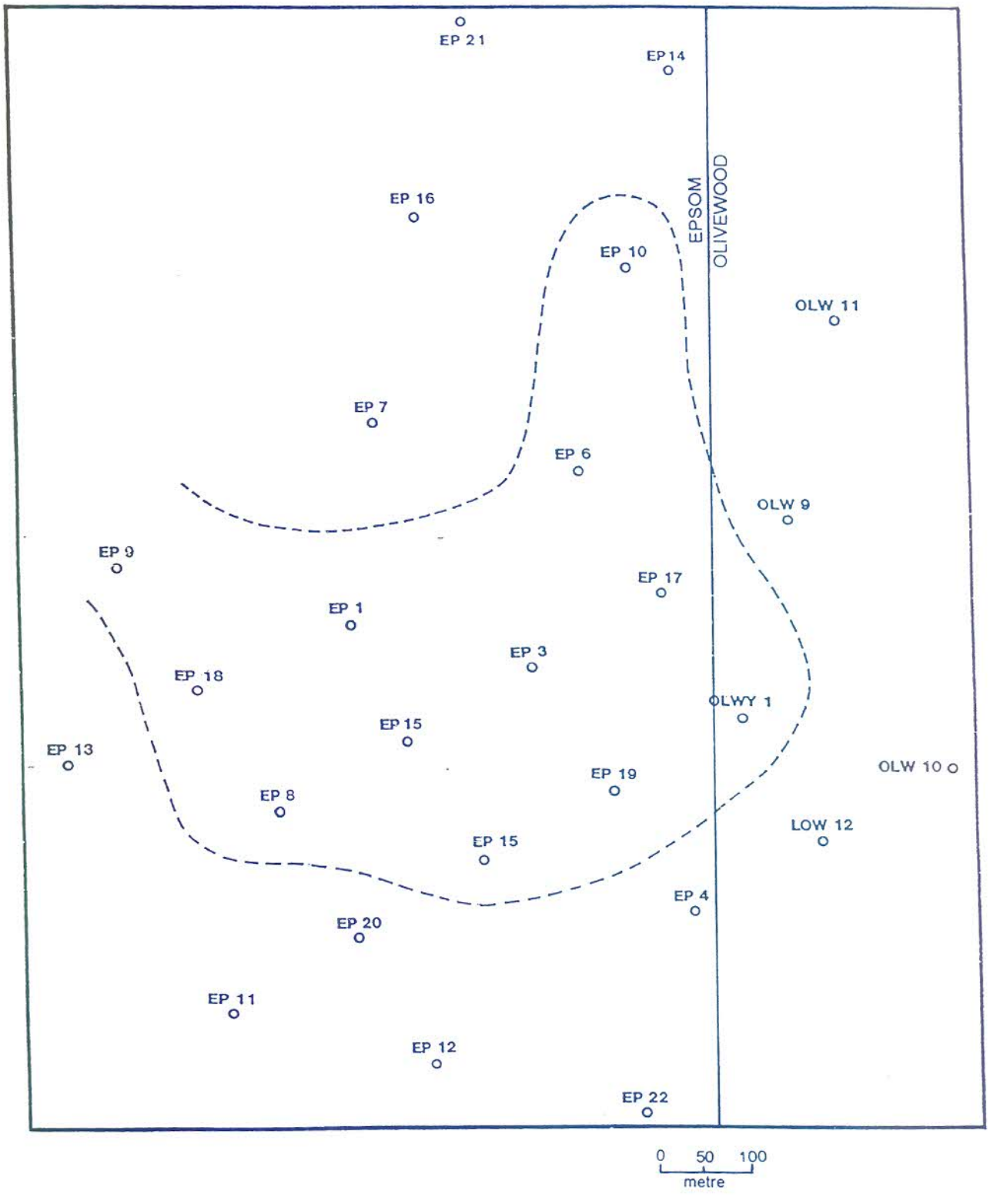

Fig. 7-6 Epsom high grade Mn deposit.

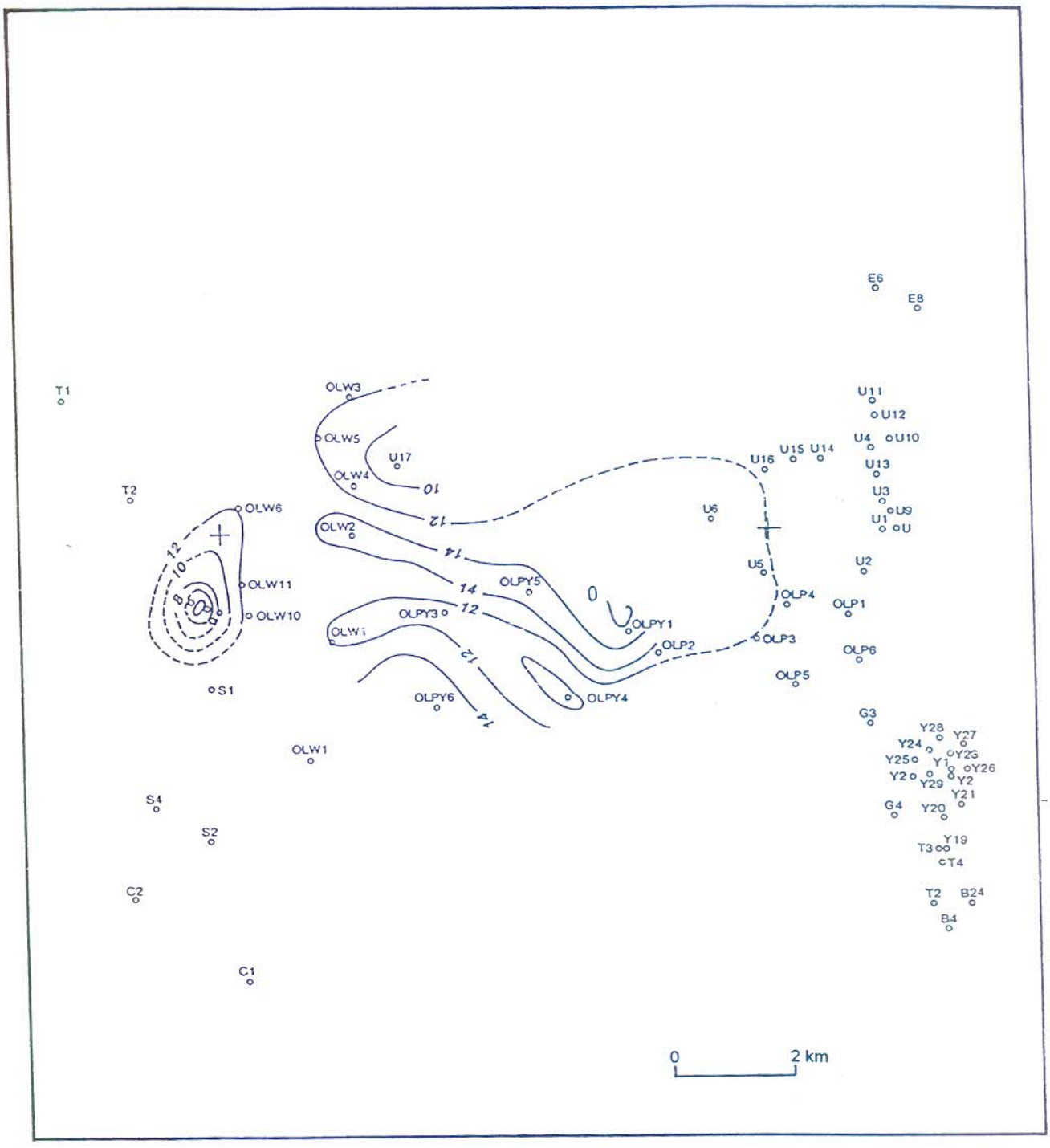

Fig. 7-7 Isopachs on the lower BIF unit covering the Epsom-Hotazel transect.

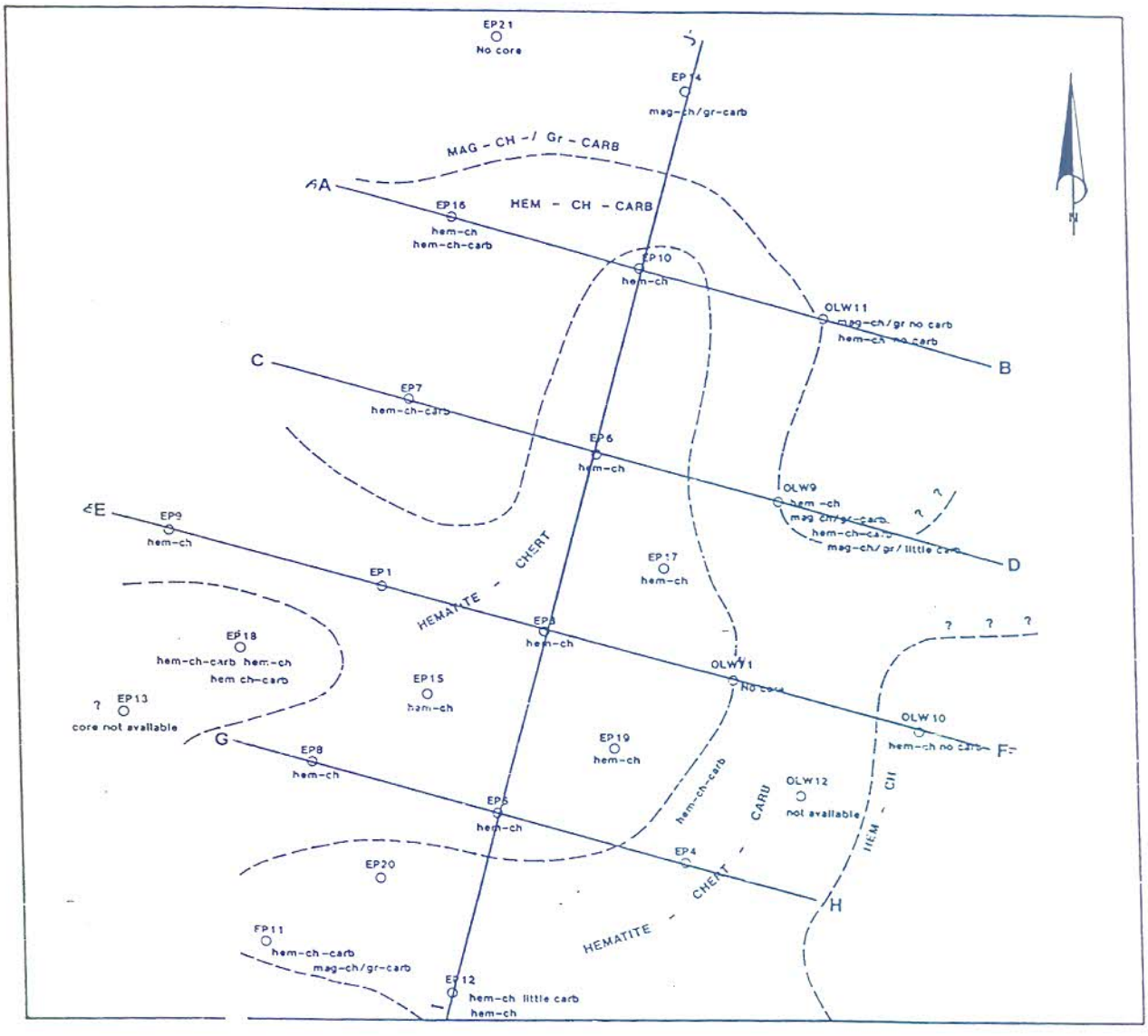

Fig. 7-8 Lateral facies distribution across the Epsom palaeohigh (Middle BIF unit). Localities of profiles lines are also shown.

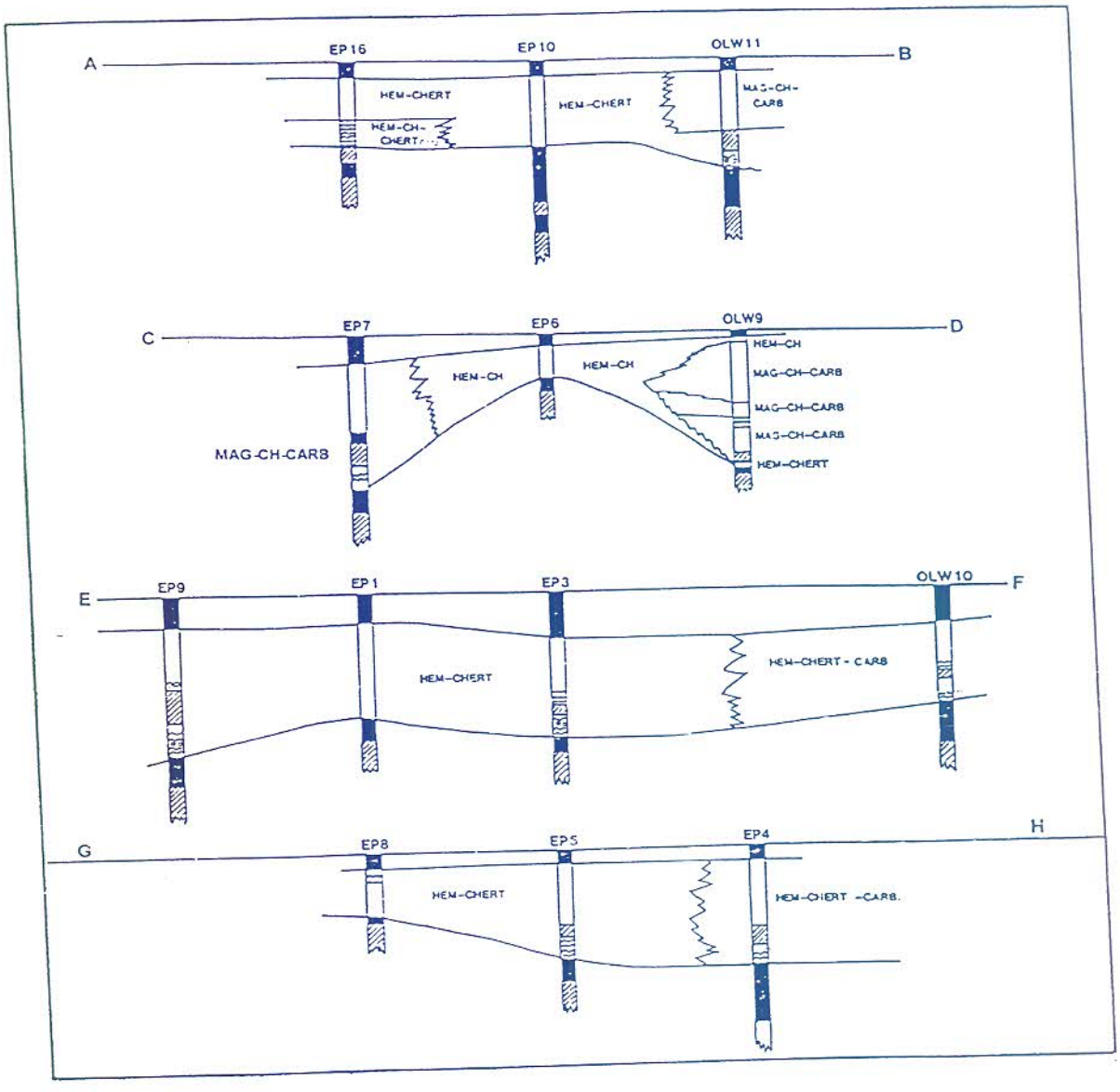

Fig. 7-9a East-west facies variation across the Epsom palaeohigh (Middle BIF unit).

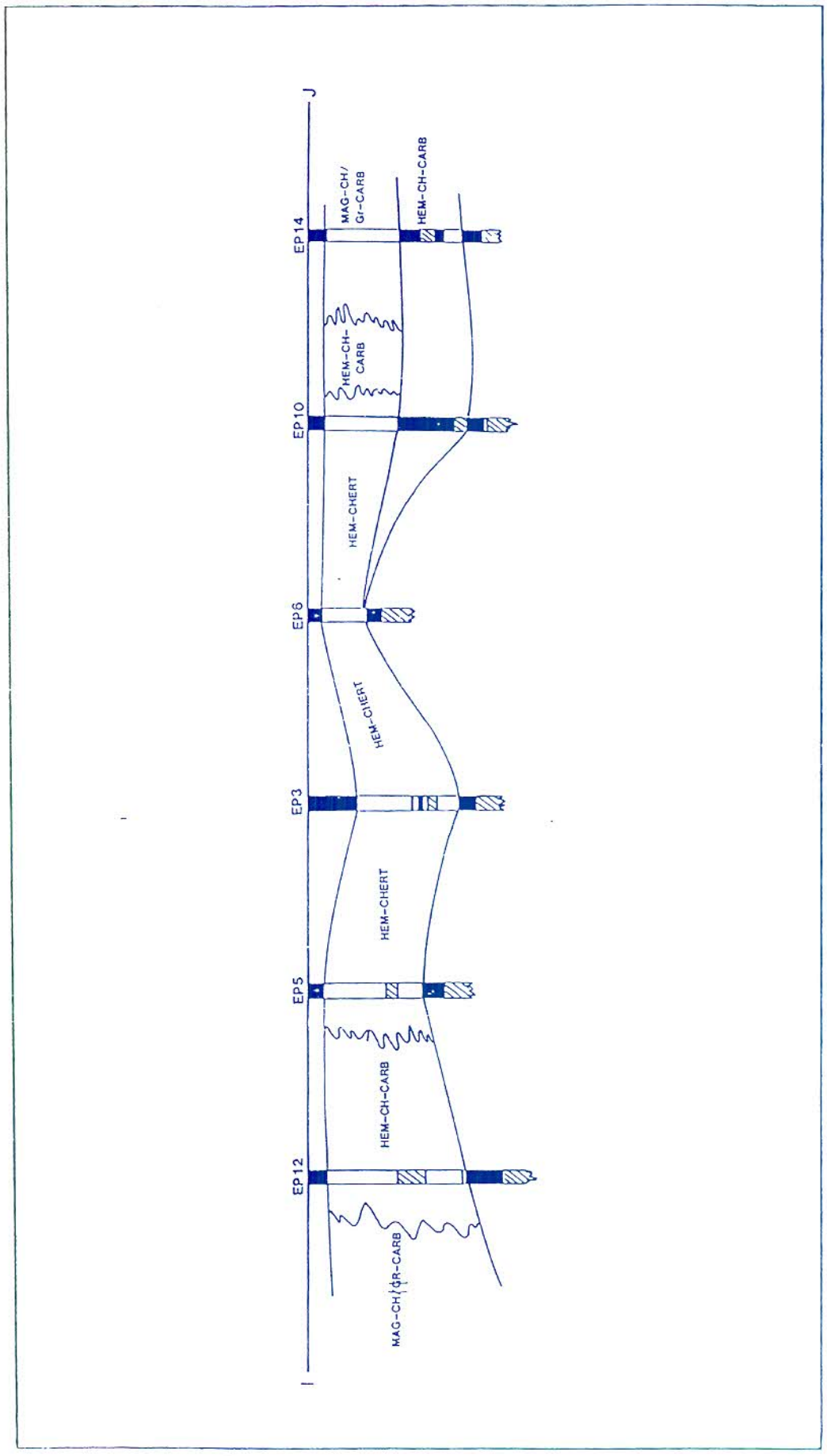

Fig. 7-9 b North-south facies variation across the Epsom palaeohigh (Middle BIF unit)

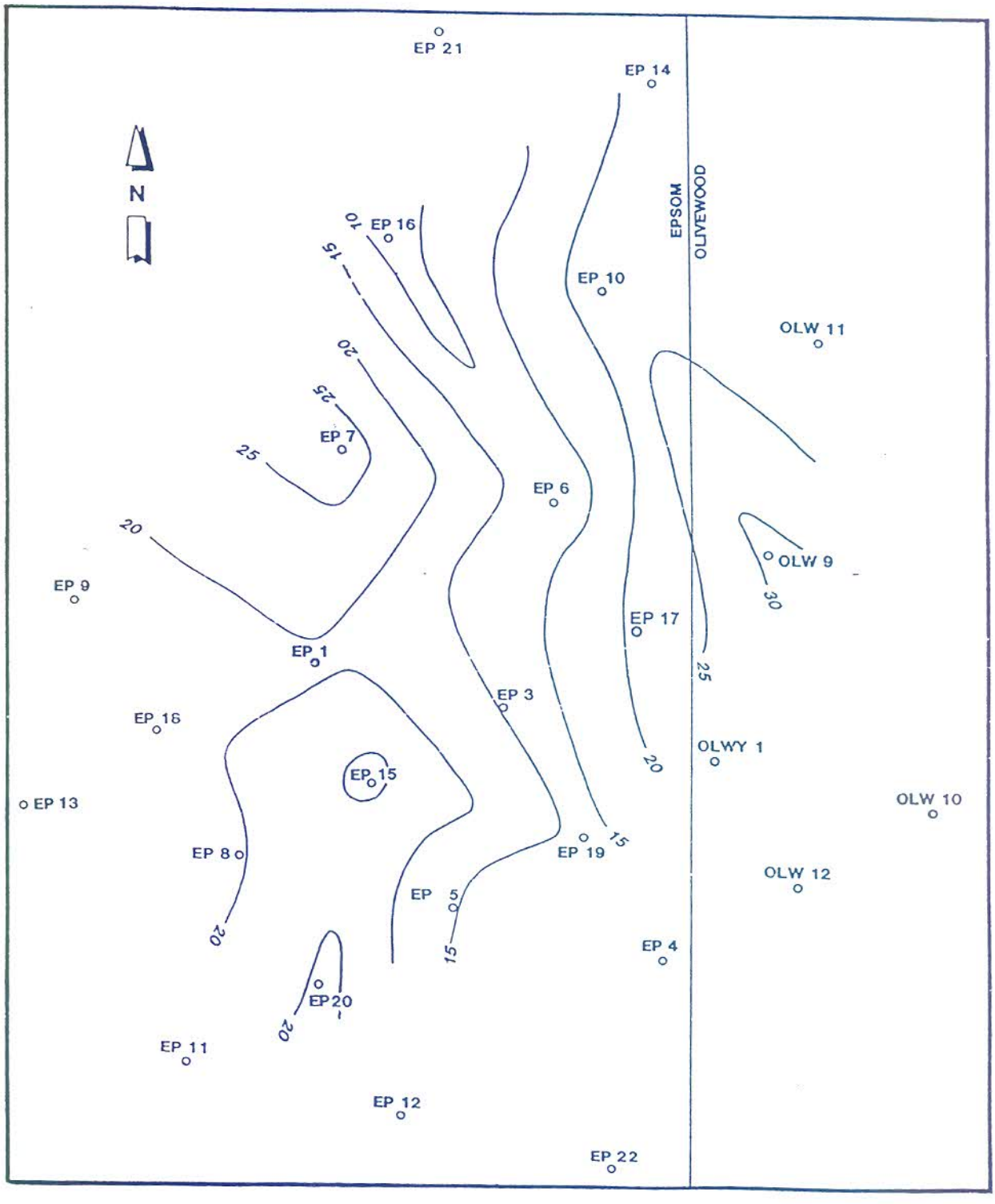

Fig. 7-10 Isopachs of Middle BIF unit across the Epsom palaeohigh.

Fig. 7.11 *Borehole EP 5 - chert waves, billows and pillows near base of Lower BIF Unit (hematite-chert facies).*

(b) Hematite-chert-carbonate facies (oxide facies)

The hematite-chert-carbonate represents a lateral gradational extent of the hematite-chert associations (Fig. 7.1, 7.5 and 7.9). Bedding features are similar to those of the hematite-chert facies. Carbonate is present in the form of ankerite. Carbonate generally occur in 5mm thick brownish coloured microbands but is also present as disseminations in chert mesobands. Coarse-grained euhedral recrystallized carbonate often rims the carbonate laminae.

(c) Magnetite/hematite-carbonate facies (oxide facies).

The magnetite/hematite-carbonate facies is found at the outer fringes of the Epsom palaeohigh (Figs. 7.1, 7.4, 7.5, 7.8, and 7.9). In boreholes EP 11, OLW 9 and OLW 11. Zones in which either magnetite or hematite dominate, are present

Fig. 7.12 *Borehole EP 5 - chert waves, billows and pillows near the base of the Middle BIF Unit (hematite-chert facies).*

Fig. 7.13 *Borehole EP3 - micro - and mesobanded rhythmites - Middle BIF Unit (hematite- chert facies).*

In the Middle BIF Unit. There is no definite pattern in the distribution of these oxides. Bedding is defined by alternating laminae of magnetite/hematite, chert and carbonate.

Magnetite is present in shiny-black microbands and ribbons generally displaying a subhedral texture. Coarse euhedral grains are common, overprinting carbonate and chert (Fig. 7.15). The chert microbands show sharp contacts with the magnetite laminae, while carbonate is present in light to brown coloured microbands. Recrystallised carbonate often occurs in individual coarse-grained microbands and as disseminations in chert.

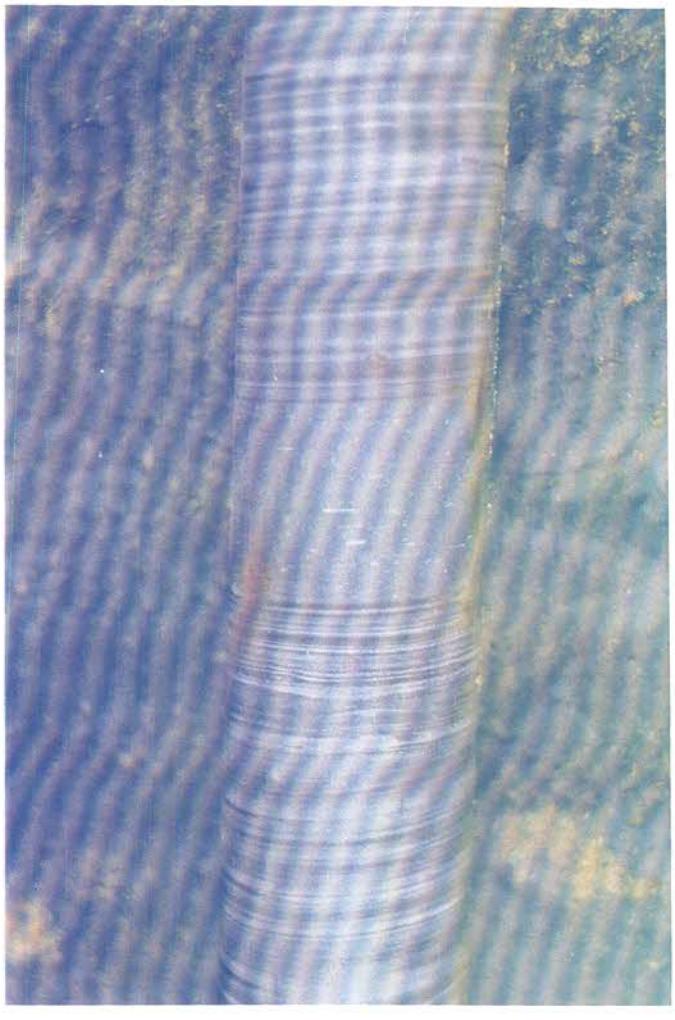

Fig. 7.14 *Borehole EP 5 - evenly micro - and mesobanded hematite-chert facies. Note the clastic textured hematite-chert bandlutite (Upper BIF Unit).*

Maculate banded iron formation is developed near the base of the Middle BIF Unit in borehole OLW 7. White chert pods, pillows and wavy disrupted chert banding occur within a massive bedded iron-carbonate matrix (Fig. 7.16). Magnetite is the

dominant iron oxide, often occurring as overgrowths on carbonate. Chert intraclasts and discs are often contained within thin (±1cm) layers. The sequence in OLW 7, comprising magnetite-chert-carbonate rhythmites, becomes more evenly bedded downwards in the stratigraphy.

(d) Greenalite-magnetite-carbonate facies (Silicate facies)

The oxide facies grades laterally (eastwards) into silicate facies rocks (Fig. 7.1). The latter facies is light to dark green in colour and comprises evenly spaced and parallel microbanded greenalite-magnetite-carbonate rhythmites. Magnetite is present as shiny-black euhedral to subhedral grains in microbands and as disseminations clearly overprinting everything else. Greenalite is present as light- to dark-green microbands with a microcrystalline texture. Carbonate occurs as euhedral to subhedral grains in light-green to brown coloured, disrupted and continuous microbands.

(e) Riebeckite-amphibole facies

This facies is best developed in the Olivepan area (Fig. 7.1, and 7.17) and comprises diagenetic fibrous subhedral aggregates overprinting everything else. Primary vestiges of greenalite-magnetite-carbonate lithologies show gradational contacts with the amphibole facies. Towards the top of the Upper BIF Unit, riebeckite occurs as massive lutites up to 1,5m thick. It is commonly present as crystals cross-cutting bedding planes. The crystalline habit of greenalite, magnetite and carbonate in zones of less severe riebeckitization is similar to that of the silicate facies.

Fig. 7.15 *Borehole OLW 7 - chert pods and pillows (grey) and magnetite waves (dark grey). Note disseminated coarse magnetite grains near base (magnetite-chert-carbonate facies).*

Fig. 7.16 *Borehole OLW 7-chert intraclasts, chips, pods and pillows near the base of the Middle BIF Unit (magnetite-chert-carbonate facies).*

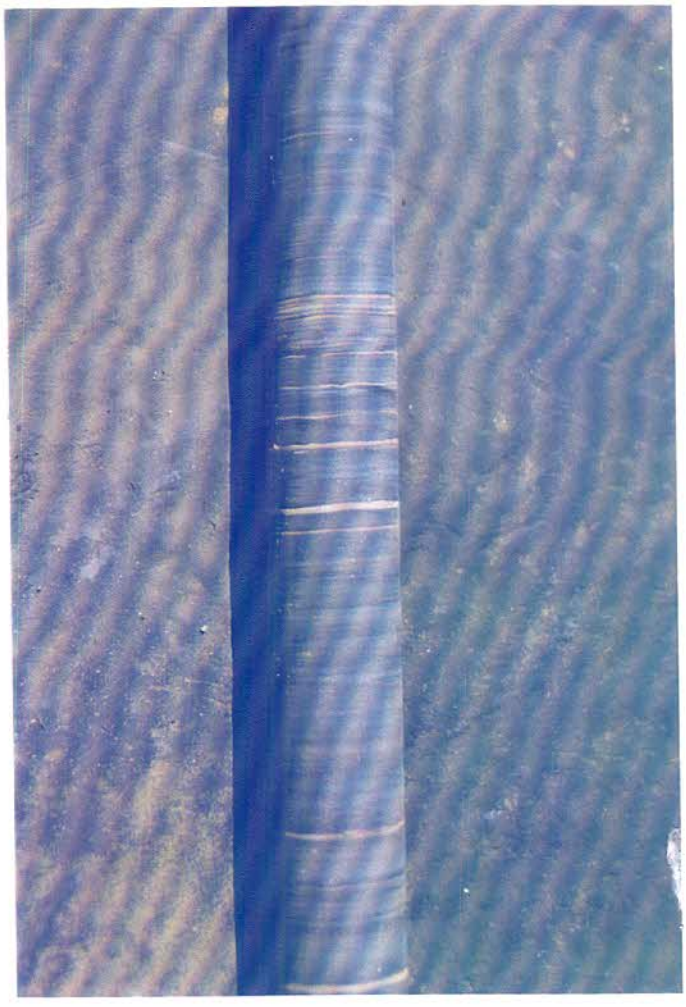

Fig. 7.17 *Borehole OLP2 - Riebeckite-rich facies in the Upper BIF Unit.*

Sandy textured deformed carbonate layers up to 6cm thick with white carbonate stringers showing coarse euhedral magnetite overprints, are often interbedded with the greenalite-magnetite-carbonate lithologies. Riebeckitic chert pods and billows are prominent near the contact with the underlying hematite-lutite above the upper Mn ore-body.

7.2.1.3 Vertical Facies Variation

Facies changes upward in the stratigraphy, from reduced facies to oxide facies iron formation, was observed in several boreholes (OLW 3, OLW 5 and OLW 7). In OLW 3, greenalite-magnetite-carbonate assemblages in the Upper BIF Unit

grade progressively upward into magnetite-chert-carbonate and hematite-chert carbonate associations (Fig. 7.1). The Middle BIF Unit in OLW 7 comprises maculate bedded magnetite-chert-carbonate facies whilst the Upper BIF Unit displays hematite-chert-carbonate facies.

The hematite-chert facies iron formation becomes more prominent upwards in the stratigraphy and was deposited over a much larger area (Fig. 7.1).

7.2.2 *The Moffat-Middleplaats-Mamatwan Transect*

7.2.2.1 Introduction

A prominent lava palaeohigh is inferred for the area towards the west of the Middleplaats mine (Fig. 5.1). Both the Lower and Middle BIF Units progressively onlap westwards onto the palaeohigh (Fig. 7.18). Borehole intersections also indicate rapid thinning particularly of the Upper BIF Unit, as the palaeohigh is approached (Fig. 7.19 to Fig. 7.21).

This transect (Fig. 7.18) deals with the lithologies developed towards the west of the lava-palaeohigh, on the farms Smuts and Moffat (Figs. 5.1 and 7.18) and to the east within the basin (Middleplaats-Mamatwan). A total of 20 boreholes were studied. Borehole profiles along this transect indicate dips of ±7° towards the west at Mamatwan, passing through a synformal structure in the central part of the basin and then reverts to ± 7° easterly dips in the area east of Middleplaats. In contrast to the Epsom-Hotazel transect, no prominent lateral facies changes were recognised.

WEST

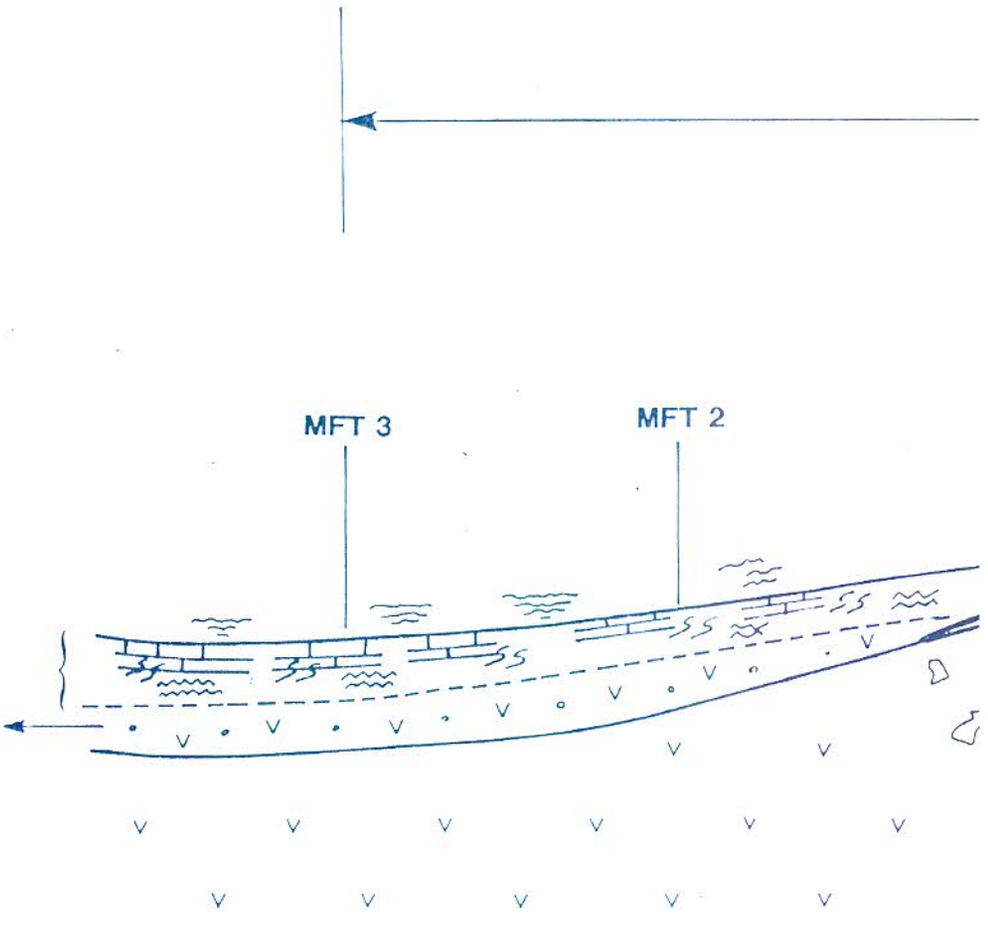

REFERENCE

- SLUMPED CARBONATE LAYERS
- WAVY BEDDING
- CHERT BILLOWS AND PILLOWS
- HEMATITE LUTITE
- Mn BODY

VERTICAL S

0
10 M
20

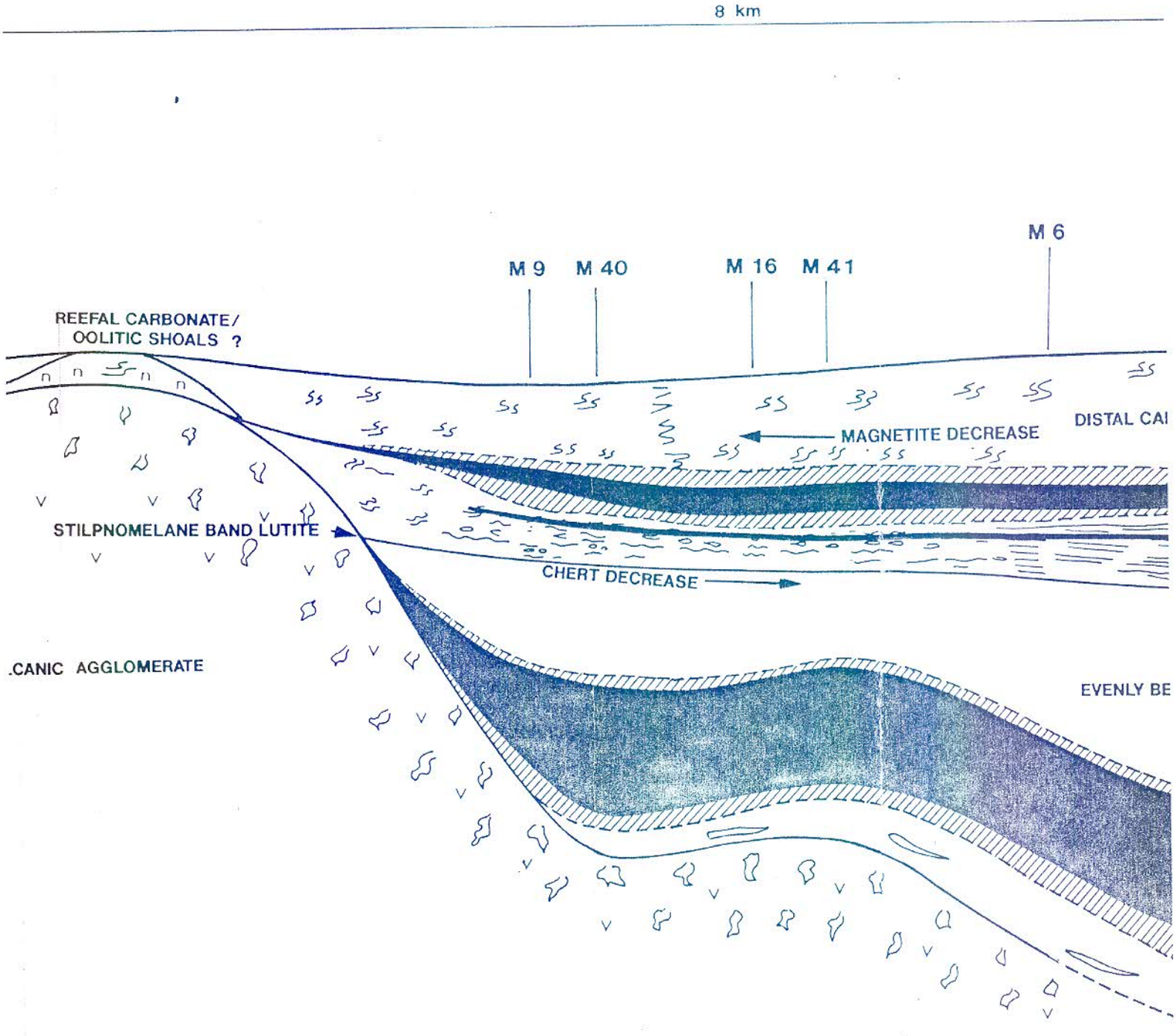

Fig. 7.18 Moffat - Middleplaats - Mamatwan transect.

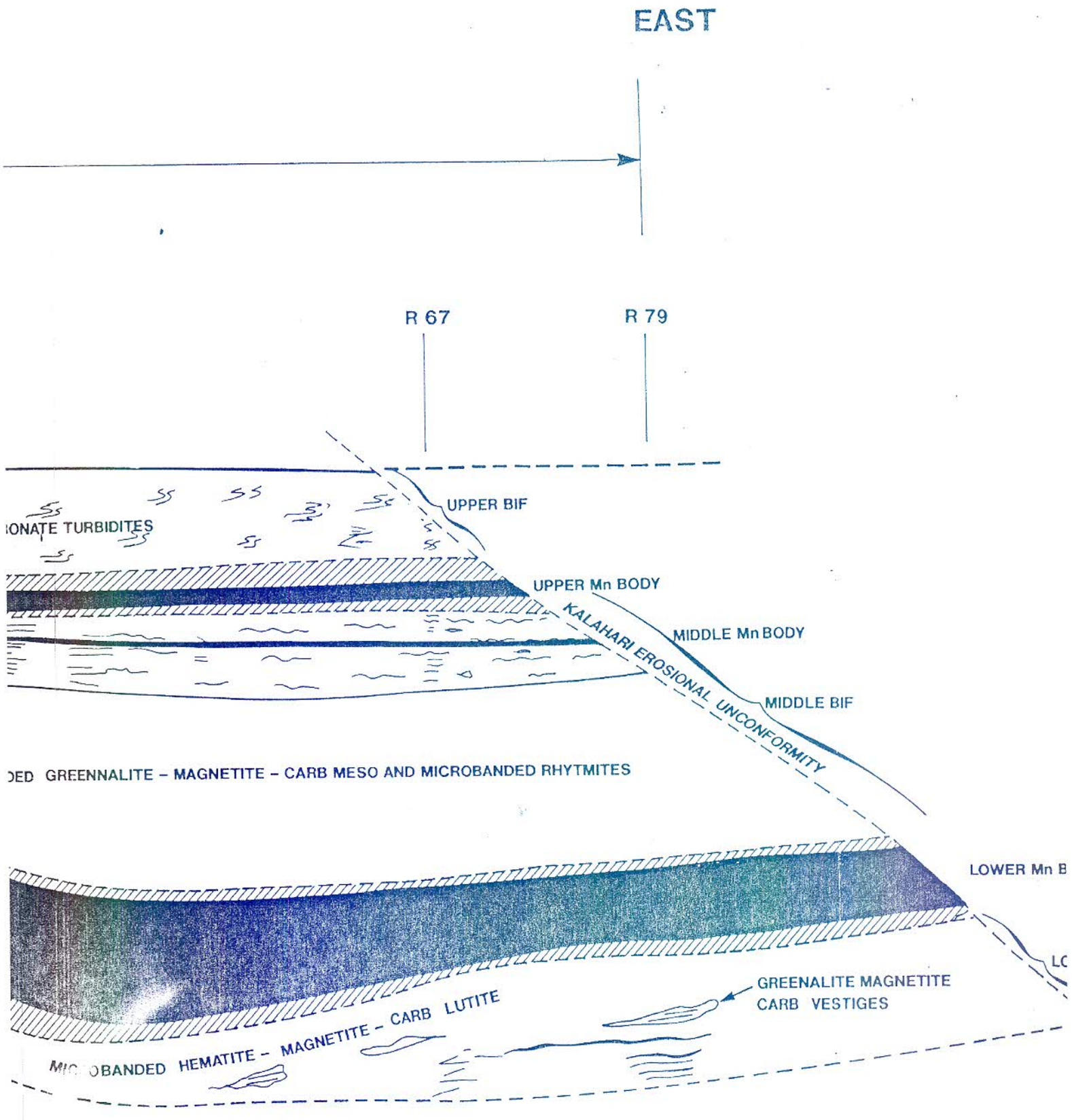
EAST
R 67
R 79
UPPER BIF
ONATE TURBIDITES
UPPER Mn BODY
KALAHARI EROSIONAL UNCONFORMITY
MIDDLE Mn BODY
MIDDLE BIF
DED GREENNALITE – MAGNETITE – CARB MESO AND MICROBANDED RHYTMITES
LOWER Mn B
LC
GREENALITE MAGNETITE
CARB VESTIGES
MIC OBANDED HEMATITE – MAGNETITE – CARB LUTITE

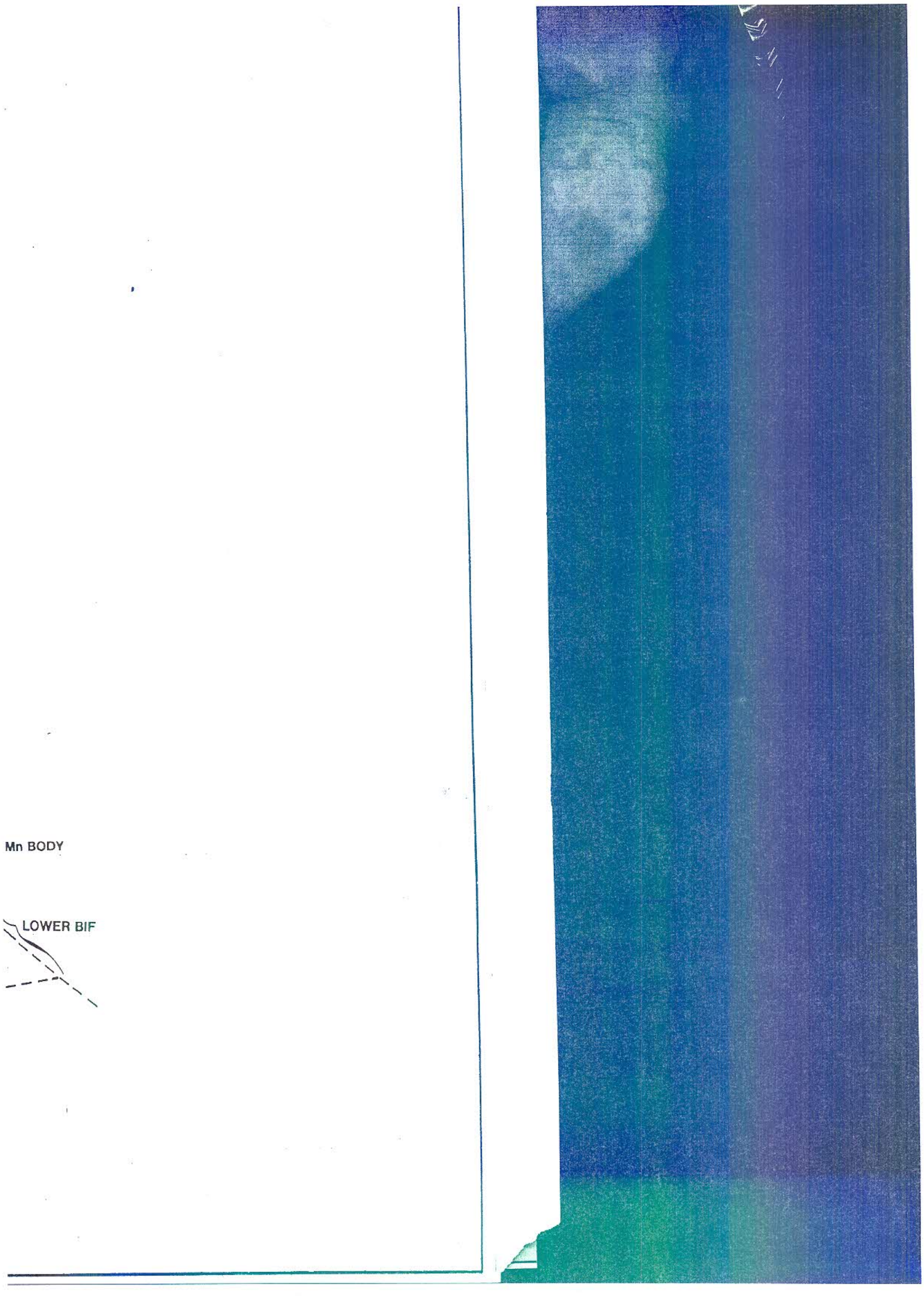
Mn BODY
LOWER BIF

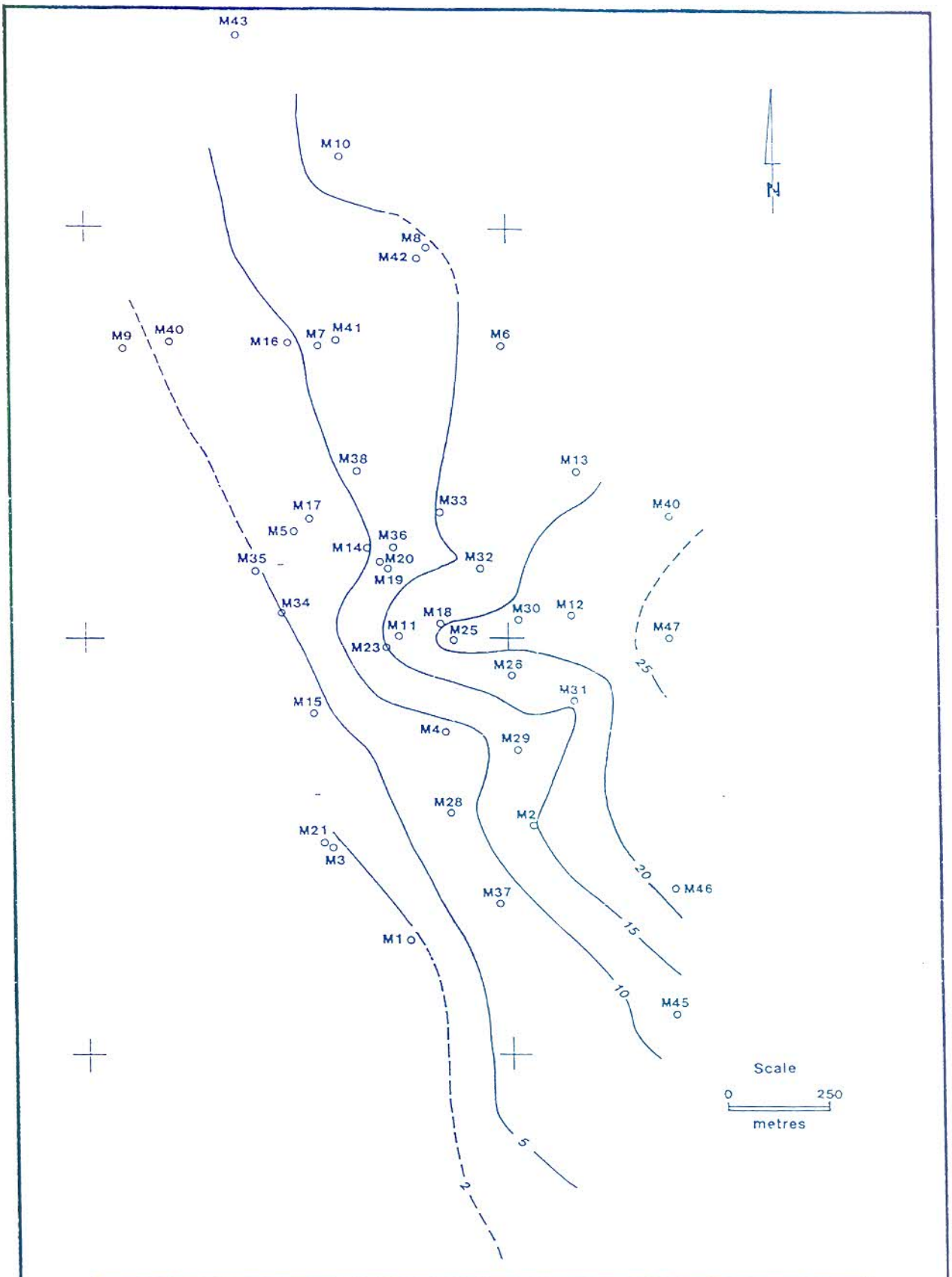

Fig. 7.19 Isopachs showing the thickness of the lower banded iron formation unit at Middleplaats (thickness in metres).

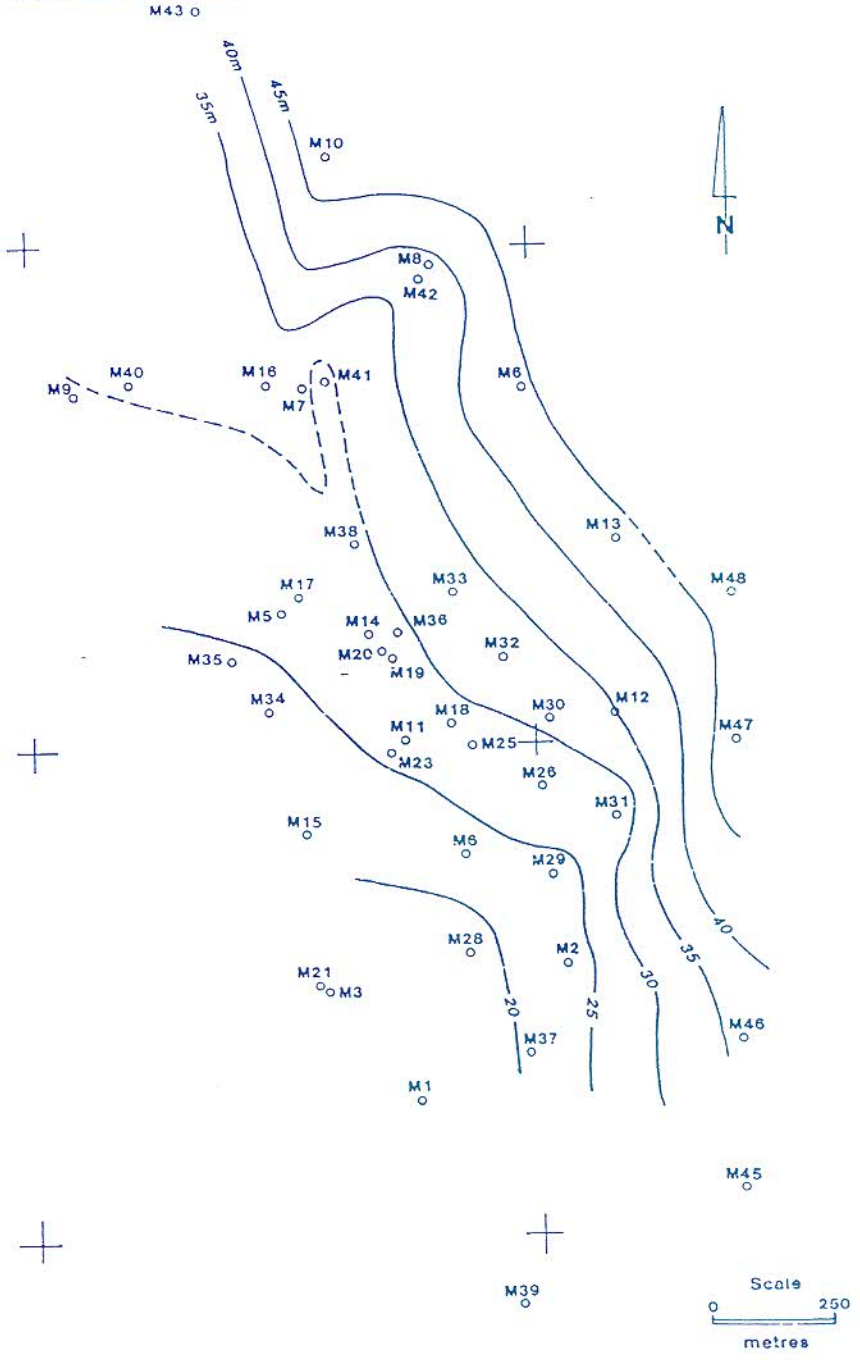

Fig. 7.20 Isopachs showing the thickness distribution of the middle banded iron formation unit at Middleplaats (thickness in metres).

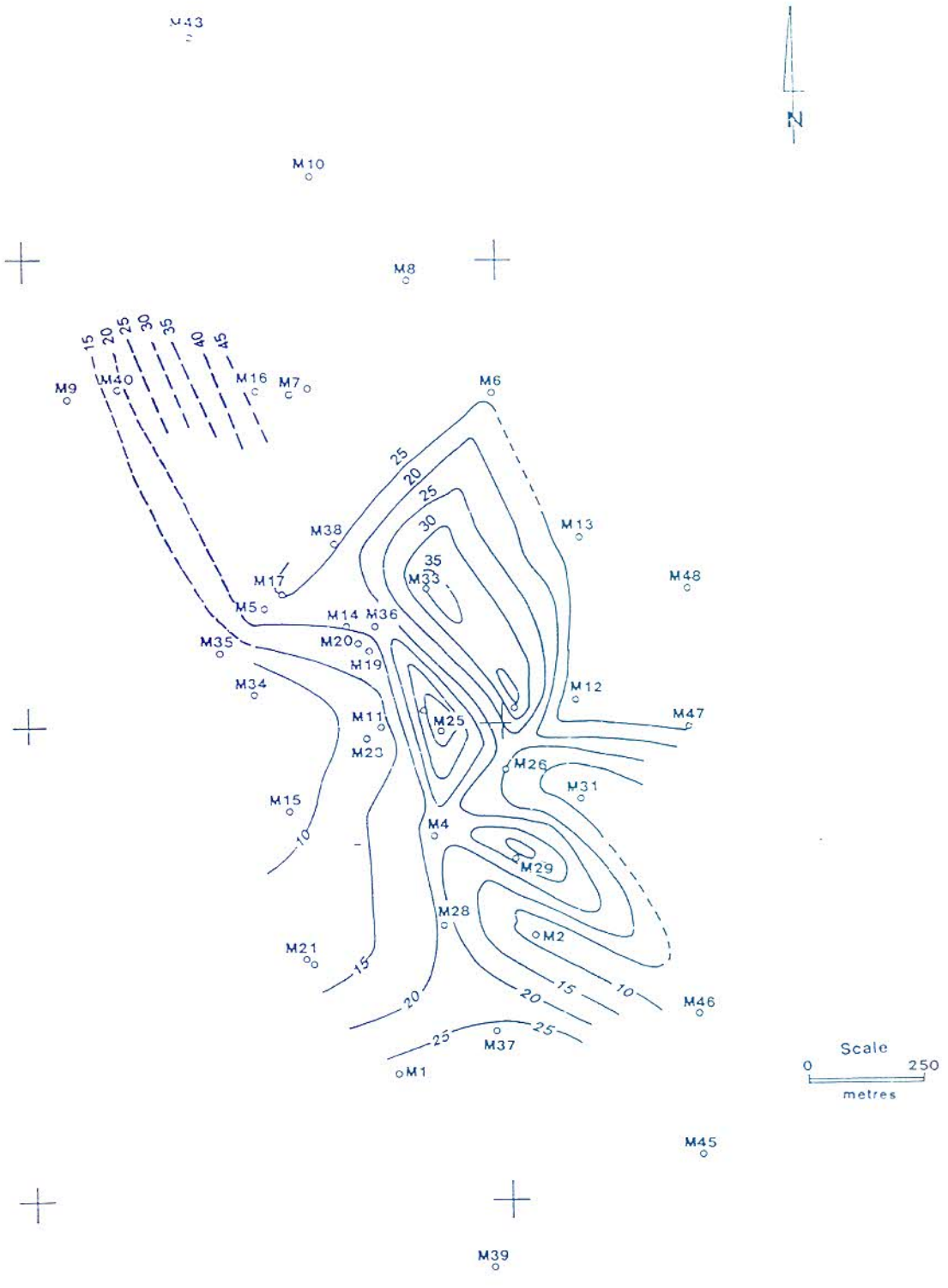

Fig. 7.21 Isopachs showing the thickness distribution of the upper banded iron formation unit at Middleplaats (thickness in metres).

7.2.2.2 Vertical Facies Variation

(a) Hematite-magnetite-carbonate facies (oxide facies)

This facies is confined to the Lower BIF Unit and comprises a magnetite-carbonate (ankerite) microbanded brick-red hematite-lutite containing vestiges of greenalite-magnetite-carbonate assemblages (Fig. 7.18 and Fig. 7.22). Contacts between the greenalite units and the oxide facies are gradational. Microbanding in the oxide facies is similar to that displayed by the greenalite-rich units. Hematite is fine-grained with a cryptocrystalline habit and imparts a brick-red colour to the rock.

Magnetite is present as coarse euhedral grains contained within 1-3mm thick laminae, often exhibiting a sieve-like texture. The magnetite laminae are generally concordant with the overall bedding but cross-cutting laminations are present in places. Ghost laminations of earlier magnetite can often be observed. Coarse euhedral carbonate, confined to 1-3mm thick grey-green microbands, is sometimes present, but the carbonates are mostly contained within very fine laminae. The carbonate in hand specimen is only detectable using acid.

The unaltered greenalite-rich units comprise greenalite-magnetite-carbonate microbanded rhythmites. The greenalite is fine-grained with a subhedral crystalline habit. These greenalite-rich horizons are not bound to the same stratigraphic horizon.

Euhedral to subhedral magnetite is present in microbands and disseminations in greenalite and carbonate. Euhedral to subhedral carbonates are contained within continuous and disrupted greenish coloured microbands.

The Lower BIF Unit is only developed within the basin in the area extending from Middleplaats to Mamatwan, onlapping onto the prominent palaeohigh west of Middleplaats (Fig 7.18).

(b) Greenalite-Magnetite-Carbonate Facies (Silicate Facies).

The facies is similar in all respects to the greenalite-magnetite-carbonate facies described in Section 7.1 (Epsom-Olivepan-Hotazel transect).

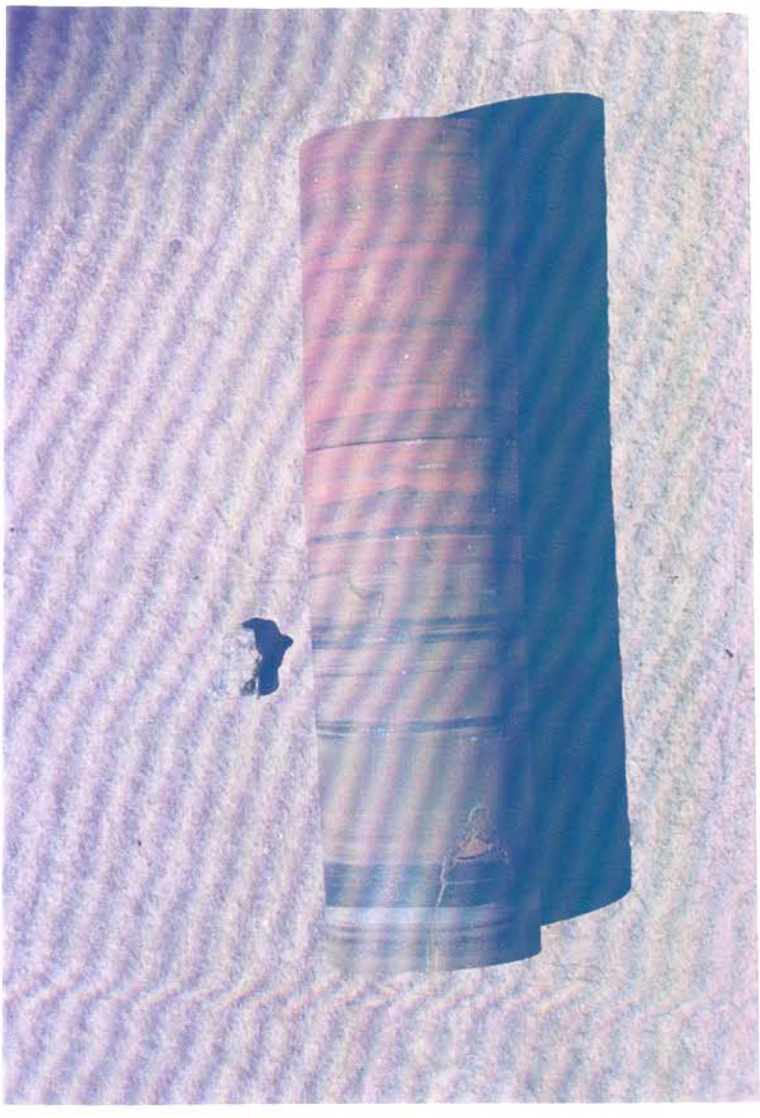

Fig. 7.22 *Borehole MA 191 - Red typical magnetite-carbonate microbanded hematite-lutite of the Lower BIF Unit - green/grey unaltered greenalite-magnetite-carbonate assemblage.*

The lower part (13-28m thick) of the Middle BIF Unit comprises evenly bedded micro- and mesobanded greenalite-magnetite-carbonate rhythmites and is subdivided into an upper and lower zone.

The upper zone (6-14m thick) is a light-green mesobanded unit. Magnetite is present mainly as coarse euhedral grains overgrowing greenalite and ankerite. Euhedral to subhedral carbonate occurs in green to brown coloured micro- and mesobands, often displaying a cross-cutting habit.

The lower zone (6-14m) is commonly dark-green to almost black in colour. Subhedral to euhederal magnetite is present predominantly in 1-3mm microbands which often exhibit a sieve-like texture. These magnetite microbands are generally parallel to the bedding. A stilpnomelane band-lutite (10-30cm thick) is present in most boreholes at Middleplaats and in some of the boreholes at Mamatwan. It is found 4-8m below the middle Mn body, roughly forming the boundary between the upper wavy bedded chert-rich unit and the lower greenalite-rich unit (Fig. 7.18).

Fine-grained to euhedral crystalline carbonates are mostly confined to fine microlaminae. The carbonate content decreases downwards while the magnetite content increases upwards.

(c) Greenalite/chert-Magnetite-Carbonate Facies (Silicate Facies).

This facies is found in the uppermost 4-8m of the Middle BIF Unit as well as in the Upper BIF Unit. Microcrystalline chert is contained within wavy disrupted mesobands, pillows and disc-lutites. The shallow water structures seem to increase in intensity towards the slope of the palaeohigh. The chert content gradually decreases from Middleplaats eastwards into the deeper basin and coincides with an increase in the greenalite content (boreholes M6, M12 and M13). In the Upper BIF Unit the magnetite content decreases as the slope of the palaeohigh is approached. At Mamatwan, however, wavy bedded chert

mesobands, chert discs and pillows alternating with magnetite and carbonate microbanded greenalite-rich rocks are present in the upper ±15m of the Middle BIF Unit.

Slumped carbonate layers are commonly interbedded within the top part of the upper sequence (Figs. 7.18 and 7.23). Magnetite is present as coarse euhedral grains in cross-cutting laminae and as disseminations in the carbonate slump layers and as overgrowths in the carbonate and greenalite micro- and mesobands. Carbonate occurs, in addition to the slumped layers, as coarse euhedral grains in cross-cutting laminae and as subhedral crystallites confined to micro- and mesobands.

7.2.2.3 Thickness Variation

(a) Lower BIF Unit (Middelplaats area)

An isopach map of the Lower BIF Unit in the Middleplaats area (Fig. 7.19) shows thickness ranging from zero in the west along the slopes of the palaeohigh, to 25m eastwards into the basin (Fig.7.19). East-west trough-shaped thickening in the central area might indicate an uneven floor palaeotopography or might be related to synsedimentary deepening of the basin. In the Mamatwan area in the east most of the boreholes were stopped short of the lava contact so that thicknesses of the interbeds are unknown.

(b) Middle BIF Unit (Middleplaats area)

The sequence, similar to the Lower BIF Unit, gradually thickens from zero metres in the west, where it onlaps on the volcanic palaeohigh, to 45m basinwards (Fig. 7.20).

In the Mamatwan, Rissik and Smart areas, the true thickness of the Middle BIF Unit is uncertain due to peneplanation by the Kalahari unconformity (Fig. 7.18). However, where preserved down dip, thicknesses range from 45m to 67m.

(c) Upper BIF Unit (Middleplaats area)

Isopach maps of the Upper BIF Unit display highly variable thicknesses. Rapid thinning of this unit towards the west suggests onlap onto the palaeohigh (Figs. 7.18 and 7.21).

7.2.2.4 Oolitic Oxide-Silicate-Carbonate Facies, West of the Palaeohigh

This facies is developed towards the west of the Middleplaats palaeohigh and was intersected in boreholes drilled on the farms Moffat and Smuts (Fig. 7.24).

It comprises massively bedded oolitic hematite-jaspilitic chert/carbonate mesobands. Grey coloured, wavy to planar bedded, coarse slumped carbonate microbands and mesobands are commonly interbeded with cryptalgal band lutites (Figs. 7.18 and 7.24).

Red-coloured jaspilitic meso- and microbands showing soft-sediment deformation are often contained within the slumped carbonate units. Replacement of carbonate laminae is also common.

Hematization, associated with stylolite structures, is present near the base of the sequence and commonly cuts across the carbonate bedding. The massive bedded hematite-carbonate units often display spherical and shard-like, peloidal-sized dolomite residues, suggesting hematization of a primary dolomitic precursor (Fig. 7.24). These units also display bright red, irregularly shaped hematite ovoids, arranged parallel or subparallel to the bedding, indicating diagenetic replacement of the dolomite residues (Fig. 7.24).

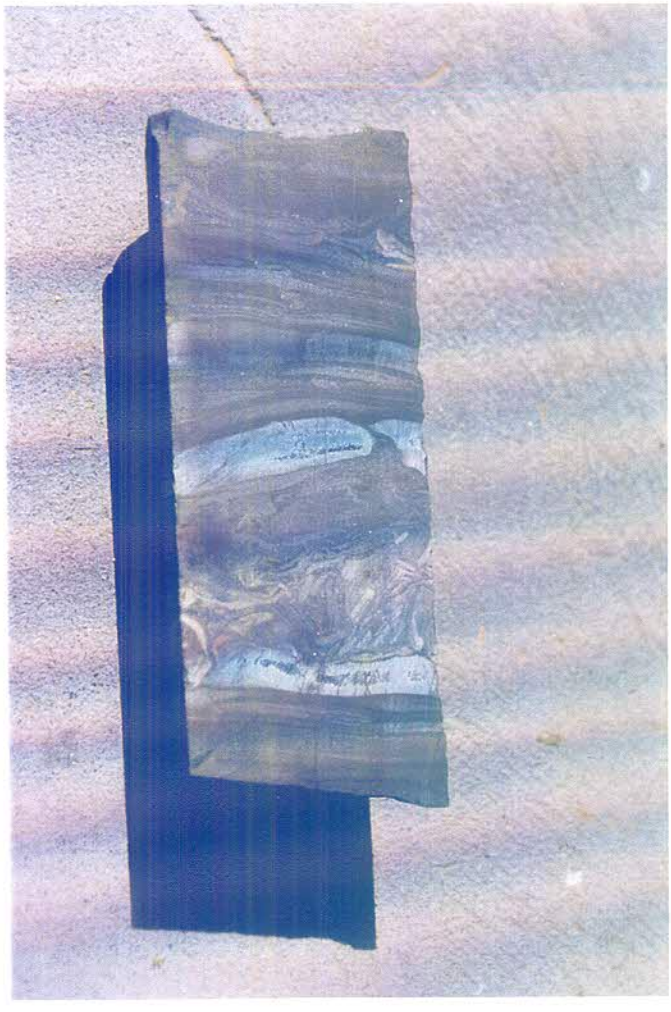

Fig. 7.23 *Borehole M10 - deformed carbonate slump layers interpreted as distal carbonate turbidite deposits.*

An oolitic manganiferous unit is generally present towards the base of the sequence, enveloped in massive bedded hematite-carbonate oolites. The sequence grades upward into crinkly chert, slumped carbonate and algal laminated band-lutites.

Fig. 7.24 *Oolitic facies BIF displaying shard and peloidal-like dolomite residues and irregularly shaped hematite ovoids. Borehole MFT 2.*

The carbonates within the laminae, slumped flow-layers and algal mats are coarse euhedral in texture with subhedral grains of carbonate disseminated within the hematite-jaspilitic chert lithologies. Coarse euhedral magnetite overgrowths and cross-cutting mesobands are closely associated with the coarse-textured carbonate units.

7.2.3 *Mamatwan-Botha-Gama-Olivepan-Transect*

7.2.3.1 Introduction

This transect roughly follows the eastern suboutcrop over a distance of 15km, extending from Mamatwan in the south to Olivepan in the north (Fig. 5.1). During Dwyka glaciation and Kalahari peneplanation, large thicknesses of the Hotazel iron formation were eroded so that core intersections, exposing the total stratigraphy close to the suboutcrop, are limited. Only 7 boreholes were examined along this transect.

The facies variation along this transect is very similar to that described along the Middleplaats-Mamatwan transect. Similar characteristics with respect to mineral assemblages, textures and sedimentary structures are displayed. Descriptions will therefore be brief, only summarising the more prominent features.

7.2.3.2. Vertical Facies Variation

(a) Hematite-Magnetite-Carbonate Facies (Oxide Facies)

This facies is confined to the Lower BIF Unit. It comprises magnetite and carbonate microbanded hematite-lutite. It is brick-red in colour and grades upwards into more massive bedded hematite at the base of the lower Mn body. Vestiges of greenalite-magnetite-carbonate microbanded rhythmites are present near the base of the succession, close to the lava contact. Transition of the greenalite-rich units into the hematite units is gradational. Hematization of the greenalite units is often patchy and erratic.

(b) Greenalite-Magnetite-Carbonate Facies (Silicate Facies)

This facies comprises well bedded magnetite-carbonate microbanded greenalite lutites of the Middle BIF Unit. The sequence shows a gradual colour change from light-green to dark-green with decreasing height in the stratigraphy. Mineral characteristics are similar to those along the Middleplaats-Mamatwan transect.

(c) Greenalite/chert-Magnetite-Carbonate Facies (Silicate Facies)

This facies is typical of the Upper BIF Unit along the Middleplaats-Mamatwan transect and comprises wavy bedded and disrupted micro - and mesobanded rhythmites. Greenalite and chert discs and pillows are prominent in borehole R67. Slumped carbonate layers are interbedded throughout. Northward (borehole B26), the lithology of the Upper BIF Unit comprises fairly evenly bedded greenalite-magnetite-carbonate mineral assemblages with minor interbedded thin carbonate slump layers. Imbricate chert clasts are present at the base. The Upper BIF Unit in B26 are overlain along a sharp contact by a Mooidraai Formation dolomite debris flow sequence, 4,1m thick. Mineral textures and occurrences are similar to those described for the Middleplaats-Mamatwan transect.

(d) Magnetite-Chert-Carbonate Facies (Oxide Facies)

The lithology of the Middle BIF Unit in borehole G4, comprises slightly wavy bedded magnetite-chert-carbonate rhythmites with minor amounts of greenalite. The prominent disrupted and deformed carbonate slumps interbedded in the Upper BIF Unit at Rissik, Mamatwan and Middleplaats, are rarely encountered in borehole G4.

7.3 Hematite-Lutites

The three mineralised bodies within the Kalahari basin, the lower, middle and upper Mn ore bodies are always enveloped by a brick-red hematite-lutite, regardless of the composition of the overlying or underlying banded iron formation facies.

The contacts between the banded iron formation and hematite-lutite are gradational often displaying wavy chert bands, billows pods and pillows at the contact, invariably over less than one meter. The hematite-lutite is essentially a mudstone consisting almost entirely of hematite micrite. Stringers, lenses and ooids of carbonate (kutnahorite and rhodochrosite) and silicates (talc, stilpnomelane, minnesotaite and bementite, the Mn equivalent of greenalite) impart a laminated appearance to the rock (Kleyenstüber, 1985). Texturally it often resembles the Mamatwan-type low-grade ores but can be quite massive when enveloping high-grade ores.

The hematite-lutite which envelopes the Mamatwan-type ore becomes darker as the manganese ore bodies are approached, and assumes a brownish purple hue signifying enrichment in manganese. A dark brown-coloured fine-grained lithotype consisting of jacobsite (manganese-bearing magnetite) marks the transition into the microcrystalline ooidal kutnahoritic braunite-lutite (low-grade ore).

The hematite-lutite which envelopes the high-grade Wessels-type ores tends to be massive. The jacobsitic transition zones at the hanging - and footwall contacts are only rarely developed.

The mineralogical composition of the hematite-lutite indicates a significant change in the chemistry of the depositional environment. The silica content of BIF decreases markedly on approaching the hematite-lutite. The quartz content is low

but can still be recognised under the microscope as a minor constituent in the carbonate matrix and ooids (Kleyenstüber, 1985). The hematite-lutite is enriched in carbonates and in manganese compared to the BIF units. Manganese is in the carbonate form either as rhodochrosite or kutnahorite.

Petrographic examination of certain hematite-lutite samples revealed the presence of tricuspate glass shards. Similar observations were made by Kleyenstüber (1985). Much of the glass was devitrified and altered to chlorite. Thin monomineralic layers of talc, a few millimetres in thickness, are present in places within the hematite-lutite and may represent altered volcanic ash.

7.4 The Manganese Ores

Kleyenstüber (1985) defined two major ore-types in the Kalahari manganese field, the Mamatwan- and the Wessels-types.

The **Mamatwan-type** represents a carbonate-bearing, quartz-free, manganese ore with a total manganese content ranging between 36 and 38%. It is the dominant ore-type in the Kalahari basin. The ore is dark brown to dull greyish-black in colour, compact and finely laminated, often distinctly banded and has a microcrystalline texture (Fig. 7.25). The fine-grained matrix (5µm) of the ore consists of braunite and carbonates. White and/or light-brown ellipsoidal carbonate ovoids, up to 2 mm in diameter, consisting of kutnahorite (Mn-dolomite) manganoan calcite and calcite, are found throughout the ore matrix (Fig. 7.25). White to pink carbonate lamellae and bands of similar composition are common, and accentuate the banding of the ore. The carbonate ooids are clearly diagenetic in origin and overprint the bedding lamination.

The Wessels-type manganese ore is massive, black and shiny (Fig. 7.26) and has an average Mn content of 46-48% Mn and a combined Mn + Fe content of about 60%. Ores with a vuggy appearance and a brecciated texture show signs of

recrystallisation and alteration. Mineralogically, the Wessels-type ore consists primarily of hausmanite and braunite II (a lower silica variety of braunite I). The known high-grade ores are restricted to the Epsom-Olivewood palaeohigh, the now defunct Hotazel open pit and the Wessels-Nchwaning area (Fig. 5.1).

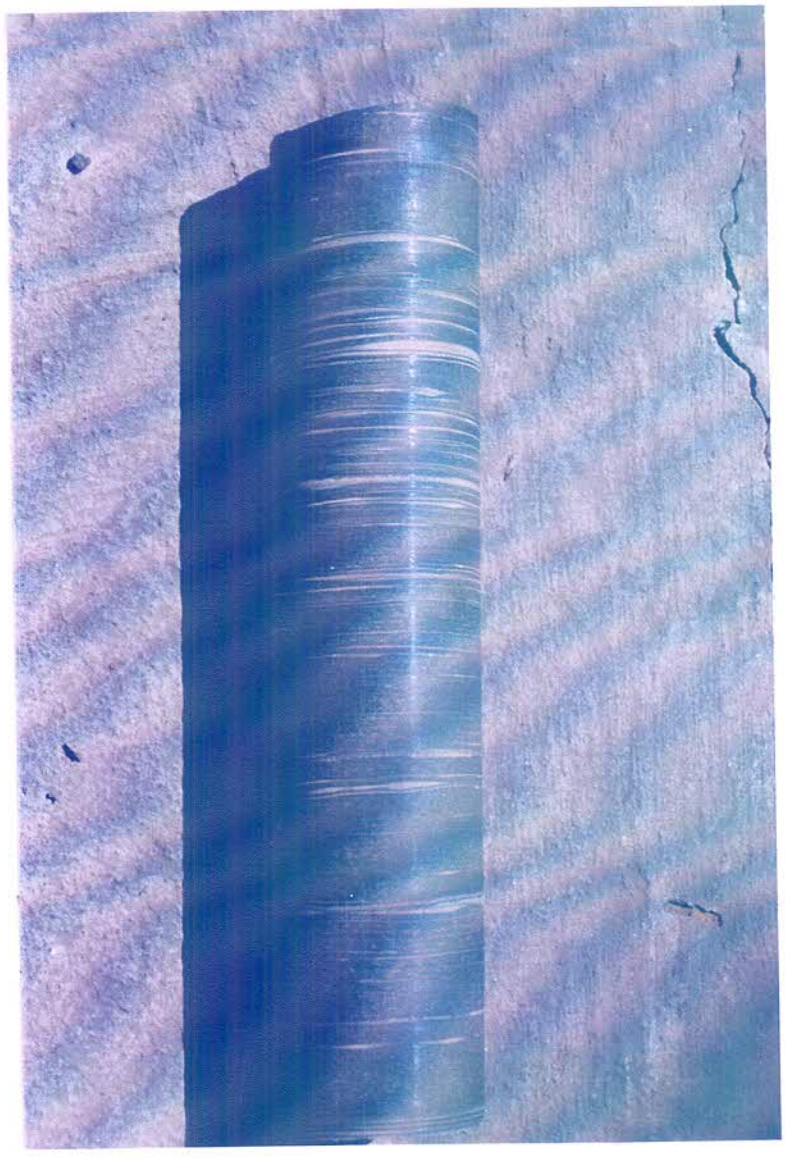

Fig. 7.25 *Typical Mamatwan-type ore. Borehole MA189.*

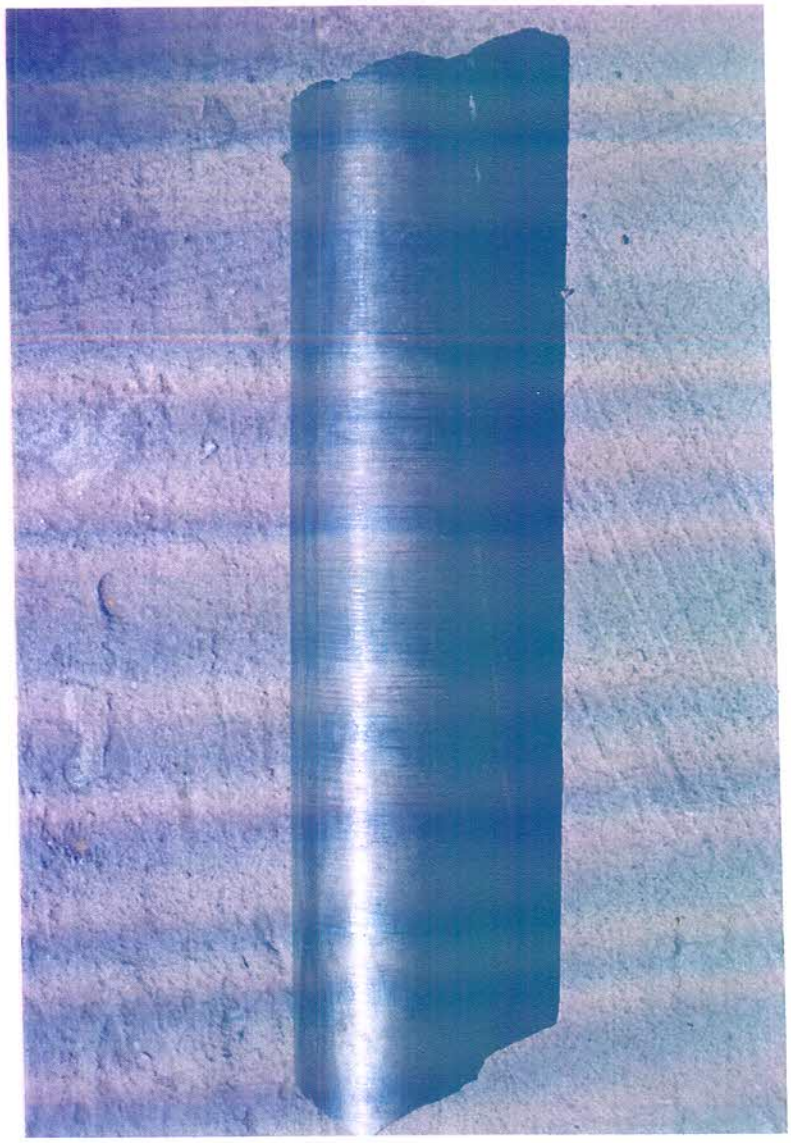

Fig. 7.26 *Wessels-type high-grade ore. Note character and shiny appearance.* Borehole HO 89.

The lower Mn ore body is the best developed, with a thickness which ranges from 40m at Mamatwan Mine to about 5m at Wessels (Fig5.1), approximately 35km towards the north of Mamatwan. The middle manganese body is not prominently developed and is on average only 2m thick (Fig. 7.18). The middle body is a hematite-lutite with a low manganese content, where it drapes over the Epsom-Olivewood palaeohigh.

The upper Mn ore body is consistently 5-6m thick. At Hotazel and Epsom/Olivewood, both the upper and lower bodies are of Wessels-type grades, whereas at Wessels/Nchwaning (Fig. 5.1) only the lower body is of high grade. The upper body in this area has a high metal content but is ferruginous in character.

The low-grade Mamatwan-type ores tend to be distinctly magnetic throughout, whereas the high-grade ores are only weakly magnetic. The high-grade manganese mineralisation at Hotazel is, however, extremely magnetic (Fig. 7.27).

7.5 The Ongeluk Lava

Compositionally, the Ongeluk lava can be classified as a tholeiitic basaltic andesite with subalkaline (low-K) affinities (Schutte, 1992). It is further subdivided, based on chemical alteration, into a regional- and Kalahari-type lava (Schutte, 1992). The petrographic and chemical characteristics of the alteration have been discussed in detail by Schutte (1992) and only the salient features are discussed here.

Regional Ongeluk Lava-type (Schutte, 1992)

Low-temperature (>150C) seafloor-type alteration was recognised within the Ongeluk lavas. The alteration is localised and is a result of the interaction of sea water with the basalt in small scale hydrothermal systems. Chemically, the alteration is characterised by the following:

(i) Pillow cores with high Na, Ca, and Mn and lower K, compared to rims, with highly variable K, high Na and Mg content and low Ca and Mn content.

(ii) Hyaloclastites exhibit a complete loss of Na and a moderate depletion of CaO, MnO and TiO_2. SiO_2 and Al_2O_3 contents are unaffected but the lavas are greatly enriched in K_2O and show increased Fe and Mn values.

(iii) The chilled margins of massive flows are altered in a similar fashion to the hyaloclastites, being enriched in K and depleted in Na.

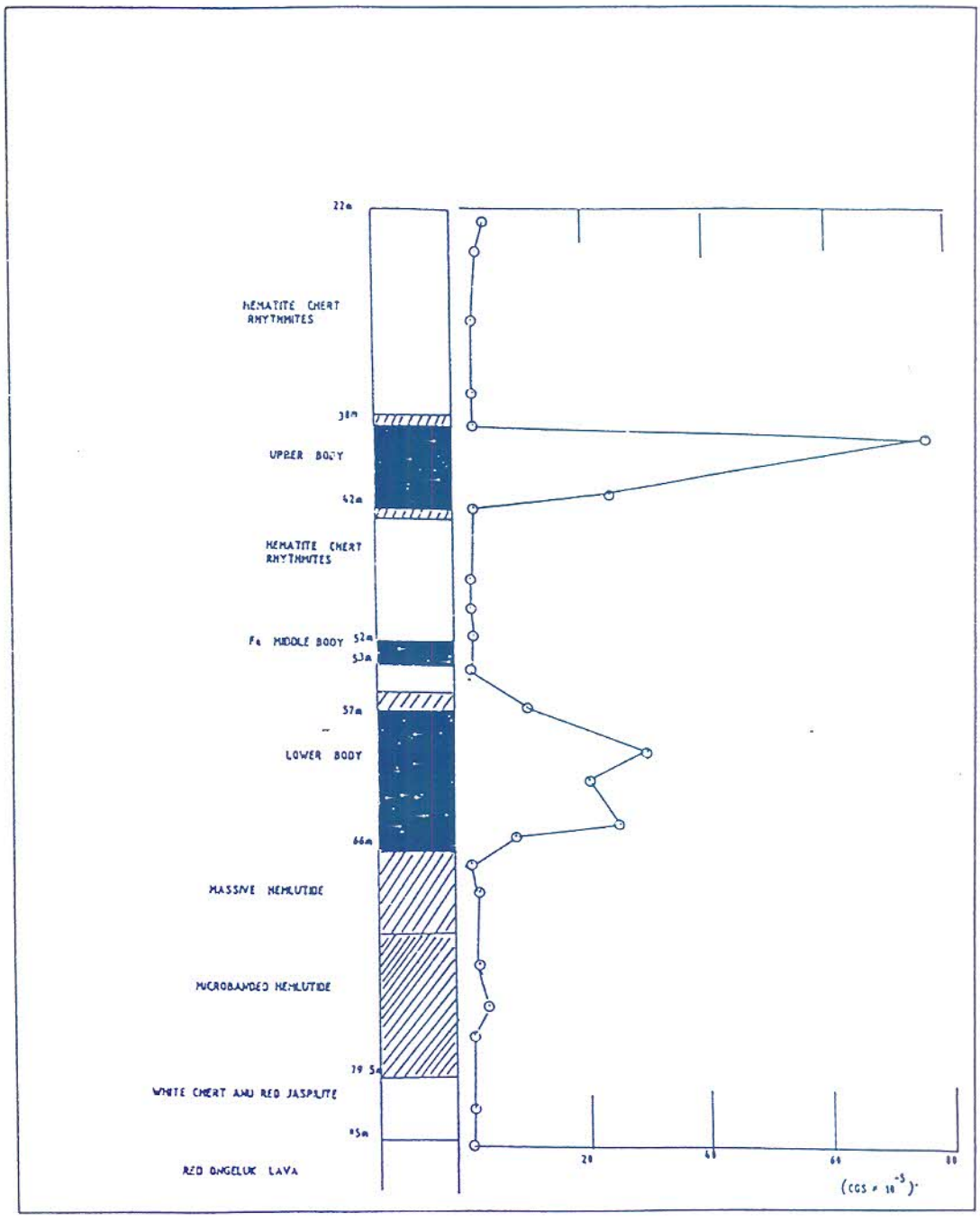

Fig. 7.27 *Magnetic susceptibility in borehole HO 89 at Hotazel.*

Kalahari-type Ongeluk Lava (Schutte, 1992)

The Kalahari-type Ongeluk lava underlies the Hotazel iron formation and is more pervasively altered. The alteration profile extends up to 150m downwards into the lavas. Macroscopically, alteration was essentially a process of hematization, with disseminated goethite and hematite which impart a characteristic maroon colour to the lava. The hematitic lavas grade irregularly downwards into greenish grey lavas, texturally identical to the regional Ongeluk lavas, which may contain hematite in veinlets rather than as disseminations. These veinlets cut across original primary structures such as pillows and flow-tops. Secondary magnetite replaces hematite with depth, while epidote may be present in places. The lava may also contain minor amounts of pyrite with depth, lining veins or vugs. The contact between the hematitic lavas and unaltered lavas is gradational and the hematized lavas at the top of the pile may grade downwards into normal greenish-grey lavas and then back to reddish lavas again.

Although the alteration profile can extend up to 150m downwards into the lavas, the most profound alteration (iron and potassium enrichment and Ca depletion) occurs right at the top of the lavas, below the BIF. Cornell and Schutte (1995) show that the highly altered Kalahari Ongeluk lava is similar to that observed at the Deep Sea Drilling Project on the Mid-Atlantic ridge hydrothermal system.

8 DIAGENETIC MODIFICATION OF THE HOTAZEL IRON FORMATION

8.1 Introduction

The precursor material of iron formations is regarded as a complex chemical precipitate containing iron hydroxide, iron-silicates and carbonates (Goodwin, 1956; James, 1966; Trendall and Blockley, 1970; Dimroth and Chauvel, 1973).

Through diagenetic processes operating close to the sediment-water interface, the unconsolidated material was converted into solid rock. Mechanisms include compaction and water expulsion from the sediment, crystallisation of the original gels and solution and precipitation of the minerals at relatively low temperatures, normally less than 100°C (French, 1973).

Researchers have concluded, based on petrographic and textural studies of the minerals making up iron formation, that chert, siderite, hematite, greenalite and possibly some magnetite represent the most primitive mineral assemblages (James, 1954 and 1966: Goodwin, 1956; Edwards, 1958; La Berge, 1964; Curtis and Spears, 1968; French, 1973). On the other hand, some of the magnetite, if not all, as well as minnesotaite, stilpnomelane, specularite, riebeckite and talc are secondary diagenetic or low-grade metamorphic products (French, 1968; Dimroth and Chauvel, 1973).

8.2 Primary iron minerals; possible candidates

There are three primary or very early diagenetic phases within the Hotazel iron formation: hematite, greenalite and iron-carbonate. It may also be possible that some of the very fine-grained magnetite flanking the Epsom-Olivewood palaeohigh is primary in origin, but the bulk of the magnetite is clearly diagenetic. The textural characteristics of the hematite in the Hotazel iron

formation suggest that it represents a primary or at the very least an early diagenetic phase, occurring as fine-grained dust and ooids in the hematite-lutite unit (Kleyenstüber, 1985). The ooids are extremely fine-grained, ranging between 5 and 10μm in diameter, and exhibit no signs of recrystallization. No evidence indicative of hematite forming at the expense of siderite was recognised (Kleyenstüber, 1985).

Greenalite is the least altered mineral and primary textures are well preserved. It is commonly microcrystalline, and may occur in fine laminations, oolites, granules and small irregular masses (Tsikos, 1994). Macroscopically, the rock is finely laminated, with a slaty appearance.

Many of the carbonate layers in the Upper BIF Unit must have been primary or a very early diagenetic phase, because they define penecontemporaneous slump folds.

8.3 Secondary Iron Mineral Phases

8.3.1 *Hematite in the Lower Iron Formation Unit*

The Lower BIF Unit in the southern part of the basin (Middleplaats and Mamatwan) as well as along the suboutcrop on Rissik and Botha (Fig. 5.1) contains zones of silicate facies (greenalite-magnetite-carbonate) iron formation within the oxide facies (hematite-magnetite-carbonate) iron formation (Fig. 7.22). The dark green greenalite-magnetite-carbonate rocks grade gradually into the hem-lutites. The silicate facies remnants (Fig. 7.22) are generally less than 2m thick and are preserved at different stratigraphic levels. This facies is texturally indistinguishable from the generally well laminated oxide facies banded iron formation. The overall effect appears to be similar to the irregular diagenetic reddening seen in many red and green shale sequences, and is presumably the

result of the oxidation of greenalite to a hematite dominated assemblage. The oxidation of the Lower BIF Unit may be related to early diagenesis or to oxidation at a later stage.

8.3.2 *Specularite in the Oxide Facies Iron Formation.*

Some of the hematite in the Hotazel banded iron formation was converted to specularite. This alteration could be diagenetic in origin, possibly due to compaction of the sequence (Kleyenstüber, 1985; Dimroth, 1979a), but could also be the result of ferruginization related to later extensional faults.

8.3.3 *Formation of Magnetite.*

Magnetite in the Hotazel iron formation typically occurs in well-defined continuous or lenticular mesobands and laminae, and as disseminations or irregular clusters and patches. It is almost always coarse- to medium-grained, well-crystallised and has a subhedral to euhedral habit. It is commonly much coarser than the chert, hematite and iron silicates, often having a grain size similar to that of the recrystallized carbonates. Much of the magnetite overprints the bedding lamination and it is clearly diagenetic in origin (Fig. 7.15).

The origin of magnetite in unmetamorphosed Archaean or Proterozoic banded iron formations is a much debated subject. Some proposed mechanisms are as follows:

(i) James (1954) regarded both hematite and magnetite to be primary precipitates within the iron formations of the Lake Superior region.

(ii) Some authors consider it to be a diagenetic recrystallization or reaction product of a primary precipitate (Gross, 1973; Dimroth and Chauvel,

1973; Klein, 1974 and 1983; Klein and Bricker, 1977). Two minerals commonly quoted as precursors for the magnetite are hydromagnetite ($Fe_3O_4\ nH_2O$) or mixtures of iron hydroxides ($Fe(OH)_3$ and $Fe(OH)_2$).

(iii) Others interpret the magnetite to have formed by the oxidation of iron-silicates (e.g. greenalite) and carbonates (e.g. siderite), or by the reduction of earlier ferric hydroxides (La Berge, 1964; French, 1968 and 1973; Han, 1972). Fockema (1967) and Beukes (1978 and 1980) regarded the magnetite from the Asbesheuwels Subgroup to be the product of recrystallization of earlier iron-bearing minerals.

Kleyenstüber (1985) recognised similar reactions to those outlined in (iii) in the Hotazel iron formation. Coarse euhedral to subhedral magnetite crystals occur as an overprint in the fine dusty hematite matrix of certain hematite-lutite samples. Kleyenstüber (1985) suggested that the magnetite formed as a result of the localised reduction of hematite during recrystallization, according to the reaction:

$$2Fe_2O_3 = 2Fe_3O_4 + {}^1/_2\,O_2$$

Hematite = magnetite + oxygen

Kleyenstüber (1985) also found indications that magnetite formed in small quantities in the hematite-lutite due to the oxidation of siderite replacing large carbonate rhombs, according to the reaction:

$$3FeCO_3 + {}^1/_2\,O_2 = Fe_3O_4 + 3CO_2$$

siderite + oxygen = magnetite + carbon dioxide

Magnetite is absent from the chert-hematite lithologies which cap the Epsom-Olivewood palaeohigh as well as from the chert-hematite succession in the vicinity of Wessels Mine (Fig. 5.1). Magnetite is present only where carbonate minerals form a significant part of the succession and therefore, diagenetic oxidation of siderite may have been an important mechanism regionally in the formation of the magnetite. In the Middle BIF Unit (greenalite-rich facies), the carbonate levels increase upwards in the stratigraphy whilst the magnetite increases downwards. The magnetite is clearly cross-cutting and disseminated, and may have formed at the expense of Fe-carbonate. Ankerite is the most common carbonate mineral and could have formed via the oxidation of Ca-Mg siderite or ferroan dolomite, according to the reaction (French, 1973):

Ca-Mg siderite + O_2 = magnetite + ankerite + H_2O.

This reaction takes place under chlorite-grade metamorphic conditions, at temperatures between 200°C and 300°C and pressures of between 2 - 3 kbar (French, 1973).

Magnetite can also form at the expense of greenalite (French, 1973), according to the reactions:

greenalite + O_2 = magnetite + quartz + H_2O

greenalite + O_2 = magnetite + minnesotaite + H_2O

The reactions take place in the field of low-grade metamorphism at temperatures of 200°C-350°C and at pressures of 2-3 kbar (French, 1973). Tsikos (1994) reported minnesotaite as a common replacement product in the Voëlwater BIF, in boreholes on the farm Rissik, in greenalite-magnetite-carbonate facies iron formation.

8.3.4 *Recrystallization of Carbonates*

Tsikos (1994) concluded that coarse-grained ankerite is the most abundant carbonate mineral in the carbonate-rich assemblages of the Hotazel iron formation. Klein and Beukes (1989) suggested that the siderite in the Asbesheuwel BIF was a primary precipitate but concluded that ankerite is commonly euhedral and appears to be of later diagenetic origin.

8.3.5 *Iron-Silicates.*

Bright-blue riebeckite is common in certain portions of the Upper BIF Unit on Olivepan (Fig. 7.17). It forms fibrous subhedral aggregates overprinting everything else and is clearly diagenetic in origin. Contacts between the riebeckitic iron formation and the surrounding rocks are gradational. Riebeckite indicates the presence of highly saline or evaporative conditions within a partly or completely enclosed depositional basin, as has been suggested for the Asbesheuwels riebeckites by Cilliers (1961), Hanekom (1966) and Beukes (1973 and 1978). Riebeckite can form by crystallisation of the saline pore fluid during diagenesis, or by sodium being leached from a sodium-silicate precursor, which then reacts with the iron-bearing amphiboles to form Na-Fe riebeckite (Eugster, 1969; Eugster and Chou, 1973). The source of the sodium has been regarded by Beukes (1983) as being fumarolic. Magnetite is generally present in the immediate surrounding of the riebeckitic layers but is not present within the layers, suggesting that it has been replaced during the formation of riebeckite.

8.4 Summary

It is evident that the Hotazel iron formation exhibits similarities in its overall diagenetic history to banded iron formations, elsewhere, in that :

i) There is evidence for three primary or early diagenetic mineral phases, i.e.: hematite, greenalite and iron carbonate.

ii) Some of the magnetite is clearly secondary

Three broad types of mineral assemblage were recognised in the Hotazel iron formation, similar to those described by French(1973) and Dimroth and Chauvel (1973) from other iron formation sequences elsewhere in the world, i.e.:

i) An early diagenetic or primary assemblage (<100 bar, <100°C) comprising hematite, chert, greenalite some carbonate and possibly a small amount of magnetite.

ii) A late diagenetic assemblage (1-2 Kb; 150-200°C) characterised by the formation of magnetite and ankerite.

iii) A low-grade (burial) metamorphic event (2-5 Kb and 200-350°C) resulting in the formation of minnesotaite, stilpnomelane, riebeckite, chlorite and talc.

9 PALAEOENVIRONMENTAL SYNTHESIS OF THE DEPOSITION OF THE HOTAZEL IRON FORMATION

9.1 Chemical and Physical Environment During BIF Precipitation

9.1.1 The Epsom Olivewood Transect

Lateral and vertical facies changes in the banded iron formation along the Epsom-Olivewood transect are defined by textural as well as mineralogical (chemical) changes. These facies changes are the product of fluctuations in water depth, oxidation-reduction potential (Eh) and pH changes in the depository.

In the Lower and Middle BIF Units, disrupted and wavy bedding, cross-laminations as well as the presence of chert waves, billows, pods and pillows within the chert-hematite facies, on and immediately flanking the palaeohigh, suggest the influence of wave action in fairly shallow water. These structures probably represent chert-hardgrounds which were broken up during periods of wave and storm activity. It is difficult to ascertain the exact water depth because the influence of waves can extend down to depths of up to 100m during periods of excessive storm activity (Gross, 1973).

In the Upper BIF Unit, evenly microbanded hematite-chert rhythmites grade upward into peloidal and clastic textured hematite-chert bandlutites. Upwards in the sequence the chert bands also get thicker and chert waves and pillows may be developed, as in borehole EP2. This would indicate an overall shallowing of the basin. In contrast to the above, no shallow water structures were recognised in either the magnetite-chert-carbonate or greenalite-magnetite-carbonate associations in the Upper BIF Unit.

Away from the palaeohigh the banded iron formation, in the lower, middle and upper units, comprises evenly and finely laminated rhythmites, interpreted as deeper water deposits below the wave base.

Shallow water structures are present in the banded iron formations immediately above and below the manganese horizons throughout the basin, which indicate a general shallowing of the depositional environment prior to the deposition of the manganese.

Depending on the oxidation-reduction potential (Eh), iron may be precipitated in either the ferric state, as an oxide, or in the ferrous state, as a silicate, carbonate or sulphide. The chemical history of the depositional environments is thus locked up in these rocks.

The lateral facies variation from hematite-chert facies on the axis of the palaeohigh, grading basinward into hematite-chert-carbonate facies and then into greenalite-magnetite-carbonate facies, indicates that the water column in the depository was stratified with respect to Eh and pH. The different iron mineral phases were therefore deposited at different levels with respect to a chemocline. Above the chemocline, in the aerobic zone, the more oxidising conditions favoured the deposition of hematite and magnetite, whilst below, in the dysaerobic zone, less oxidising and more alkaline conditions favoured the deposition of greenalite and carbonate.

Chert-rich lithologies are preferentially associated with the hematite and magnetite-rich iron formations occurring on the Epsom-Olivewood palaeohigh and its immediate flanks. Chert is relatively soluble in alkaline conditions but insoluble in acidic conditions, as explained in chapter 6.

It is now generally accepted that the Precambrian atmosphere was richer in CO_2 than that of the present day (Schidlowski, 1987). A dilute acid, HCO_3-, is formed when CO_2 combines with rainwater and may have caused the near surface waters being more acidic. Silica was probably concentrated by evaporative mechanisms, resulting in the deposition of chert when the pH was lowered during abnormal influxes of more oxygenated, fresher, near surface water into the depositional basin (Klein and Beukes, 1989; Morris, 1993).

Indications are that the depository became more oxidising over a much wider area during the deposition of the Upper BIF Unit. The hematite-chert facies within the Upper BIF Unit is laterally far more extensive away from the Epsom-Olivewood palaeohigh than its lower counterparts, and extend from OLW3 in the east to EP2 in the west (Figure 7.1).

Vertical facies changes were observed in several boreholes. In OLW3, for example, the succession starts with evenly and finely laminated deep water greenalite-magnetite-carbonate rhythmites at the base of the Upper BIF Unit,

and grades into magnetite-chert-carbonate facies and upwards into hematite-chert-carbonate associations, indicating progressive shallowing and change in redox potential.

Klein and Bricker (1977) produced stability diagrams indicating equilibrium assemblages very similar to those observed in the Hotazel iron formation. They concluded that ankerite commonly occurs with hematite in the more oxidised, oxide-carbonate facies. Siderite does not form with hematite in nature due to the high PCO_2 required for its formation. They concluded also that the greenalite stability field is always separated from the $Fe(OH)_3$ field by the presence of magnetite.

Riebeckite-rich facies (OLP 2) and a carbonate-rich facies (OLP 7) are present to the east of borehole OLW 3. These facies contain graded sandy layers which pass upwards into finer lutite layers with alternating deformed carbonate layers. These sediments exhibit cross-lamination, rip-up clasts, convolute lamination and evidence of soft sediment slumping, and are interpreted as truncated Bouma sequences typical of distal fine-grained turbidites. The riebeckite mineralization in OLP 2 and OLP 7 is clearly diagenetic and is interpreted as representing the product of crystallisation of a sodic brine or saline fluid, generated in the originally alkaline conditions, within the sediment pore space. Alternatively, sodium could be concentrated in shallow water by evaporation, contemporaneous with the precipitation of carbonates over the Epsom palaeohigh. Continuous evaporation generated intensely saline conditions. Mixing of groundwater with the brines and a steep gradient, allowed seepage towards the central part of the basin (OLP 2 area).

Eastwards along the transect, shallow water conditions are suggested by the dominance of wavy bedded chert-magnetite-carbonate rhythmites over greenalite within the Middle BIF Unit (borehole G4). The iron formation partings between the manganese horizons are also thinner, suggesting shallow water hematite-chert facies further to the east (Hotazel outlier). The hematite-chert facies in the Hotazel outlier are similar to those from Epsom-Olivewood, although the manganese bodies are much thicker.

The banded iron formation sequence along this traverse closely resembles that in the model proposed by James (1954) for the deposition of iron formations.

9.1.2 The Moffat-Middleplaats-Mamatwan transect

The Lower BIF Unit shows no lateral or vertical facies variation along this transect and the characteristics were discussed in chapter 7. The lower 13-28m of the Middle BIF Unit is generally an extremely well laminated silicate facies (greenalite-magnetite-carbonate) which probably was deposited below the wave base in an alkaline environment below the chemocline.

The mineral association towards the top of the Middle BIF Unit and in the Upper BIF Unit is distinctly different to that along the Epsom-Olivewood transect. Boreholes situated close to the Middleplaats palaeohigh exhibit a build-up of chert in association with greenalite in all the iron formations above the middle Mn body. The chert is often jaspilitic in composition and invariably shows wavy bedding. The magnetite content in the Upper BIF Unit also decreases markedly on approaching the palaeohigh. These mineralogical and textural features suggest a shallower, more anoxic and slightly acidic depositional environment adjacent to the Middleplaats palaeohigh. However, it cannot be ruled out that diagenetic alteration of greenalite to form chert and ankerite rather than magnetite and ankerite may have been important.

The absence of primary hematite oxide facies, the presence of abundant chert within the greenalite Upper BIF Unit and the decrease in magnetite on approaching the Middleplaats palaeohigh are anomalous, but could be explained by one or more of the following:

(i) The palaeohigh west of the Middleplaats mine probably was a prominent feature with considerable relief as indicated by the progressive onlap of the different BIF and the abundance of turbiditic carbonate layers in the Upper BIF Unit. Thick hyaloclastites underlying the Hotazel iron formation are interpreted as gravity flows down the slopes of the palaeohigh. It is therefore possible that the bulk of the Hotazel iron formation was deposited in dysaerobic conditions beneath the chemocline.

(ii) Above the middle Mn body, the carbonate content increases upward in the sequence. Deformed carbonate bands are interpreted as gravity flow-layers suggesting a carbonate reefal complex over the Middleplaats palaeohigh. This is also supported by the gradational transition from BIF to dolomite at the Hotazel-Mooidraai Formation contact. (Fig. 10.6).

Carbonate buildups are known to be extremely fast (Schlager, 1981) so that at the time of deposition of the Upper BIF Unit, steep prograding unstable depositional slopes could have triggered gravity flows into the deeper basin, explaining the carbonate flow-features in the Upper BIF Unit. A thin layer of ferruginous oolite and carbonate-rich material between the Mooidraai dolomite and the Ongeluk lava (Fig. 7.18) is interpreted as ferruginised dolomite suggesting that the Mooidraai dolomite was deposited on the palaeohigh contemporaneous with the deposition of the Hotazel iron formation in the basin.

The high organic carbon supply in the vicinity of the reef depressed the oxygen levels and resulted in a less oxic environment, thereby preventing the precipitation of hematite in the basin and also of magnetite closer to the palaeohigh.

(iii) A volcanic ash band (stilpnomelane layer) within the Middle BIF Unit in the Middleplaats-Mamatwan area suggests the presence of an effusive centre in this area, also during the development of the Ongeluk lava volcanic belt. Reactive components of the ash changed the chemistry of the water. In addition, the oxidative capacity of sunlight to precipitate iron oxide was modified by the consequent turbidity, in both the atmosphere and in the water, causing more reduced and acidic conditions in the vicinity of the palaeohigh.

In a discussion of Algoma-type iron formations, Goodwin (1973) and Gross (1965) concluded that reduced iron formation facies are common in the vent area while oxide facies, forming thicker and more extensive units, occur distal to the extrusive centres. Fumarolic activity (assisted by evaporitic concentration) may have caused the waters in the vicinity of the palaeohigh to become supersaturated in silica.

The features of the Hotazel iron formation along the northerly directed traverse from Rissik to Gama (Fig. 5.1) are similar to those of the Moffat-Middleplaats-Mamatwan traverse, except that the entire Middle BIF Unit comprises evenly and well laminated rhythmites, in contrast to the presence of wavy bedded chert bands in the upper part of this unit along the latter traverse. The stilpnomelane band also pinches out in a northerly direction towards Botha and Gama. The facies preserved in this third transect indicate deposition under tranquil

conditions below the chemocline. However, the mineralogy in borehole G4, namely chert-magnetite-carbonate, is indicative of a more oxygenated and acidic environment, possibly more distal to an effusive centre. The drastic thinning of the Middle BIF Unit from approximately 70m in borehole R67 to approximately 4m in borehole G4 on the farm Gama, suggests deposition on the flank of a palaeohigh.

9.2 Chemical and Physical Environment During the Precipitation of the Hematite-lutite and Associated Manganese Units.

The manganese mineralization of the upper and lower bodies as well as the associated enveloping hematite-lutite form "blanket-like" deposits which cover the entire basin regardless of the character of the underlying or overlying BIF. In this regard it is similar to the manganese mineralization developed in many of the so called "manganese giants of the world" (e.g. Nikopol and Groote Eyland) where the mineralised zone forms a transgressive layer capping a sequence of clastics. These clastics generally show a lateral facies change from a near-shore or shoreline facies to a deeper water shelf facies (Roy, 1981).

The hematite-lutite demarcates a number of profound chemical and water depth changes that periodically affected the entire basin. It marks a more oxidised depositional environment throughout the basin with hematite as the primary mineralogical phase. This was most likely the result of basin-wide shallowing which is supported by the ubiquitous development of a thin zone of chert-rich iron formation at the interface between the hematite lutite and the BIF's. The chert is in the form of thin laminae, waves, billows, pillows and pods. The hematite lutite, according to Kleyenstüber (1985), marks a change in the pH of the environment with the first appearance of carbonate, typically as wisps and ellipsoids, in rocks where carbonate is absent from the underlying or overlying BIFs (hematite-chert facies). In addition, there is very little silica in the hematite lutite, indicating that the environment had become more alkaline. The hematite lutite also marks the first appearance of significant manganese mineralization in the form of carbonate.

As conditions became more oxidising and alkaline, the less mobile iron started to precipitate as hematite. The solution became progressively more depleted in iron and saturated in manganese, eventually resulting in the precipitation of manganese as Eh and pH conditions rose. The water chemistry controlled the

deposition of the interbedded manganese facies in a way similar to the manner in which the BIF facies were affected. Manganese oxide (silica- and carbonate-poor), hausmanite and braunite II were present within hematite-chert oxide facies iron formation and braunite I (silica and carbonate-rich) manganese units were interbedded within the silicate facies iron formation. Deposition of manganese was followed by a transgressive phase causing the environment to become progressively deeper, less oxygenated and less alkaline, precipitating the next influx of iron as hematite, grading into the next BIF unit. This cycle was repeated three times, as is evident from the stratigraphic column.

Altered glass shards in certain hematite-lutite samples from just below the lower Mn body (Kleyenstüber, 1985), the blanket-type geometry and the presence of talc layers within the hematitelutites, suggest a strong volcanogenic origin. The volcanism probably caused abrupt basin-wide chemical changes during the precipitation of the hematite-lutites.

9.3 Palaeoenvironmental Synthesis

The Lower and Middle BIF Units are characterised by two broad facies types, i.e.:

(i) A thinner shallow water oxide facies which is found draping over intrabasinal highs in the north-western portions of the basin, from Epsom-Olivewood through Wessels and Nchwaning to Hotazel, and

(ii) A thicker silicate facies was deposited below the wave base at a depth in excess of 100m in quiet tranquil conditions and below a chemocline in alkaline conditions.

A thick succession of carbonate facies banded iron formation was deposited during Upper BIF Unit times, as distal turbidite flows along the basinal slopes in the southern, south-eastern and eastern parts of the basin. At the same time, deep water rhythmites were still being deposited under alkaline conditions in the depocentre (Umtu 17 area, Fig. 7.1) while shallow water oxide facies iron formation was deposited over a much wider area in the northern parts of the basin. Conditions were highly saline close to the depocentre which resulted in the deposition of riebeckite in the OLP 2-OLP 7 area on Olivepan.

9.4 Character of the Depository

The tholeiitic Ongeluk lavas were erupted onto continental crust undergoing subsidence (Schutte, 1992), probably during a period of extensional thinning accompanied by high-angle faulting.

The basin floor was characterised by large-scale undulations such as the prominent palaeohigh at Middleplaats and by an intrabasinal high at Epsom/Olivewood. These intrabasinal highs resemble volcanic mounds currently forming in the vicinity of modern oceanic ridges, both in size and shape (see examples from Rona and Scott, 1993). Variations in the thickness (Fig. 7.2, 7.3, 7.19 and 7.20) of the banded iron formation units indicate an irregular lava floor.

The abnormal thickness of the Middle BIF Unit (± 70m in borehole R67) in the Mamatwan-Middleplaats area suggests that the lava palaeohigh west of Middleplaats may have been bounded by a growth fault. This is supported by the fact that the northern and eastern margins of the high are demarcated by a sharp linear magnetic anomaly. A prominent and rapid facies change within the Mooidraai dolomite sequence from reefal carbonates to turbiditic carbonates also occurs across this lineament, suggesting a change in slope-angle.

The presence of a proximal shoreline in the western part of the basin is suggested by the way in which the Upper BIF Unit onlaps onto the Ongeluk lava floor (Fig. 9.1). At the farm Constantia, the upper Mn body rests directly on the lavas, whilst in borehole SMD 2 on the farm Simondium, all three manganese horizons are present but the interbedded iron formation partings are very thin. The thickness of the Middle BIF Unit ranges from 3-5m.

De Vries Klein (1991) classified the Griqualand West basin as a passive continental margin rift-type. Sediment loading probably also contributed to the basin development as a great thickness of sediment, principally the Ghaap Group, accumulated on the margin of the Kaapvaal Craton, prior to the deposition of the Postmasburg Group. Subsidence due to thermal decay possibly also played a role in the basin development.

The Hotazel iron formation accumulated in a basin deep enough to allow the formation of turbiditic sediments, as well as a stratified water column. The abundance of greenalite facies iron formation which can only be precipitated in alkaline conditions, implies that the basin must have been closed or partially closed. The absence of clastics and the distinctive aluminium-deficient character of both the manganese and iron formations indicate a starved basin. From the above it is suggested that the Hotazel iron formation accumulated either in:

(i) A shallow marine setting inaccessible to clastic detritus, similar to the Bahama Platform, where the hinterland is of extremely low relief. This is identical to the model proposed by Schutte (1992) for the deposition of the Ongeluk lava, or

(ii) On the continental slope in a fault-block dam-type situation as depicted in Fig. 9.2.

9.5 A Possible Genetic Model

9.5.1 *Source of the Manganese, Iron and Silica*

A volcanogenic source for the origin of the manganese, iron and silica is suggested by the intimate relationship between the Hotazel iron formation and Ongeluk volcanism i.e.:

(i) The contact between the Hotazel banded iron formation and the Ongeluk lavas is conformable, as viewed in borehole cores, as well as in the exposure in the Hotazel open pit, where the iron formation has sagged into spilitised pillows.

(ii) Manganese mineralization associated with iron formation is present at various localities within the Ongeluk lava. Thin horizons of iron formation occur within the Ongeluk lava on the farms Rissik and Goold. On the farm Gravenhage in the Avontuur Basin, manganiferous sediments are also present in the volcanic pile below the contact with the Hotazel iron formation. On the farm Kaffirkop, some 60 km south of Postmasburg, lenses of jaspilite with manganese mineralization occur within the Ongeluk lava. The increase of Mn and Fe toward the top of the altered

reddened (Kalahari-type) lavas establishes a strong genetic link with the overlying iron formation.

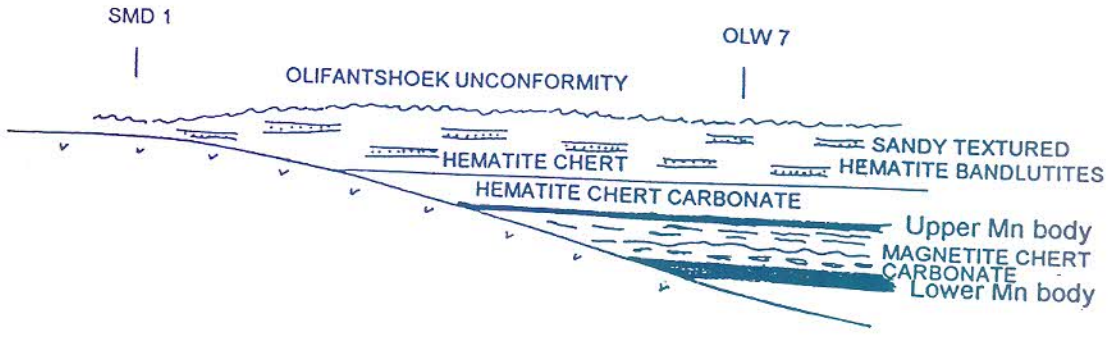

Fig. 9.1 *Schematic profile based on boreholes Olivewood 7 and Simondium 1 showing the transgression of the Upper BIF Unit onto the Ongeluk lava.*

(iii) Pronounced lateral facies changes such as that described for the study area are more characteristic of Algoma-type iron formation than a Superior-type iron formation (Gross, 1983). The latter is generally characterised by vertical facies changes.

(iv) The interbedded stilpnomelane band in the middle BIF unit in the Middleplaats-Mamatwan area suggests penecontemporaneous volcanism.

(v) Diagnostic element plots indicate that both the Wessels- and Mamatwan-type ores as well as the BIF are of hydrothermal origin (Fig. 9.4, 9.5, 9.8, and 9.9). The plot in Fig. 9.10 is contradictory suggesting a supergene origin, however Nickolson (1992) states that Mn-oxides (Wessels-type ore) display a strong adsorbtion capasity for elements like Ba, Cu, Li, Mo, Pb, Sr, V and Zn. The Hotazel Formation is depleted in Al (Fig. 9.11 and 9.12).

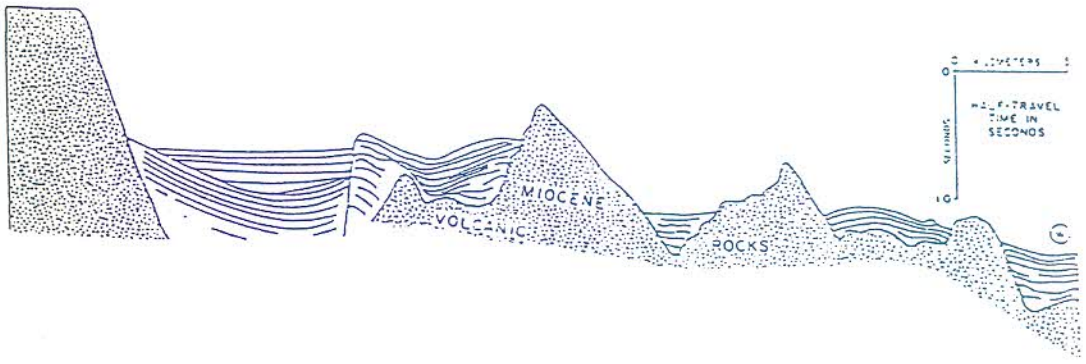

Fig. 9.2 *Fault-block dams, continental slope system, Baja California, Mexico (from Brown and Fisher, 1977).*

The genetic association between the Ongeluk volcanism, the BIF and associated manganese mineralization suggests that the source of the Fe, Si and Mn is probably derived from the Ongeluk lava pile, and not from weathering of the Transvaal dolomite sequence or any other clastic source of a similar age on the Kaapvaal Craton, as was proposed by de Villiers (1970).

The Kalahari alteration bears remarkable similarities to that observed in portions of the Troodos ophiolite complex in Cyprus (Gillis and Robinson, 1985). Over a wide area (2km x 3km) along the northern flank of the Troodos Complex, the uppermost 20 to 200m of the pillowed lava flows are green to reddish in colour, highly oxidised and leached. This alteration is believed to be the result of prolonged seafloor weathering over a topographic high. The assemblages of secondary minerals in this zone are very similar to those recovered from the upper portions of the present day oceanic crust where similar processes are invoked. The oxidised zone is absent where the extrusive sequence is overlain by a relatively thick sequence of synvolcanic umber (Fe-Mn sediment). Gillis and Robertson (1985) suggest that the umbers were deposited in topographic lows on the seafloor. These would have formed an early impermeable layer that prevented seawater from percolating downwards into the upper part of the lava pile. A similar setting could be invoked for the Kalahari-type alteration. The iron

necessary for the Kalahari alteration process could have been derived either from iron originally present in a reduced form as a sulphide, or alternatively, it was derived from alteration of mafic minerals deeper in the system. The iron contents in the ferruginised lava, up to 30% are much higher than in the regional Ongeluk lavas (Schutte, 1992). Such high levels are unlikely in primary igneous rocks, suggesting the addition of iron to the system. Mn, Fe and Si can be leached in the following ways i.e.:

(i) By leaching of Mn, Fe and Si from an extruding lava pile at a shallow level by acidified and reduced seawater.

(ii) Convective circulation of descending seawater through deep fractures or porous zones. The seawater becomes heated and enriched in metals which are finally debouched onto the ocean floor.

(iii) Deep seated derivation of the metals through degassing (generation of CO_2 emanations) in conjunction with the differentiation of pyrolite into peridotite and basalt in areas of mantle upwelling.

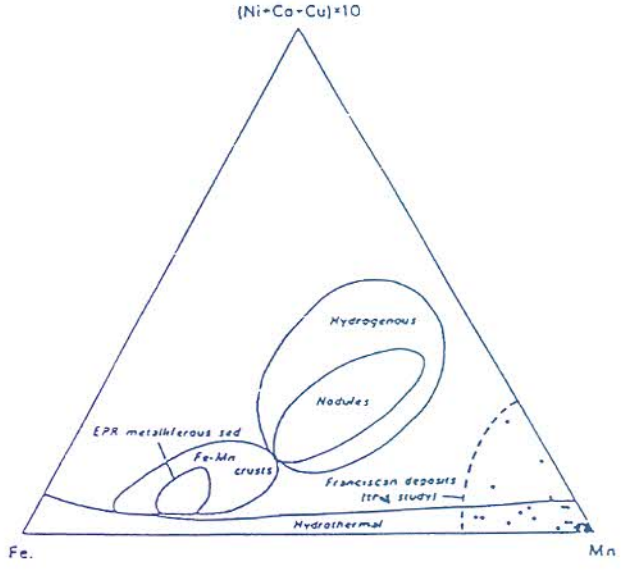

Fig. 9.3 *Ternary diagram showing Fe vs Mn vs (Ni+Co+Cu) x 10 for manganiferous marine deposits. The diagram compares data from ore lenses of the Franciscan deposits with generalised fields for hydrogenous sediments and hydrothermal deposits after Bonatti et al. (1972). Also shown are fields of East Pacific Rise metalliferous sediments after Corliss and Dymond (1973), and fields of intermediate Fe-Mn crusts and ferromanganese nodules taken from Toth (1980) (from Crerar et al., 1982). Key for geochemical plots Fig. 9.4 and 9.5.*

KALAHARI MANGANESE FIELD

BASIN ANALYSIS PROJECT

GEOCHEMICAL PLOTS OF WESSELS AND MAMATWAN TYPE MANGANESE MINERALIZATION

○ MAMATWAN TYPE Mn

■ WESSELS TYPE MANGANESE

COMPILED BY M SMITH

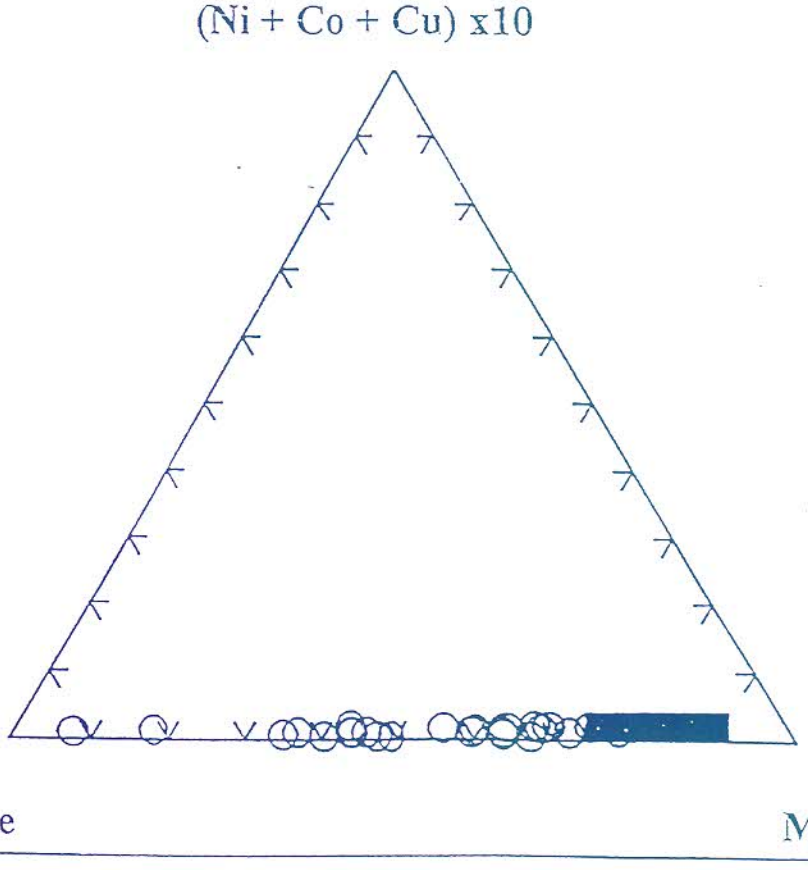

Fig. 9.4

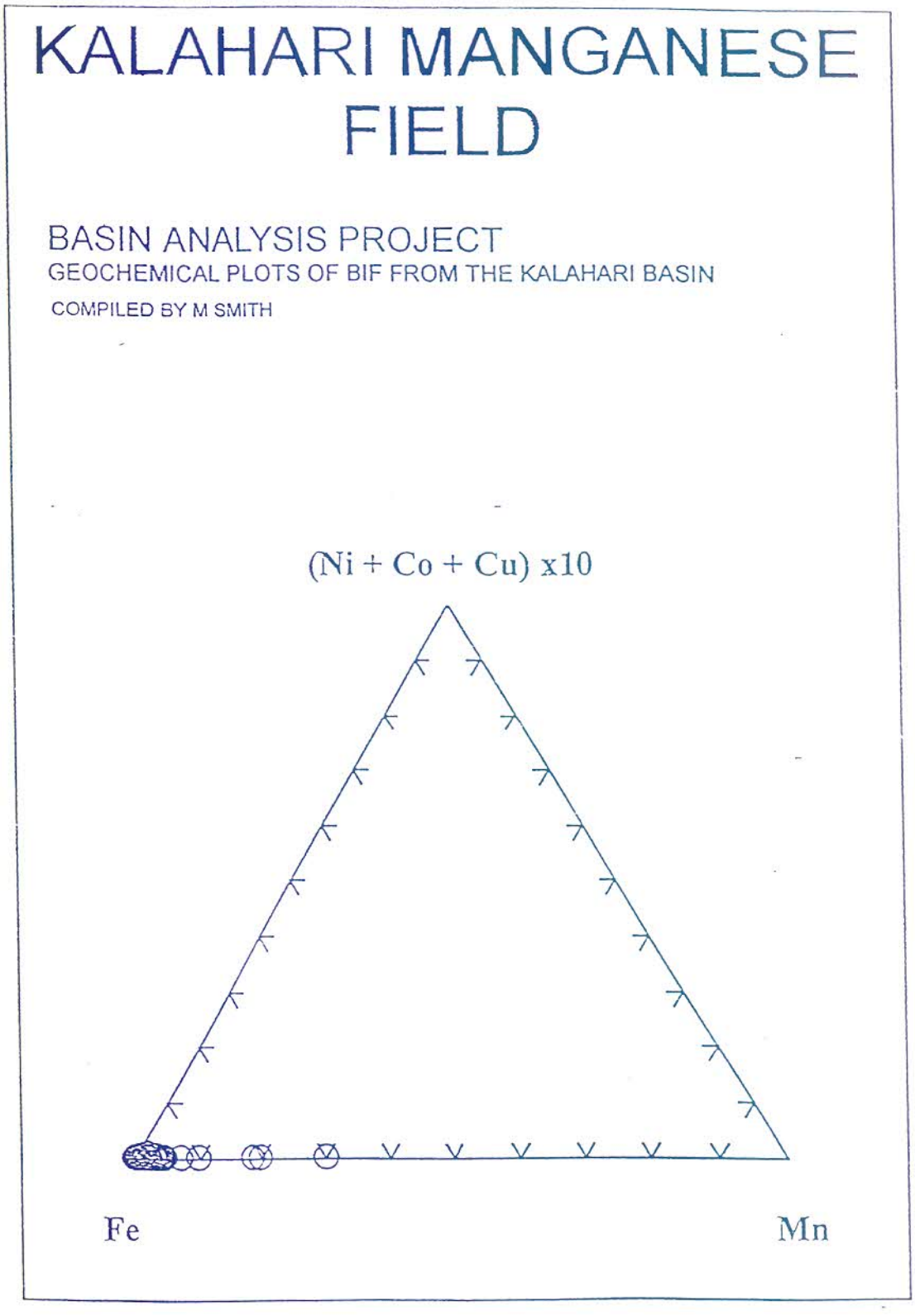
KALAHARI MANGANESE FIELD
BASIN ANALYSIS PROJECT
GEOCHEMICAL PLOTS OF BIF FROM THE KALAHARI BASIN
COMPILED BY M SMITH
(Ni + Co + Cu) x10
Fe
Mn

Fig. 9.5

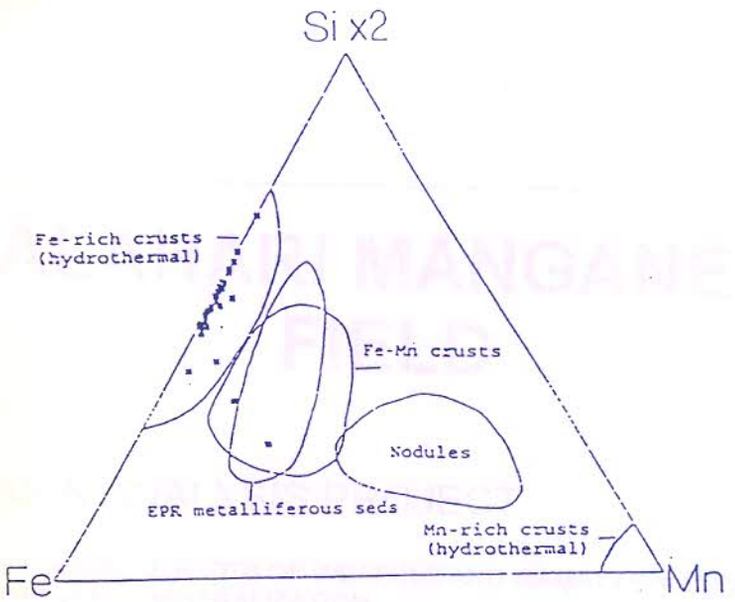

Fig. 9.6 *Ternary diagrams of Fe-Si (x 2)-Mn showing the positions of rocks from the study area (filled squares) relative to the fields of various marine sediments (after Bonatti et al., 1972 ; in Tsikos, 1994). Diagram is key to geochemical plots Fig. 9.8 and 9.9.*

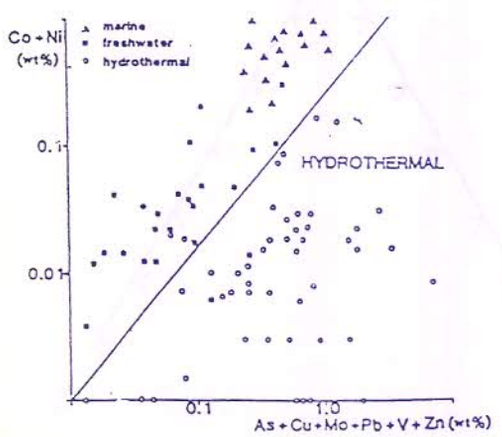

Fig. 9.7 *Diagnostic plot to differentiate supergene and hydrothermal manganese oxides. Note that because of their high metal content, dubhites plot in the hydrothermal field: however, these can be recognised using the Pb-Zn plot (after Nicholson, 1992). Diagram is key for geochemical plot Fig. 9.10*

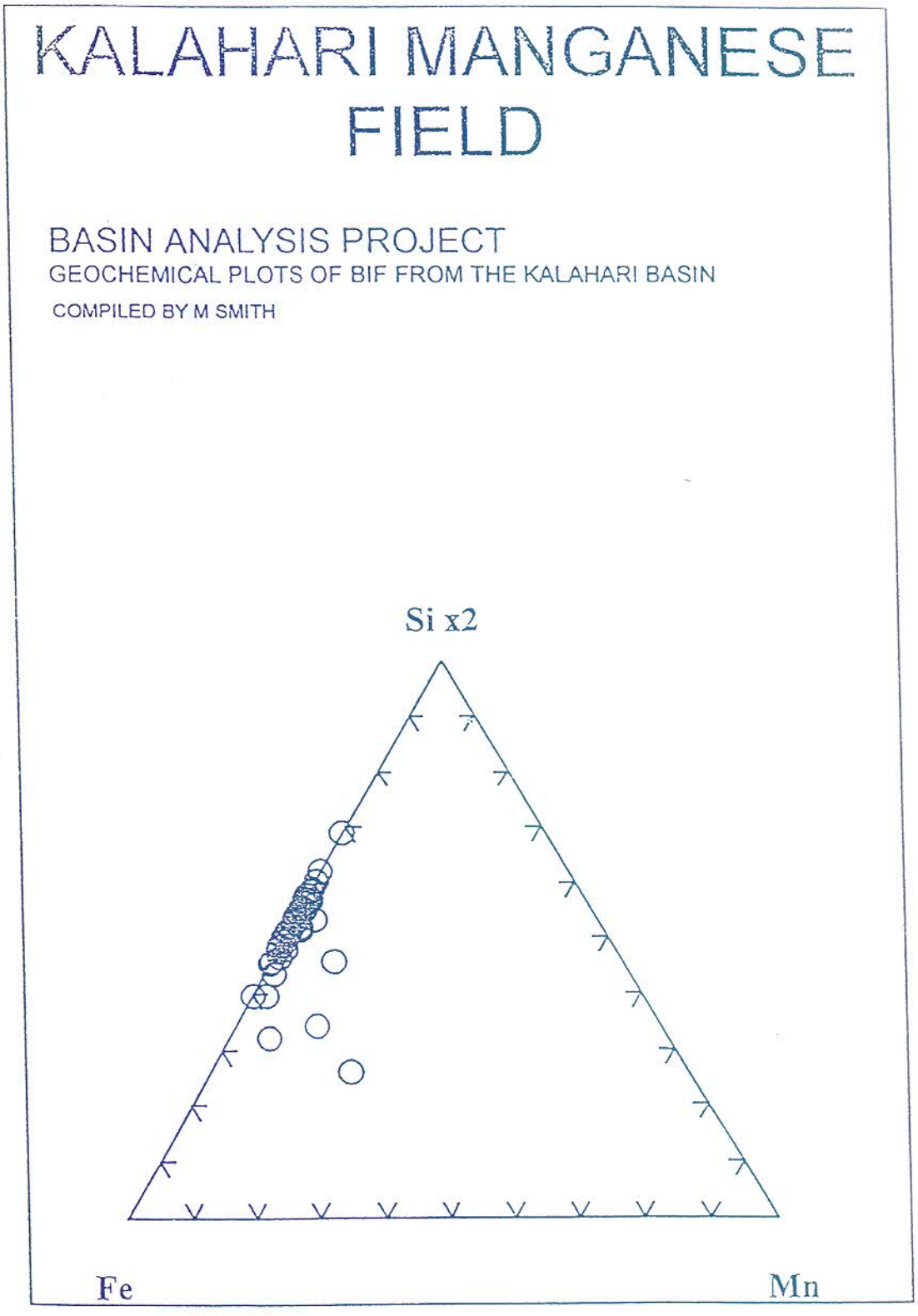
KALAHARI MANGANESE FIELD
BASIN ANALYSIS PROJECT
GEOCHEMICAL PLOTS OF BIF FROM THE KALAHARI BASIN
COMPILED BY M SMITH
Si x2
Fe
Mn

Fig. 9.9

KALAHARI MANGANESE FIELD BASIN ANALYSIS PROJECT

GEOCHEMICAL PLOT OF MANGANESE MINERALIZATION

○ WESSEL TYPE Mn
▩ MAMATWAN TYPE Mn

COMPILED BY M SMITH

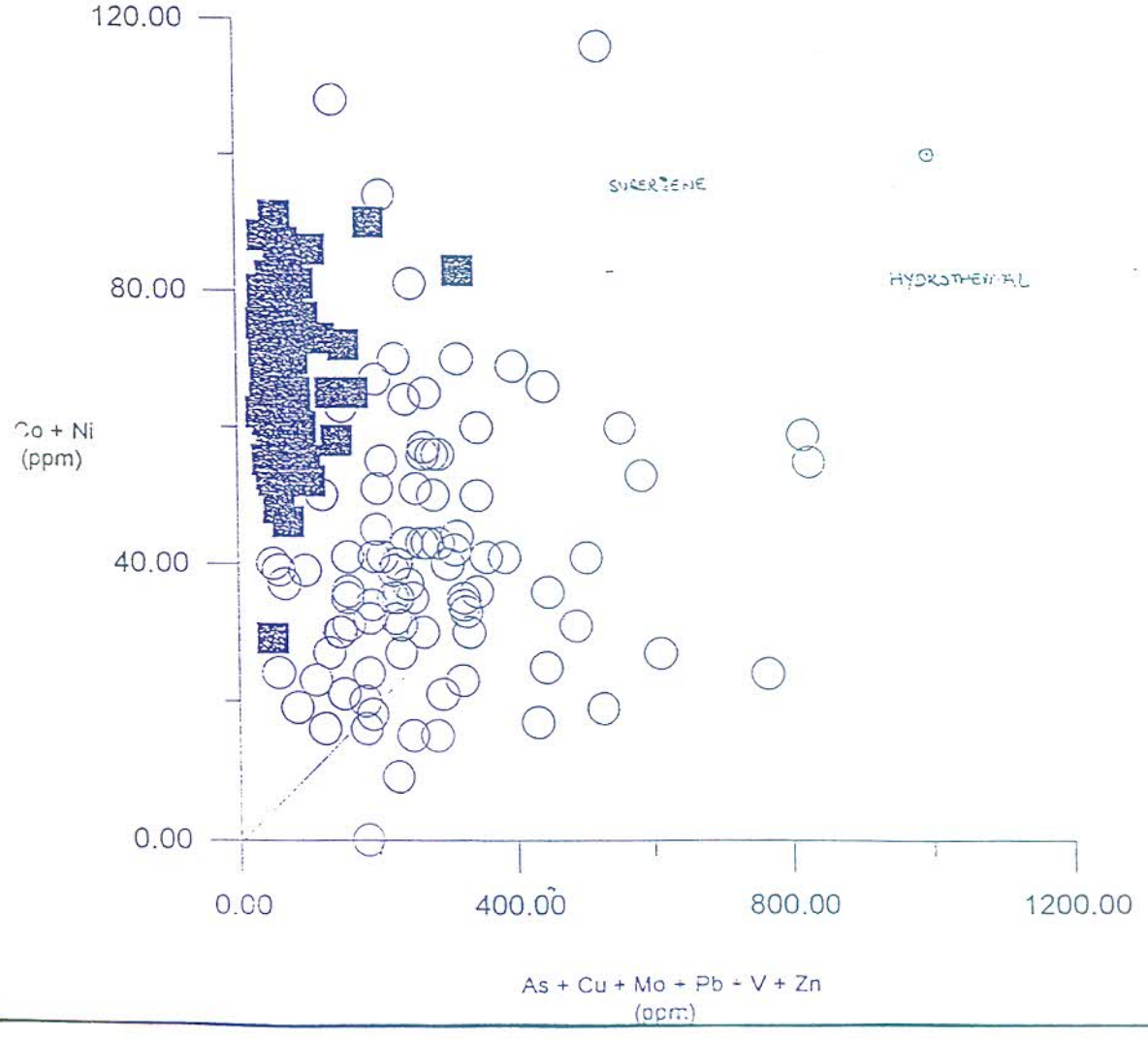

Fig. 9.10

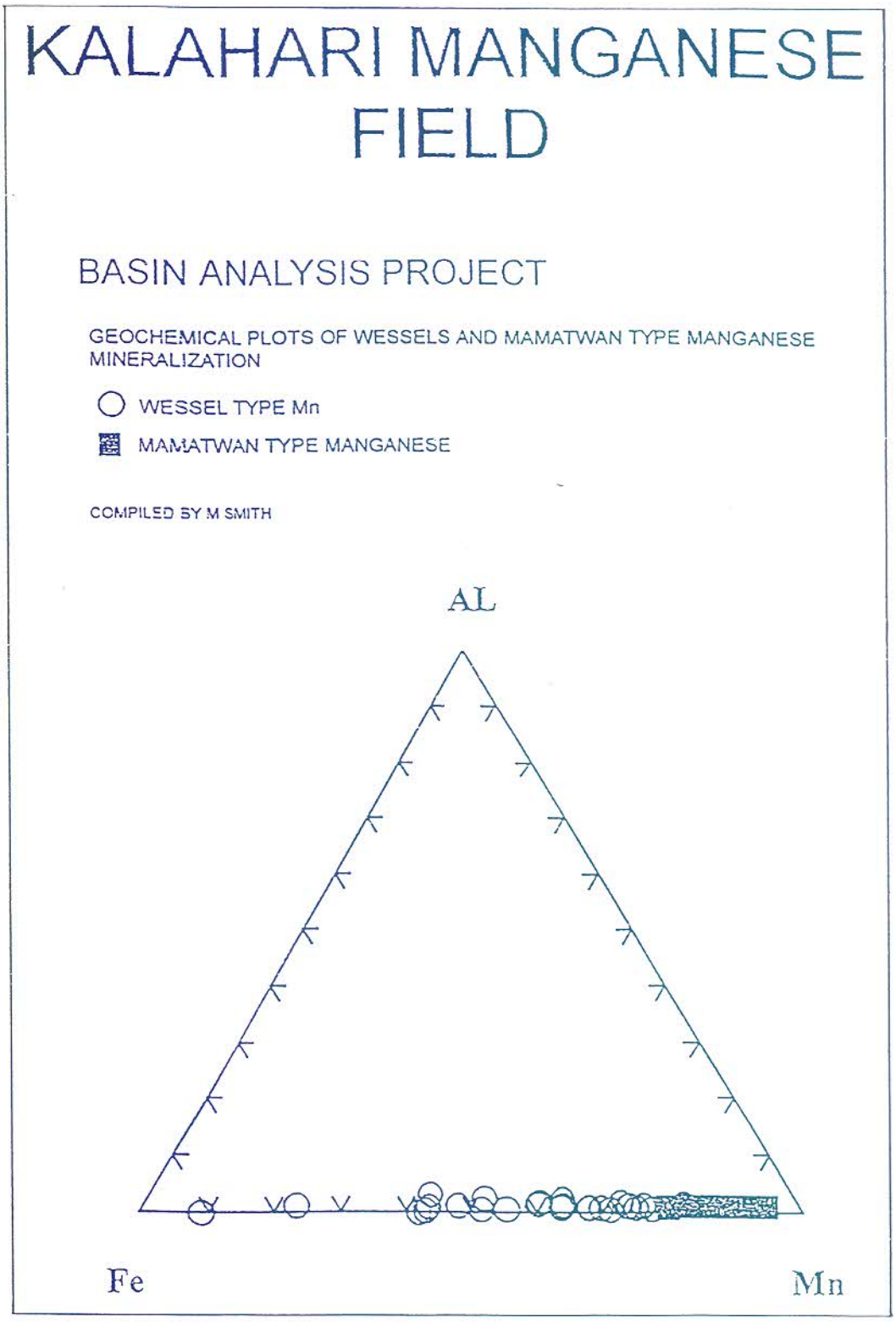
KALAHARI MANGANESE FIELD
BASIN ANALYSIS PROJECT
GEOCHEMICAL PLOTS OF WESSELS AND MAMATWAN TYPE MANGANESE MINERALIZATION
WESSEL TYPE Mn
MAMATWAN TYPE MANGANESE
COMPILED BY M SMITH
AL
Fe
Mn

Fig. 9.11

KALAHARI MANGANESE FIELD

BASIN ANALYSIS PROJECT

GEOCHEMICAL PLOTS OF BIF FROM THE KALAHARI BASIN

COMPILED BY M SMITH

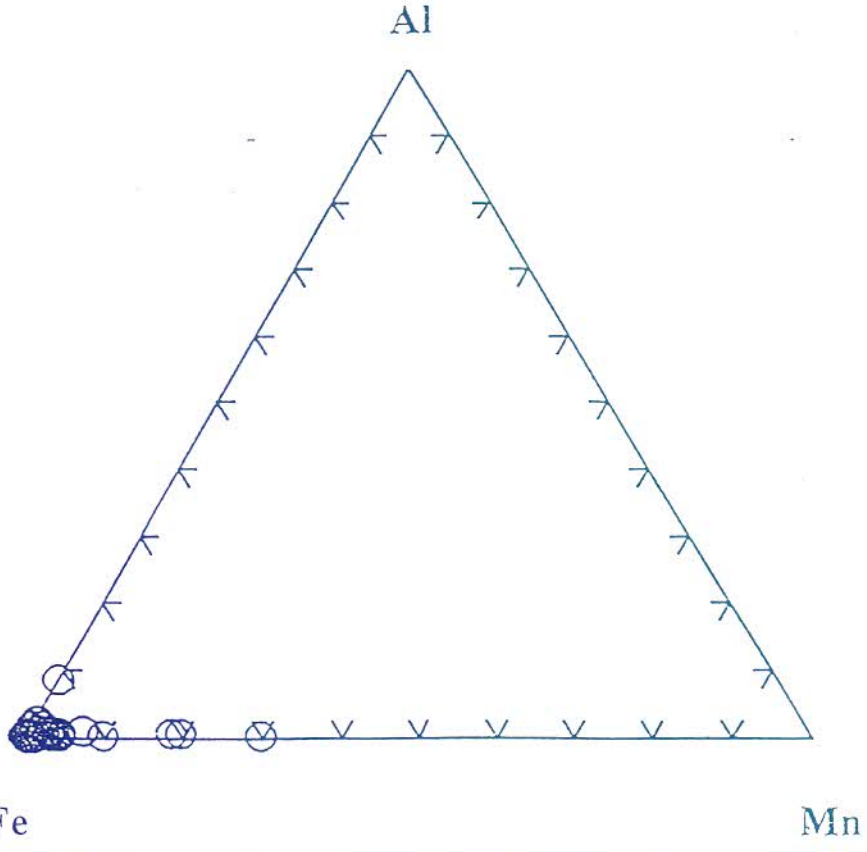

Fig. 9.12

9.5.2 *Deposition of Manganese*

Two genetic models can explain the origin of the Hotazel iron formation and its associated manganese mineralization, i.e.:

(i) a sedimentary model in which both Mn and Fe were deposited from upwelling anoxic water onto the continental shelf, and

(ii) a volcano-sedimentary model.

9.5.2.1 Upwelling of anoxic water

Schissel and Aro (1992) merged the model of Button *et al.* (1982), which explains the origin of BIF in continental margin sequences, and that of Cannon and Force (1983), Frakes and Bolton (1984) and Force and Cannon (1988), which discuss the origin of manganese mineralization in near-shore and marine settings (see Chapter 6.6.2). Stratigraphic evidence within the Hotazel iron formation favours the presence of a chemocline and supports such a model (Figure 9.13). The silicate facies (greenalite-magnetite-carbonate) iron formation were preferentially deposited below the chemocline, whilst the oxide facies (hematite-chert) iron formation was deposited just above. The hematite lutite which contains significant manganese and carbonate mineralization would equate with the manganese-carbonate facies of Schissel and Aro (1992). Force and Cannon (1988) stressed that carbonate deposition is not only dependent on Eh and pH levels but also on the partial pressure of carbon dioxide. Minor fluctuations in CO_2 levels can result in the preferential deposition of manganese-carbonate and this may explain the presence of carbonate ooids in the hematite lutite and manganese oxide-silicate (braunite I) horizons.

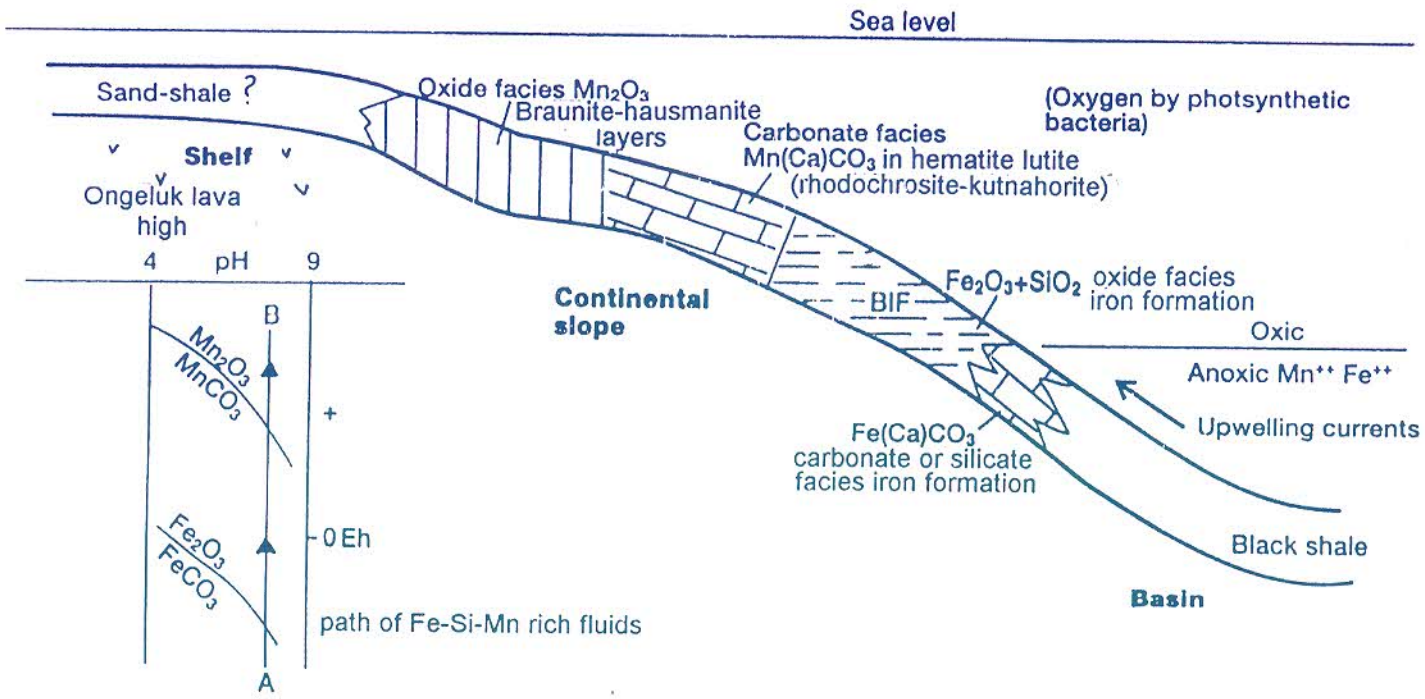

Fig. 9.13 *Cannon and Force (1983) model for deposition of manganese from upwelling anoxic waters,modified to include banded iron formations (after Button et al., 1982). Modified after Schissel and Aro, 1992,for the Kalahari Manganese Field .*

The three fold cyclicity of manganese and iron within the Hotazel iron formation can be explained as a reflection of three discrete periods of transgression with associated strong upwelling currents which moved anoxic manganese- and iron-charged water over a sill and into the basin. The manganese would have been deposited during the regressive portion of each cycle when the waters shallowed and became oxygenated prior to a fresh influx marking the following transgressive event.Trace element plots (Fig. 9.4, 9.5, 9.8 and 9.9) presented above suggest a hydrothermal source for the iron and manganese, either derived from exhalation of metal-rich fluids or leaching of the lava pile deeper in the ocean, as seen along many of the mid-oceanic ridges and rises at present.

9.5.2.2 Volcanogenic-sedimentary model

The upwelling model has recently been challenged by Cornell and Schutte (1995) because they doubted the existence of a chemocline during deposition of the Hotazel iron formation. They regard the entire iron formation as being of oxide facies and proposed a volcano-sedimentary model for the origin of the Hotazel iron formation and associated manganese deposits (Figure 9.14). The model advocates the presence of a major hydrothermal exhalative system in the Ongeluk lava immediately below the Kalahari Manganese basin. The locus of the Kalahari-type alteration in the Ongeluk is considered to have been situated close to an extrusive vent which supplied heat and CO_2 (possibly also from the underlying dolomite). CO_2 is a necessary component of the hydrothermal fluid to cause the mobilisation of high field strength (HFS) elements. Sea water was drawn from a large area, heated at depth and then disgorged on to the sea floor. During the heating stage the fluid interacted with large volumes of lava, became saturated in K, Rb, Ba, Mn and Fe and also acquired HFS elements as carbonate complexes. Prior to emerging at the sea floor as a Proterozoic "black smoker", the fluid cooled, mixed with oxygenated sea water and began

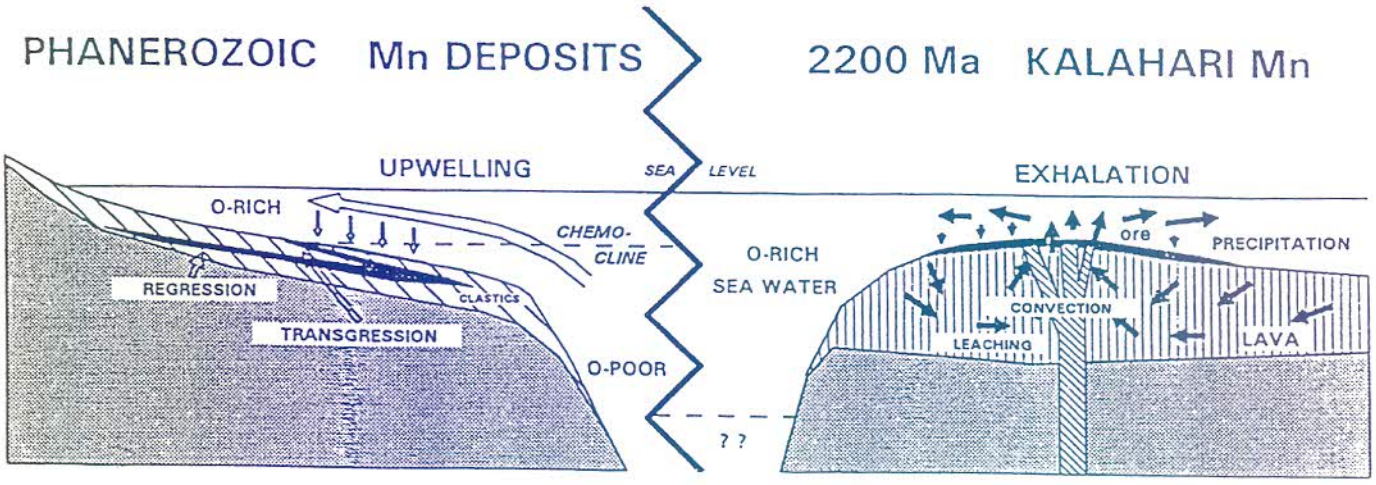

Fig. 9.14 *Comparison of models for Mn ore formation in Phanerozoic and Proterozoic (Kalahari Mn) continental shelf environments (after Cornell and Schutte, 1995).*

precipitating its dissolved load in the Ongeluk lava. On entering the sea, further cooling and oxygenation led to the precipitation of hematite, Mn-carbonate and oxide ores. The zonation between manganese and iron is explained by the interplay between the Eh and pH during flocculation. Cornell and Schutte (1995) draw analogies with deposits forming at present day mid-oceanic ridges.The model presented by Cornell and Schutte (1995) is non-specific with regard to the area of discharge and the tectonic setting of the depositional site. The model in particular fails to account for the following important features:

(i) The distinctive red Kalahari alteration is confined to the lavas around Wessels Mine and the area to the north (Boerdraai), possibly Hotazel Mine as well as in borehole EP 1 on the Epsom-Olivewood palaeohigh, and would therefore appear to mimic the distribution of oxide facies iron formation.

(ii) Deposits currently forming along the mid-oceanic ridges are typically small, thin, lenticular bodies and are nowhere near the size or continuity of the Hotazel iron formation. (iii) Deposition of the iron formation would effectively cap and seal the lavas preventing the flow of

hydrothermal fluid. No evidence of any large-scale syndepositional hydrothermal brecciation or alteration of the iron formation was recognised.

9.5.3 *Synthesis*

The formation of the Kalahari basin may be related to rifting associated with the Ongeluk lava phase. Wilson (1963) suggested that rifting may be initiated by upwelling of hot mantle (the "hotspot" theory). Upwelling over the mantle plume results in uplifting and doming, commonly along old lines of crustal weakness. This causes crustal thinning which generates horizontal tensional stress resulting in crustal failure along extensional faults. On surface, the only expression may be high angle extensional faults which may become listric with depth (Bott, 1975 and 1982). Volcanism commonly precedes or follows the uplift event.This study proposes the Kalahari basin to be a half-graben along a growth fault flanking a submerge volcanic seamount (the Middleplaats palaeohigh) (Fig. 9.15). This is similar to the present day Atlantis II Deep in the Red sea, which is a stratified basin with respect to salinity, temperature and Eh (Berkel, 1982).Seawater from outside the present confines of the basin descended through the lava pile, through the more permeable parts such as flow tops, lava tubes, buried talus piles, hyaloclastites and fractures zones. Dewatering as a result of compaction by the overlying sediments may also have been a contributory source. These fluids became heated with depth and leached Si, Mn, Fe and other elements from the porous lava in a manner similar to that proposed by Cornell and Schutte (1995). The fluids were preferentially discharged at intrabasinal highs (Epsom-Olivewood, Hotazel, Wessels-Nchwaning) flanking the western and northern margins of the basin and began precipitating in the uppermost lavas causing a moderate to intense ferruginization. Much of the Mn^{2+} and Fe^{2+} would stay in solution within the hot oxygen-poor and acidic hydrothermal fluid. Away from the discharge areas, the hydrothermal fluid would

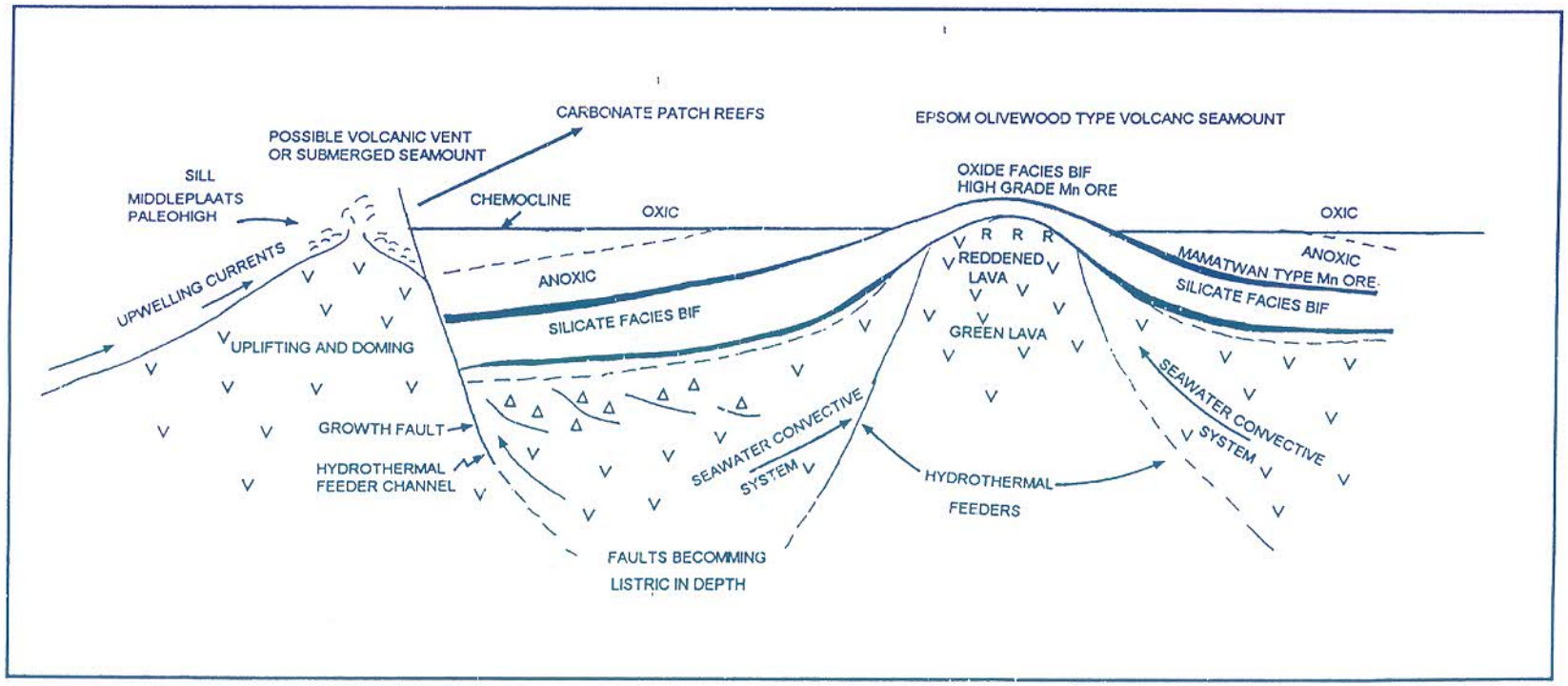

Fig. 9.15 *Cartoon sketch illustrating a proposed model for the deposition of the Hotazel Iron Formation.*

react with cold and more oxygenated seawater. As a result metal began to precipitate accumulating in topographic lows flanking the discharge areas. Alkaline conditions below the chemocline would further facilitated the precipitation process. Iron would precipitate at slightly lower pH and Eh conditions, whilst manganese, because of its higher solubility, would precipitate at slightly elevated Eh and pH conditions. Higher Eh and pH conditions were reached as the hydrothermal plume approached equilibrium with the seawater or during an influx of fresh oxygenated seawater over the Ongeluk palaeohigh (sill) west of Middleplaats which separated the basin from the deeper ocean. Manganese would have initially been deposited as a carbonate, and as Eh conditions increased, as an oxide. The cyclic stacking of iron and manganese could be explained in this model as a reflection of episodic hydrothermal activity or as an episodic transgression of oxygenated seawater over the basin sill.

9.6 Factors controlling the distribution of the Wessels-type high-grade ores

The distinguishing characteristics between the Wessels-type and Mamatwan type ores are summarised in Table 9-1. At present there are three schools of thought as to the genesis of the high-grade Wessels-type ores i.e.:

(i) Hydrothermal fluids spreading out fan-like along thrust planes and upgrading Mamatwan-type ore (Kleyenstüber 1985).

(ii) Hydrothermal fluids altering Mamatwan-type ore along major north-south and minor east-west trending normal faults and fractures (Gutzmer and Beukes, 1995 : Burger and Beukes, 1995: Gutzmer, 1996).

(iii) Hydrothermal upgrading as a result of seawater convection through the Ongeluk lava pile (Cornell and Schutte, 1995).

Alteration and upgrading of the ore in the vicinity of high-angle faults can be illustrated in the Wessels mine and in the Hotazel pit. Beukes *et al.*, 1995, Gutzmer and Beukes, 1995 and Burger and Beukes, 1995 concluded that the Wessels-type ore was formed by hydrothermal alteration of primary Mamatwan-type ore along post-Olifantshoek north-south and east-west trending normal

faults and fractures. Most of the alteration took place along the north-south trending faults which are the predominant structures in the area. Mamatwan-type ore is generally preserved in the cores or centres of fault bounded blocks whilst the high-grade Wessels-type ores are developed between the Mamatwan-type ores and the ferruginised zones adjacent to the faults (Fig. 9.16). Beukes and Gutzmer (1995) proposed a model in which the hydrothermal fluids moved from the fault conduits in a series of metasomatic fronts (Fig. 9.17). Successive fronts overprint each other laterally as the zones of alteration next to the fault zone widened away from the conduit. This study has indicated a number of previously unknown features:

(i) High-grade Wessels-type ore is confined to hematite-chert facies BIF.

(ii) Low-grade Mamatwan-type ore occurs within hematite-chert-carbonate and greenalite-magnetite-carbonate facies BIF.

(iii) In the high-grade areas, the BIF partings are thin. Wavy bedding is common, indicating deposition over topographic highs.

The association of the high-grade oxide facies (silica and carbonate-poor Mn) hausmanite and braunite II ores with the hematite-chert facies BIF is regarded as a reflection of the primary sedimentological controls within the depository.

The restriction of high-grade ore to a particular banded iron formation facies also implies that the distribution of high-grade ore will show a strong palaeotopographic control related to the overall configuration of the basin. This is confirmed by the fact that the higher grade bodies are characteristically thinner and contain thinner partings (Table 9.1) indicating that they preferentially formed either as a drape over Ongeluk lava palaeohighs or possibly, also along the margins of the basin where progressive onlap would result in a similar thickness distribution.

TABLE 9.1: **DISTINGUISHING CHARACTERISTICS BETWEEN THE WESSELS AND MAMATWAN - TYPE ORES**

WESSELS HIGH GRADE TYPE	MAMATWAN LOW GRADE TYPE
♦ Confined to oxide facies hematite-rich banded iron formation. No carbonate present.	♦ Within magnetite-rich oxide facies, carbonate facies and silicate facies banded iron formation.
♦ Host iron formations richer in Fe and silica.	♦ Host iron formations poorer in Fe and silica.
♦ Often in tectonically complex areas.	♦ Invariably in relatively undeformed areas
♦ Ore is bright and shiny massive, brecciated or vuggy.	♦ Ore is dull and well laminated.
♦ Mn content high (47-48%).	♦ Mn content lower (37% - 38%).
♦ Fe content higher (11 - 14%), may have interlayered Fe ore.	♦ Fe lower (4 - 6%).
♦ Mn/Fe ratio 4:1.	♦ Mn/Fe ratio 8.5:1 to 10:1.
♦ SiO_2 higher (6 - 9%).	♦ SiO_2 lower (4 - 6%).
♦ CaO lower (4 - 6%) and MgO lower (0,5 - 1,5%).	♦ CaO higher (12 - 16%) and MgO higher (3 - 5%) indicating abundant carbonate.
♦ High barium.	♦ Low barium.
♦ Enriched in Cu, Pb and Zn (Sn not as marked).	♦ Depleted in Cu, Pb and Zn.
♦ Boron distinctly lower.	♦ Boron distinctly higher.
♦ Higher temperature mineralogy: hausmannite, braunite II, manganite	♦ Lower temperature mineralogy braunite (hausmannite) and kutnahorite.
♦ Ore horizons and partings between are thinner. At Hotazel ore horizons very thick but partings just as thin.	♦ Opposite.
♦ Where relatively undeformed, as at Epsom/Olivewood, is a circular patch surrounded by lower grade material.	♦ Regionally extensive.
♦ No Mooidraai present, directly overlain by Olifantshoek strata.	♦ Overlain by Mooidraai dolomite except where removed by erosion along suboutcrop.

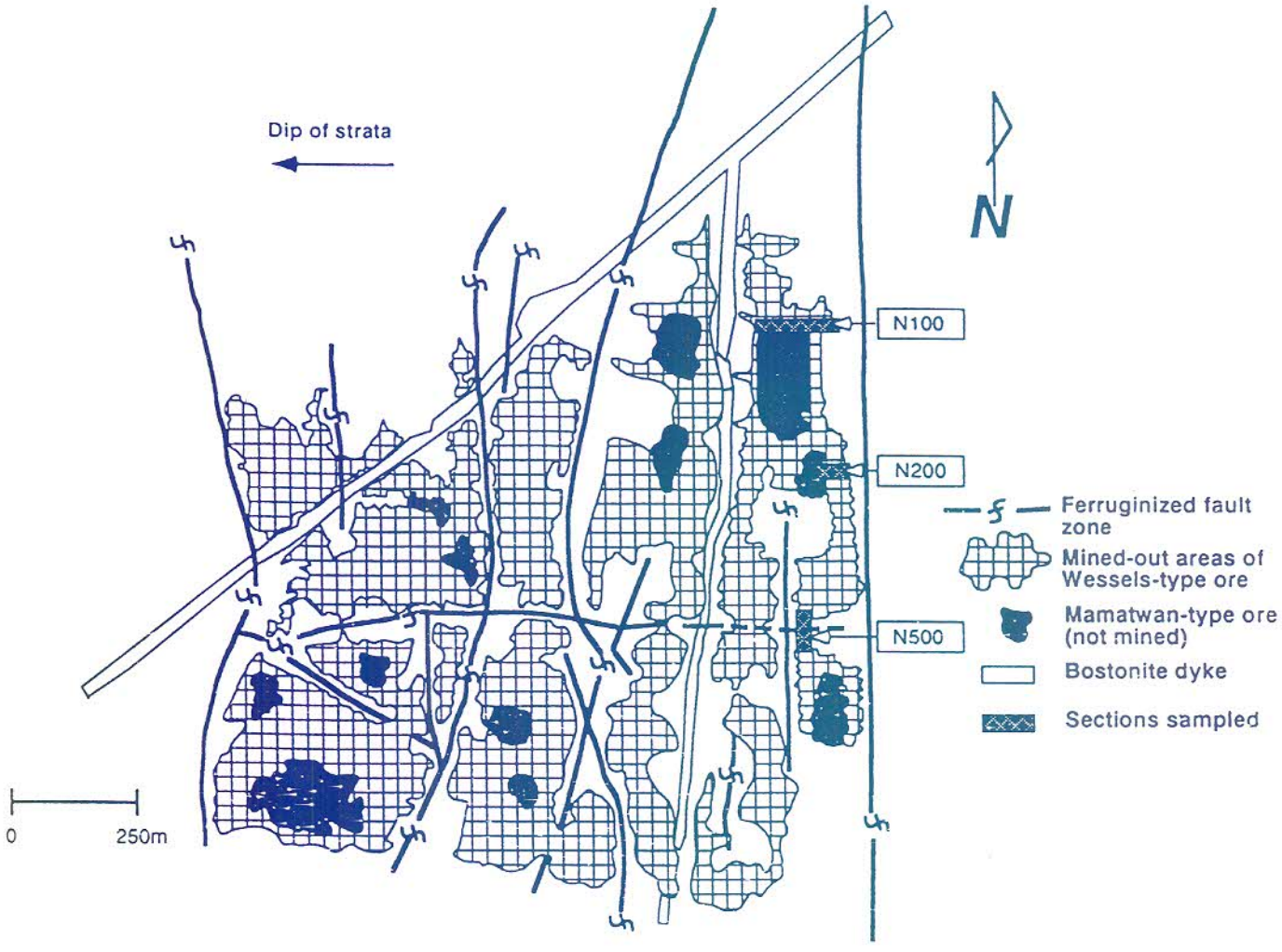

Fig. 9.16 *Simplified stope plan of the sampling area in Wessels Mine showing the location of traverses sampled (after Beukes et al., 1995).*

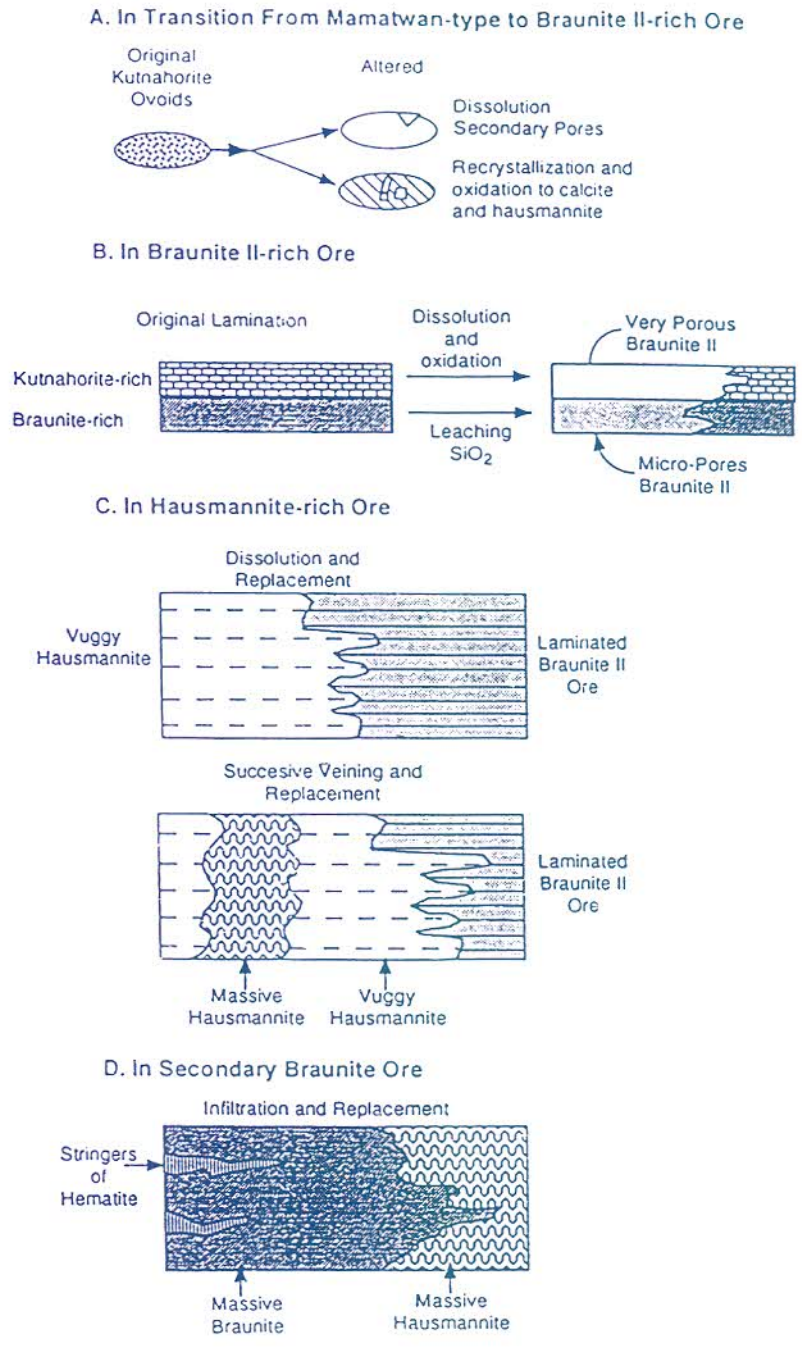

Fig. 9.17 *Diagram illustrating characteristic textural changes with increasing degree of alteration during the transformation of low-grade Mamatwan-type ore to high-grade Wessels-type ore (after Beukes et al., 1995).*

10. MOOIDRAAI FORMATION

10.1 Introduction

The Mooidraai Formation is preserved along a northerly trending belt extending from the farms Chelmsford 365 and Leonard 363 in the south to Umtu 281 in the north-west of the study area (Fig. 5.1). It is absent along the western and northern part of the Kalahari Basin. The greatest preserved thickness is on the farms Heuningdraai 334 and Umtu 281, where it reaches a thickness of 180m and 184m, respectively.

A total of 15 boreholes were used in this study. The Mooidraai Formation is subdivided into four facies which are common to most carbonate platforms (Fig. 10.1, after Wilson, 1975) i.e.:

(i) A slope facies along the south-western boundary of the Kalahari basin, extending north and north-eastwards into the basin.

(ii) An organic build-up belt on the shelf margin. This facies is inferred from borehole intersections in the basin and towards the south-west of Middleplaats, on the farm Moffat 366.

(iii) A winnowed (shelf-edge) lime-sand belt flanking the build-up belt towards the south-west.

(iv) Shelf lagoon facies developed towards the middle-shelf.

The Mooidraai Formation shown in Fig. 4.6 (compiled by Beukes, 1983) should be regarded as a cartoon-type summary and not a true representation at any one locality.

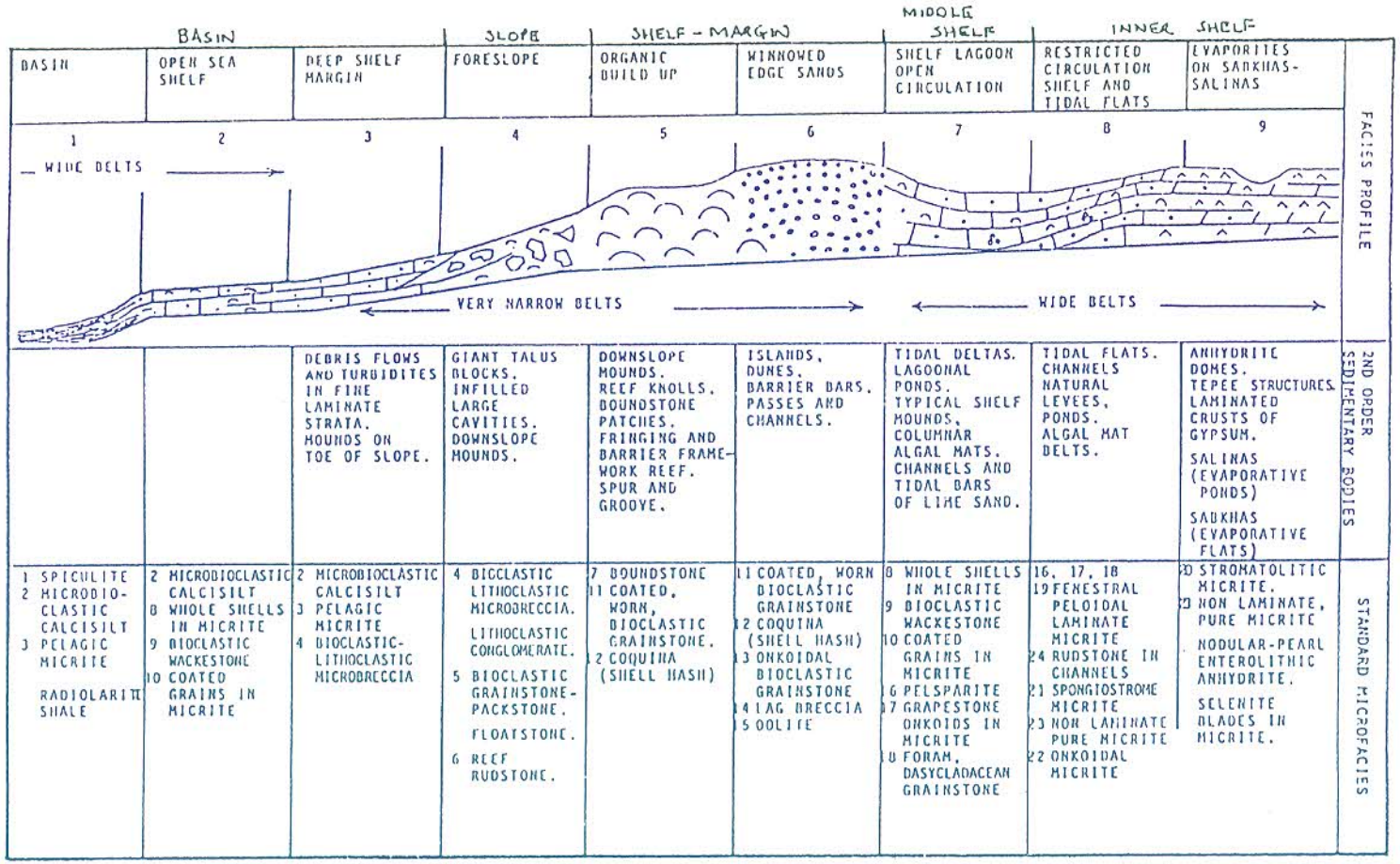

Fig. 10.1 *Synopsis of Standard Facies Belts for carbonaye deposits, reviewing second order bodies of sediment and standard microfacies associated with each belt (After Wilson, 1975, with modifications from Beukes, 1986).*

144

10.2 Slope facies

10.2.1 *Olivepan-Umtu*

The Upper BIF Unit of the Hotazel iron formation, along a traverse from borehole U17 to OLP 7, is overlain by a dolomite breccia along a sharp contact (Fig. 10.2 and Fig. 10.3). The breccia comprises angular (1-3cm) fragments of dolomite and chert, set in a coarse sandy-calcareous matrix. It thins towards the east from 11m in U17 to 0,2m in OLP 5. It is clast-supported, with upward-fining tendencies in the thinner parts. The orientation of the fragments is random.

Dolomite and chert breccia units, with a thickness of up to 8.0m, are also present higher up in the stratigraphy (Fig. 10.3). Correlation between breccias units is difficult because they apparently occupy different levels in the stratigraphy.

The bulk of the Mooidraai Formation comprises thin bedded to planar laminated rhythmites. Thin partings of fine silty material alternate with sandy clastic-textured dolomite layers, a few centimetres thick. The clastic layers exhibit micrograded bedding. The silty partings are dark brown and ferruginous, and may on rare occasions reach up to 2cm in thickness. In the absence of silty partings, the sequence comprises laminated or thinly bedded, buff to grey-coloured dolomites.

Dark-brown, red or pink-laminated ferruginous dolomites up to 8m thick, are generally developed halfway up the stratigraphy (Fig. 10.3). Hematite-chert bandulites and disseminated magnetite may also occupy this stratigraphic position in some boreholes (Fig. 10.3 and 10.4).

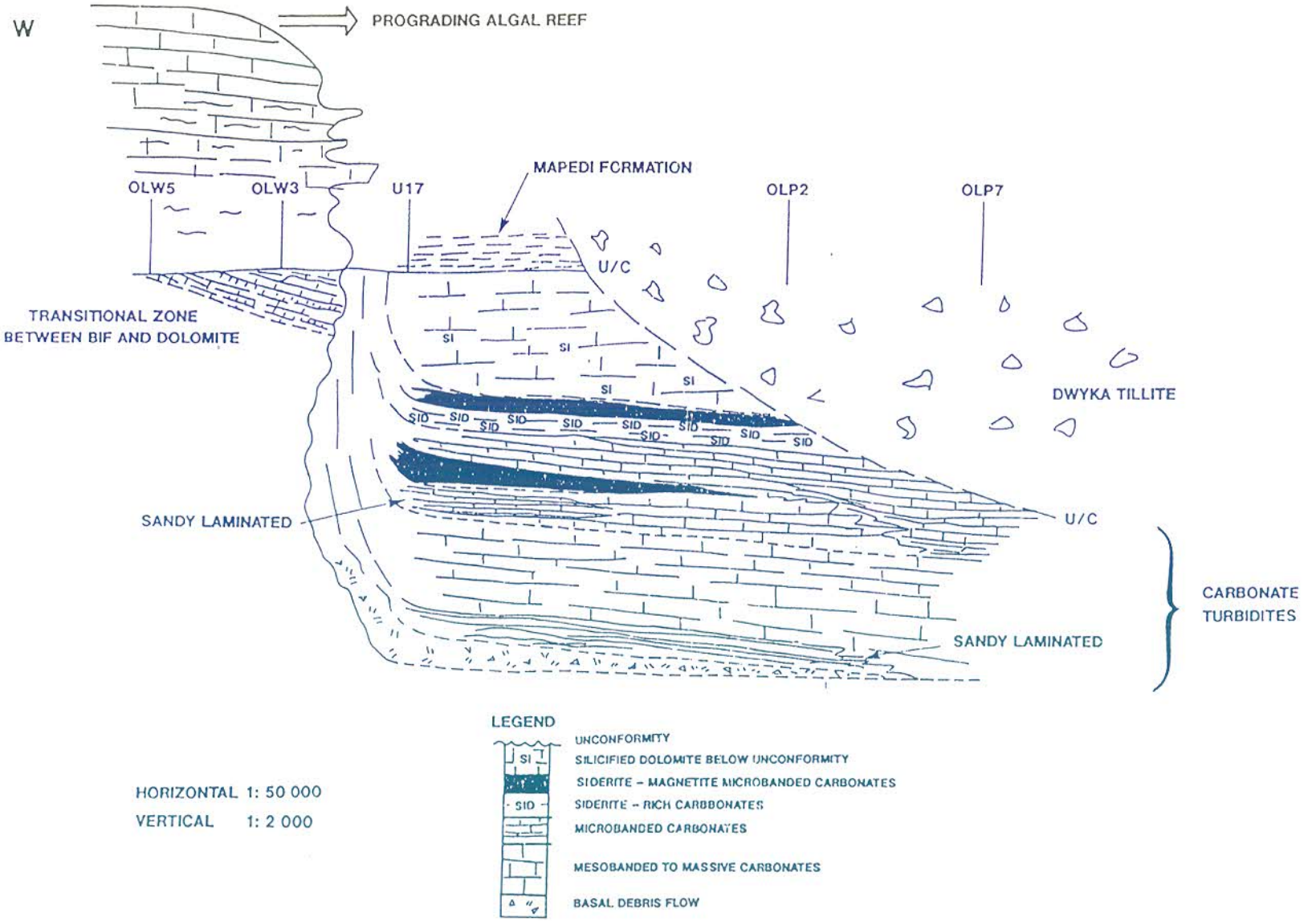

Fig. 10.2 *Evidence for a patch reef on the Epsom-Olivewood palaeohigh.*

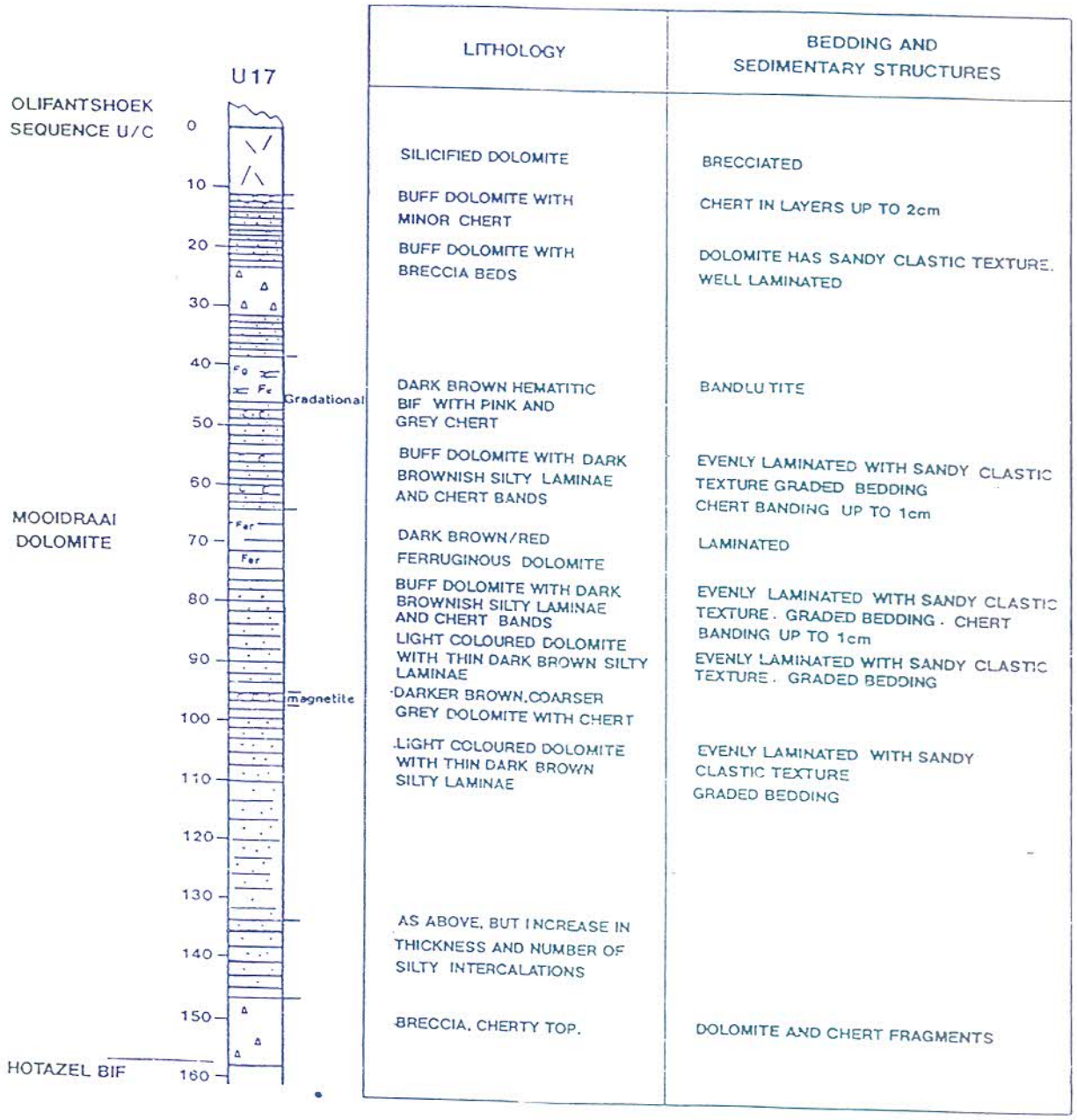

Fig. 10.3 *Stratigraphy of the Mooidraai dolomite in borehole U17 on the farm Umtu 281.*

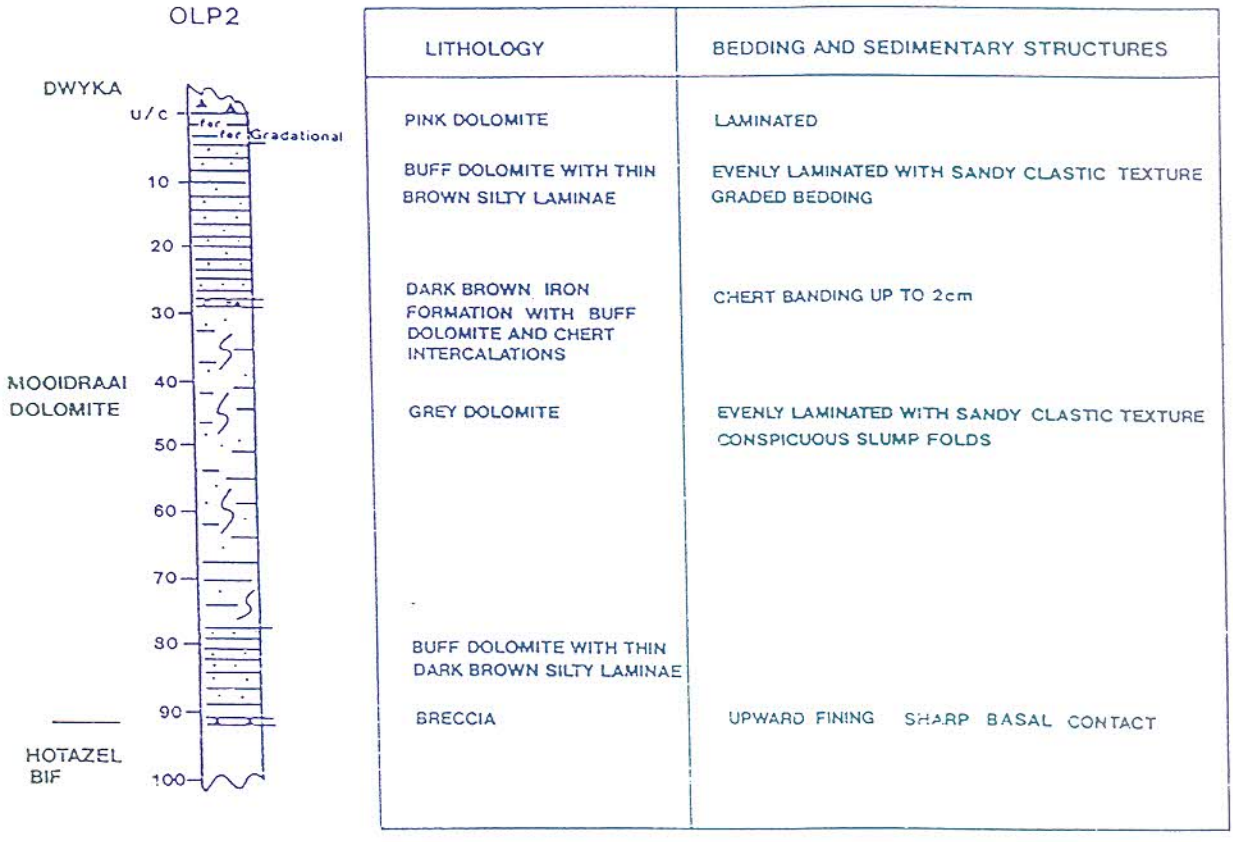

Fig. 10.4 *Stratigraphy of the Mooidraai dolomite in borehole OLP2 on the farm Olivepan 282.*

Chert bands (2-3cm thick) with associated slump folds may be present higher up in the stratigraphy. The top of the Mooidraai Formation, directly underneath the Olifantshoek unconformity, comprises buff coloured massive to brecciated silicified dolomites (Fig. 10.3).

10.2.2 *Middleplaats area*

The slope facies in this area (Fig. 10.5) differs noticeably from the slope facies in the Umtu-Olivepan area, i.e.:

(i) It is much more cherty and fractured towards the top.

(ii) Brecciation is much more common.

(iii) The sandy dolomites can be coarser-grained and are reverse or normally graded, massive bedded, evenly bedded or cross-laminated.

(iv) Cryptalgal laminations, often ferruginised, mark the transition from the Hotazel iron formation into the Mooidraai dolomite formation (Fig. 7.14)

10.3 Organic Built-up Belt

Evidence of a reefal complex, over the Middleplaats palaeohigh, is suggested by the presence of cryptalgal laminae and the gradational character of the transition between the Hotazel iron formation and the Mooidraai dolomite formation in some boreholes (Fig. 10.6). In borehole M13 (Middleplaats 332), a 3.5m thick transition zone is marked by algal laminated ferruginous dolomite alternating with wavy bedded greenalite-magnetite-carbonate rhythmites. Disrupted carbonate flow-layers (carbonate-turbidite flows) in the Upper BIF Unit further to the east (deeper part of the basin), suggest a carbonate source towards the west.

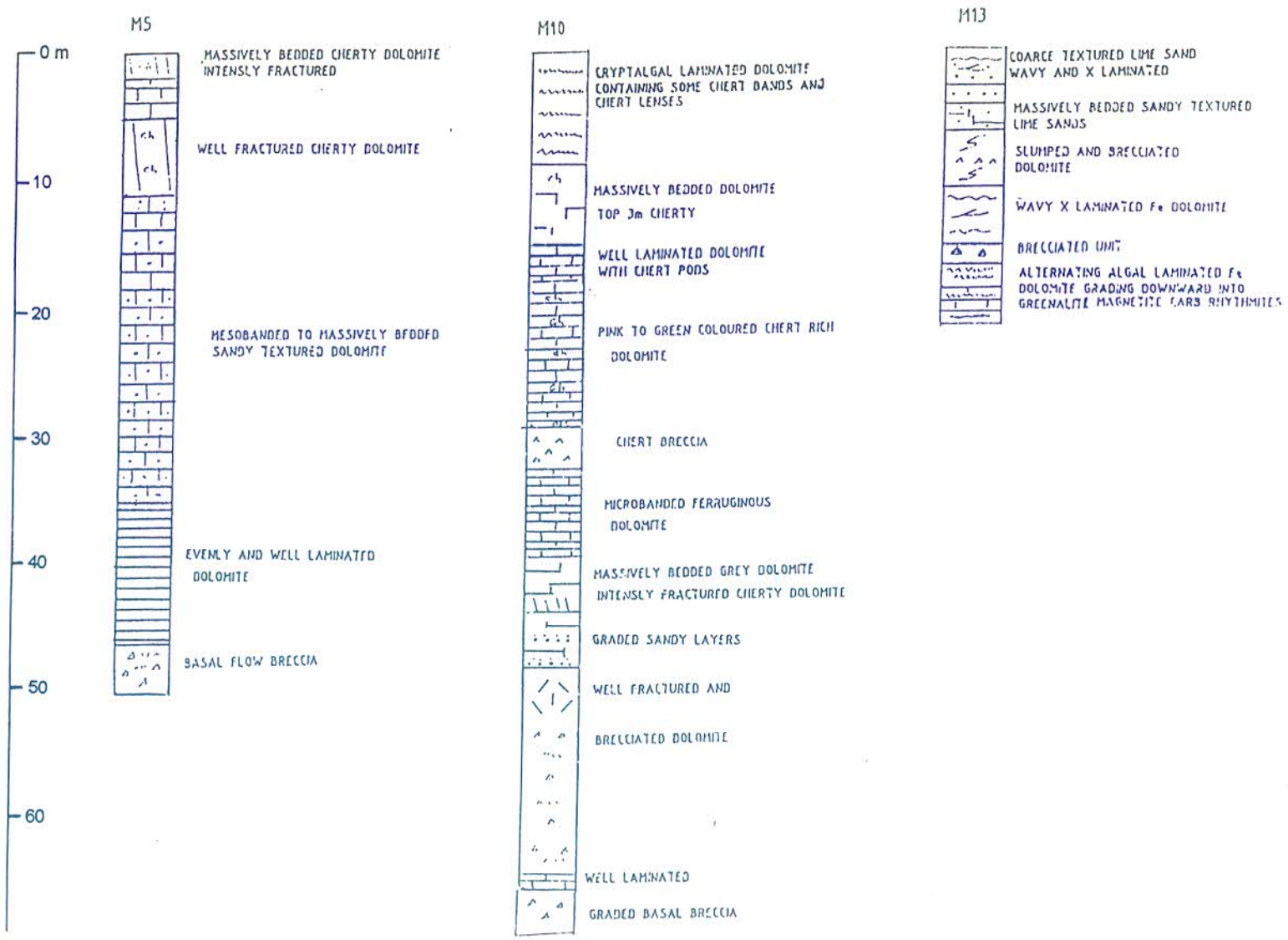

Fig. 10.5 *Stratigraphy of the Mooidraai Formation in the Middleplaats area.*

10.4 Winnowed lime-sand belt

This lithology was discussed in chapter 7.2.2.4 under the heading oolitic-oxide-silicate-carbonate facies (Fig. 7.11). This unit thins towards the south from about 16m in borehole MFT 2 to ± 10m in MFT 4 (Farm Moffat 366; Fig. 5.1). It directly overlies amygdaloidal Ongeluk lava and comprises a ferruginous-oolitic and pelliodal carbonate-rich sequence. Grey-coloured dolomite lenses are often present. The sequence becomes more cherty towards the top. Chert waves and billows alternate with algal laminated mesobands and carbonate turbidite flow layers grading upwards into the cryptalgal laminated dolomites (Fig. 10.7).

10.5 Shelf Lagoonal Facies

This facies is subdivided into three units (Fig. 10.7) i.e.:

Unit 1

The lower unit (Unit 1) comprises grey, dark to dark-grey cryptalgal laminated dolomite with abundant fine disseminated pyrite. This unit thickens towards the southwest from about 16m in borehole MFT 2 to about 39m in borehole MFT 4 (Moffat, 366) over a distance of 1.5km.

Unit 2

Unit 1 is overlain along a sharp contact by a grey-coloured micro - to mesobanded dolomite with pyrite in stylolites and joints. The angle of bedding (in drilhole core) varies throughout the unit and could be a reflection of the presence of large-scale domal stomatolites. The unit thins towards the southwest from 5m at borehole MFT 2 to 3m in borehole MFT 4 (Moffat 366) suggesting that the lime-sand was derived from the platform edge further towards the northeast.

Fig. 10.6 *Gradational contact comprising cryptalgal laminae in the transition between the Hotazel iron formation and the Mooidraai dolomite formation in the Middleplaats (332) area.*

Unit 3

The laminated facies of Unit 2 grades upwards into grey-coloured massively bedded and often brecciated dolomite. Secondary porosity such as calcite-filled veins, fissures and vugs is present. The original thickness of this unit is uncertain because it is truncated at the top by the Olifantshoek unconformity.

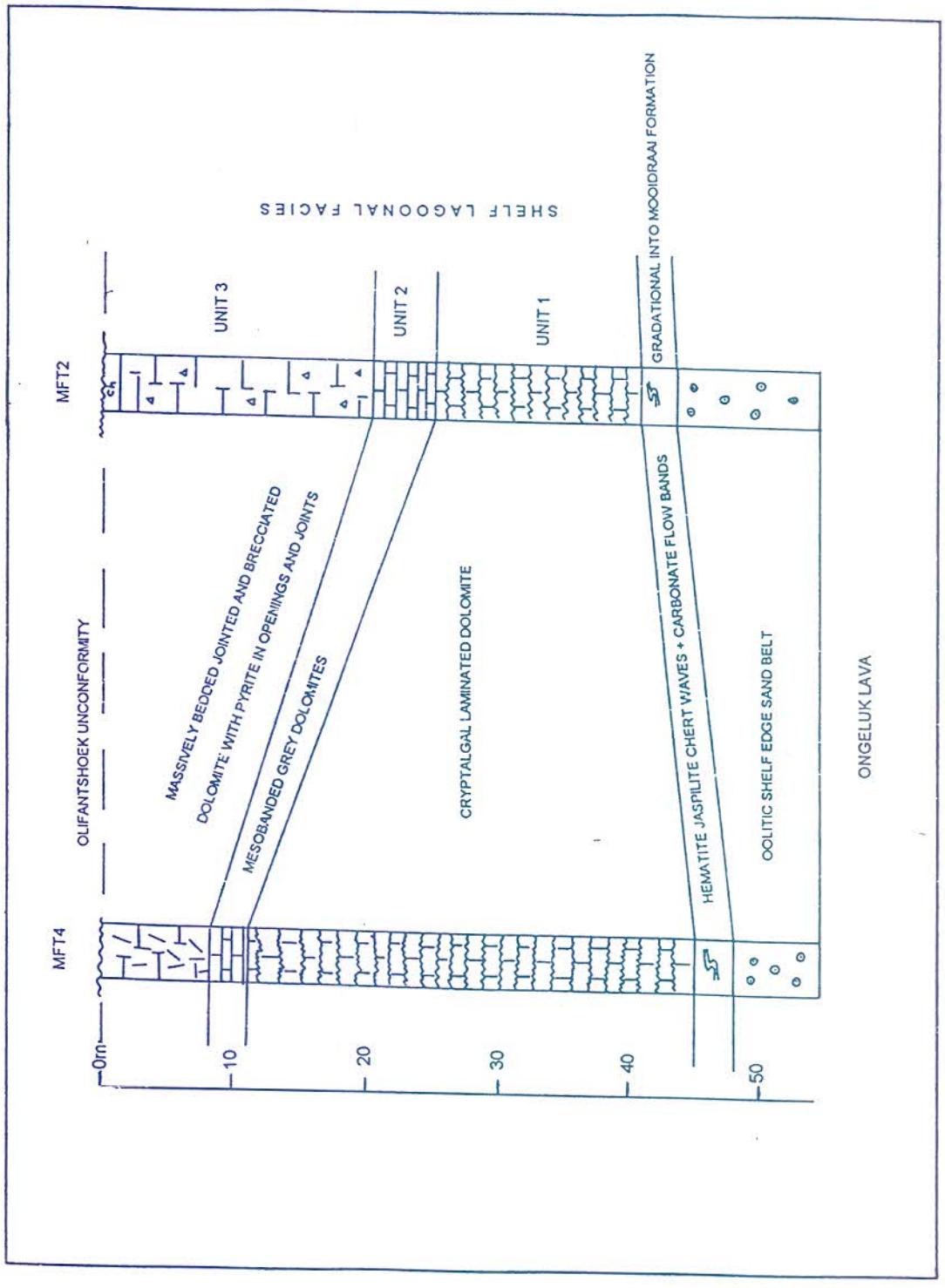

Fig. 10.7 The Mooidraai dolomite stratigraphy on the Farm Moffat 366.

10.6 Depositional setting of the Mooidraai Formation

10.6.1 *Introduction*

Carbonate sediments are born, not made and are formed close to the environment of deposition in three broadly defined environments (Fig. 10.8)of carbonate accumulation (James, 1979). Wilson (1975) further subdivided the expected facies distribution within a carbonate sequence deposited on shelves in tectonically stable areas, into nine standard belts (Fig. 10.1).

10.6.2 *Shelf-edge sand belt*

The thin vineer of ferruginous oolitic sediments capping the Ongeluk lava is regarded as ferruginised dolomite grainstones, representing winnowed platform-edge sands. The unit thins towards the south, indicating a sediment source towards the north or north-east (Fig. 10.9).

Shelf margin sediments commonly comprise a complex of oolitic or skeletal sand shoals (James, 1954). The reefal complex inferred over the Middleplaats palaeohigh could also represent a reef mound. Reef mounds commonly develop a mound cap at the end of the growth cycle (Wilson, 1975). The mound caps may comprise a thin layer of encrusted or lameller forms, domal forms or winnowed lime-sands.

10.6.3 *Shelf lagoonal facies*

The relationship between stromatolitic morphology and depositional environment is well documented by James (1954). Columnar to club shaped forms occur in subtidal or lower intertidal flats rimming headlands, where they are exposed to both wave and tidal action. Domal forms are characteristic of lower energy

environments in the lower to middle intertidal zone and in the vicinity of a protective bank. Horizontal algal units grow preferentially in the low energy high intertidal zone, while digitate column structures tend to develop in tidal pools. The domes are largest in the subtidal or lower intertidal environments, decreasing in size upward and finally merging with strataform mats in the upper intertidal zone above the zone of active sediment movement.

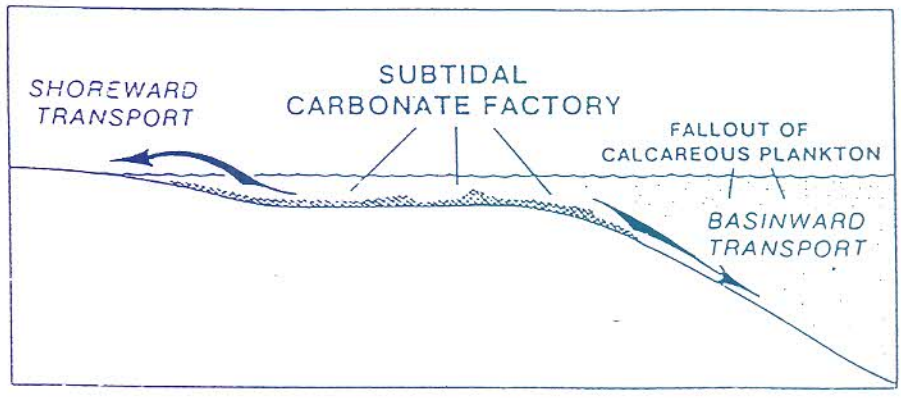

Fig. 10.8 *Main zones of carbonate accumulation, with most of the carbonate in waters less than 30 metres deep (after James, 1979).*

The darkish coloured algal laminated dolomite (Fig. 10.7 and Unit 1 in Fig. 10.9) caps the oolitic shelf edge sand belt and is regarded as algal mats within a low-energy environment. The overlying laminated dolomite unit (Unit 2; Fig. 6.9) can either be regarded as the product of build-up from carbonate debris, periodically shed from the Middleplaats palaeohigh, or it might represent a large domal stromatolite sequence deposited in a deeper subtidal to a lower intertidal environment, in a lagoonal setting. The sharp contact with the underlying Unit 1 favours debris flows as a mechanism of deposition. Variation in the angle of dip of the bedding in drill core (Unit 2) could be indicative of large scale domal

structures. However, the presence of the latter at this stratigraphic level would suggest a deepening of the depositional environment and prograding of a deeper water subtidal facies over an intertidal algal mat facies, which is in contrast to popular belief that carbonate sequences generally show shallowing (shoaling) upwards features (James, 1954). In addition, the contact with the overlying massively bedded unit is gradational, suggesting that these two facies are part and parcel of the same depositional episode.

The absence of internal laminations in the massive micrite (Unit 3) on the farm Moffat (366) suggests that it was deposited in extremely shallow water. Exposure to meteoric water and associated weathering (karstification) could explain the vuggy brecciated and veined character of the unit.

The facies accumulations discussed above are regarded as sediments deposited in belts 6 and 7 of the Wilson (1975) facies model (Fig. 10.1).

10.6.4 Slope Facies

Accumulation rates in carbonate build-ups are characteristically much greater than the rate of subsidence of the shelf (Schlager, 1981), resulting in the development of unstable slopes (overhangs) during progradation into the basin. Slope deposits (James 1954). owe their origin to downslope creep and subsequent dislocation which ultimately lead to movement of large masses of slope material, resulting in gravity flows (turbidity currents).

(i) Umtu Olivepan area (Fig. 10.2)

The graded, slumped, clastic textured rhythmites with silty partings are interpreted as the products of sediment gravity flows (turbidity currents) which moved fine carbonate detritus off the adjacent shallow shelves downslope into the basin (Beukes, 1983). This environment is situated below the wave base at a

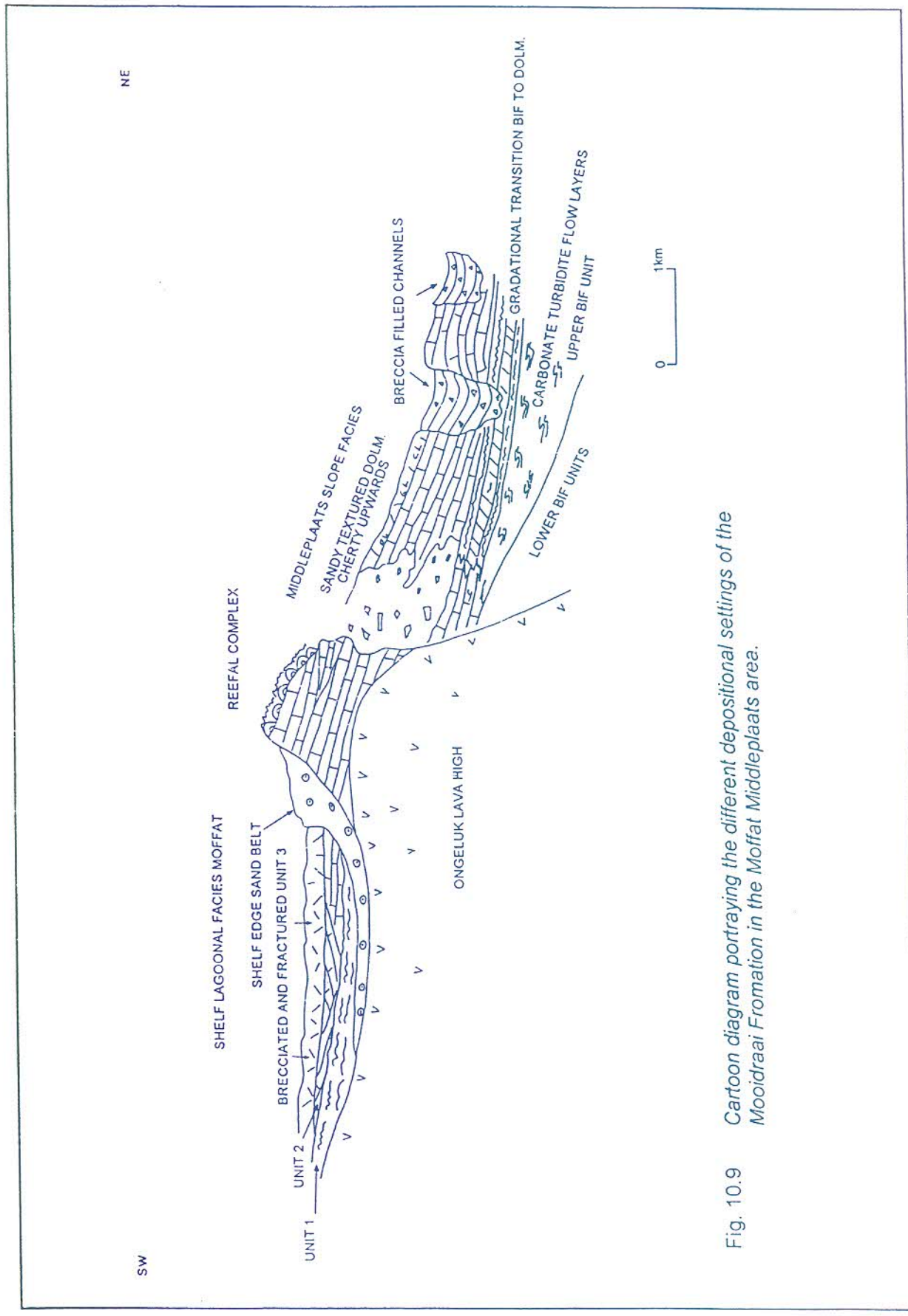

Fig. 10.9 *Cartoon diagram portraying the different depositional settings of the Mooidraai Fromation in the Moffat Middleplaats area.*

depth of 200 to 300m, barely at the oxygen level. The thin silty layers may in part also represent mud which was deposited directly from the surface waters well away from the platform margin. The iron-rich horizons are an indirect result of slow sedimentation (Wilson, 1975). Silica could have been concentrated via evaporatic mechanisms since the seawater was probably already saturated with respect to amorphous silica (Drever, 1974).

The basal breccia forms a laterally extensive sheet, which on the east-west trending Epsom-Olivewood-Olivepan transect, displays a distinctly lenticular geometry, suggesting a channel-type deposit with the long axis trending north-south. It is interpreted as a toe-of-slope slump breccia, with the clasts as either distally derived fragments from the south (Middleplaats palaeohigh), or more proximaliy derived debris (Epsom-Olivewood palaeohigh), or both. The near absence of disrupted carbonate turbidite flow layers in the Upper BIF Unit in boreholes OLP2 and U17 (Fig. 7.1) may suggest a more distal source.

The inferred reefal complex on the Epsom-Olivewood palaeohigh periodically produced material which was carried as debris flows into the basin. The sharp erosional contact at the base of the basal breccia in borehole U17 (Fig. 10.2 and 10.10) is indicative of the base of debris flow deposits.

ii) Middleplaats area

The presence of coarse-grained lime-sand units with more abundant interbedded flow breccia units, suggests a more proximal depositional environment for the slope facies in the Middleplaats area. These lime-sands are massive, with intercalated cross-bedded units. James (1954) proposed two types of depositional environments for such rocks,both may apply here i.e.:

(i) Below a platform margin of considerable slope with an abundant supply of lime-sand, by a mechanism of grain flow (mass flow of cohesionless grains

along steep slopes) rather than as turbidity current deposits, where clasts and grains are supported by fluid turbulence.

Fig. 10.10. *Sharp erosional contact at the base of the basal breccia in borehole U 17.*

(ii) Reworking of previously deposited slope sediments by bottom currents (contourites of Beukes, 1986). The massive beds would be the products of

downslope mass movement produced at a rapid rate near the platform margin during large storms. Sedimentary structures in the cross-bedded deposits indicate the action of bottom currents. These currents often run parallel to the slope or platform margin (contour currents) and may rework the earlier deposits. The currents may also be responsible for winnowing out the upper portion of the turbidites, removing the fine layers and leaving a sequence composed only of shallow water clasts and divisions A and B (Bouma, 1962) of the Bouma sequence, capped by cross-bedded lime-sand.

11. CONCLUSIONS

A volcanogenic-sedimentary model is proposed for the origin of the Kalahari manganese basin.

The basin formed in a topographic low flanking the Middleplaats volcanic palaeohigh. An inferred growth fault adjacent to the palaeohigh induced the half-graben shape of the basin. Seawater from outside the present confines of the basin descended through the more permeable parts of the volcanic pile, became heated with depth and leached Fe, Mn and silica from the Ongeluk lava. These fluids together with metal-laden hydrothermal fluids of volcanogenic origin, introduced the metals to the depository.

The Hotazel iron formation accumulated in a clastic free, stratified water body in which iron and silica were in solution below a redox boundary. Expansion of the redox boundary to relativly shallow depths allowed the transport and precipitation of iron and manganese on the shallow shelves. Progressive precipitation systematically diluted the waters of iron, possibly coupled with a coherent and progressive climatic change and contraction of the redox boundary which initiated the deposition of the Mooidraai Formation. Expansion and contraction of the redox boundary isassumed by many authors to be related to glacial activity (Klein and Beukes, 1989; Carrigan and Cameron, 1993). Evidence for sea-level change is locked up in the rock record of the Postmasburg Group. The onset of the Postmasburg sequence is marked by glacial sediments (Makganyene diamictite) and it was terminated during the deposition of the Mooidraai dolomite.

The Olifantshoek, Dwyka and Kalahari unconformities removed vast thicknesses of the Voëlwater Subgroup. The thickness is nevertheless estimated at 400m [200m Hotazel Formation, 200 m Mooidraai Formation). A major unconformity

separates the chemical and bio-chemical sediments of the Voëlwater Subgroup from clastic sediments of the overlying Olifantshoek Supergroup.

A number of mineralogically and texturally distinct facies were identified in the banded iron formations of the Voëlwater Subgroup. The Epsom-Hotazel transect includes the ellipsoidal intrabasinal Ongeluk lava (Epson) palaeohigh. Shallow water oxide facies (hematite-chert) hosting high-grade (Wessels-type) Mn ore is developed over the Epsom palaeohigh. Towards the east, the BIF units increase in thickness, accompanied by facies changes from hematite-chert through hematite-chert-carbonate, magnetite-chert-carbonate into deeper water greenalite-magnetite-carbonate associations (Fig. 7.1). Further east, on the farm Olivepan 282, riebeckite is prominent in the Upper BIF Unit. Still further east, in borehole G4, the Middle BIF Unit thins to about 4m, consisting mainly of chert-magnetite and carbonate lithologies deposited on the flank of the inferred Hotazel palaeohigh. The hematite-chert and, in places, the magnetite-chert-carbonate facies are characterised by disrupted and wavy bedding, chert billows, pods and pillows. The deeper water silicate facies (greenalite-magnetite-carbonate) comprise evenly microbanded rhythmites which represent the dominant facies-type in the KMB. Deformed carbonate slumped layers, interpreted as gravity flow layers, are interbedded within the silicate facies iron formation in the BIF sequences above the middle manganese horizon, along the Moffat-Mamatwan and Mamatwan-Olivepan transects. There is evidence for three primary or early diagenetic mineral phases: hematite-chert, the iron silicate greenalite and iron carbonate. Most of the magnetite in the magnetite-chert-carbonate assemblages is regarded as primary or early diagenetic.

Secondary mineral phases includes the following:

(i) The bulk of the magnetite in the greenalite-magnetite-carbonate facies possibly formed through the oxidation of Ca-Mg siderite and of greenalite.

(ii) Ankerite formed through the oxidation of siderite.

(iii) Riebeckite formed during the crystallisation of saline pore fluid during diagenesis

(iv) Partial hematisation of the greenalite-magnetite-carbonate facies in the Lower BIF Unit within the southern portion of the basin.

(v) A stilphnomelane bandlutite in the Middle BIF Unit in the southern part of the basin, representing an volcanic ash band.

The basin waters were Eh/pH stratified. Above the chemocline conditions were oxidising and slightly acidic, resulting in the precipitation of hematite-chert (oxide) facies BIF, hosting high-grade oxide facies Mn ore. Below the chemocline, reducing and slightly alkaline conditions favoured the precipitation of greenalite-magnetite-carbonate facies BIF, hosting low-grade, carbonate and silicate-rich Mn ore.

Shallower water features are evident at the contacts between the BIF and hematite-lutite units enclosing Mn ores, suggesting the deposition of manganese during a regressive phase followed by a transgressive phase, resulting in the precipitation of the next BIF unit.

The mineralogical composition of the hematite-lutite, which envelopes the Mn ore horizons, confirms a chemical change in the depositional environment. Higher Eh conditions during the onset of a regressive phase caused a change in the precipitate from BIF to a hematite-lutite mudstone. No free silica in the form of quartz or chert is present, while the carbonate content increased markedly, indicating a rise in pH that ultimately resulted in the precipitation of manganese. The next transgression caused a gradual drop in Eh and pH, ending the deposition of Mn, and causing the deposition of the next hematite-lutite, followed by a BIF phase.

The Mooidraai Formation is divided into four broad facies:

(i) Slope facies along the south-western boundary of the Kalahari basin, extending north and north-east into the basin,

(ii) An organic build-up belt on the shelf margin.

(iii) A winnowed (shelf-edge) lime-sand belt.

(iv) Shelf lagoon facies developed towards the middle shelf, west of the Middleplaats palaeohigh.

REFERENCES

Alterman, W. and Hälbich, I. (1990). Thrusting, folding and stratigraphy of the Ghaap Group along the south-western margin of the Kaapvaal Craton. S. Afr. J. Geol., v. 93, pp. 553-566.

Alterman, W. and Hälbich, JW. (1991). Structural history of the south-western corner of the Kaapvaal Craton and adjacent Namaqua Realm. New observations and a re-appraisal. Precam. Res., v. 52, pp. 133-166.

Behrend, F. (1936). Eisen und Schwafet fordende Gasquellenaus den Kameni Inseln. In: Reck, H.(ed). Santoren der Werdegang eines Inselvulkans und sein Ausbruch, 1925-1928, 2, Andrews and Steiner, Berlin, pp 323-327.

Beukes, NJ. (1973). Precambrian iron formations of Southern Africa. Econ. Geol. v. 68, pp. 960-1004.

Beukes, NJ. (1978). Die karbonaatgesteentes en sy ysterformasies van die Ghaap Groep van die Transvaal-Supergroep in Noord-Kaapland. PhD thesis (unpubl.), Rand Afrikaans Universiteit, Johannesburg, 580 p.

Beukes, NJ. (1980). Stratigrafie en litofasies van die Campbellrand-Subgroep van die Proterofitiese Ghaap-Groep,Noord-Kaapland. Trans. Geol. Soc S. Afr., v. 83,pp141-170.

Beukes, NJ. (1980a). Lithofacies and stratigraphy of the Kuruman and Griquatown iron-formations, northern Cape Province, South Africa. Trans. Geol. Trans. Geol. Soc. S. Afr., v. 83, pp. 69-86.

Beukes, NJ. (1980b). Suggestions towards a classification of and nomenclature for iron formations. Trans. Geol. Soc. S. Afr., v. 83, pp 285-290.

Beukes, NJ. (1983). Palaeoenvironmental setting of iron-formations in the depositional in of the Transvaal Supergroup, South Africa. In: Trendall, A.F. and Morris, R.C. (Eds.), Iron-formation: Facts and Problems, Elsevier, Amsterdam, pp. 131-209.

Beukes, NJ. (1984). Sedimentology of the Kuruman and Griquatown iron-formations, Transvaal Supergroup, Griqualand West, South Africa. Prec. Res., v. 24, pp. 47-84.

Beukes, NJ. (1985). Finale verslag oor die sishen ystererts en Kalahari mangaan afsettings. CSIR National Geoscience programme, unpubl. open file report, 49 p.

Beukes, NJ. (1986). The Transvaal Sequence in Griqualand West. In: Anhauesser, C. and Maske, S. (Ed.) Mineral deposits of Southern Africa. Geol. Soc. S. Afr., v. 1, pp. 819-828.

Beukes, NJ. (1987). Faciers relations, depositional environments and diagenesis in a major early Proterozoic stromatolitic carbonate latform to basinal sequence, Campbell Rand Subgroup, Transvaal Supergroup, Southern Africa. Sedimentary Geology, v. 54, pp. 1-46.

Beukes, NJ and Smit, CA. (1987a).. New evidence for thrust faulting in Griqualand West, South Africa: IIOmplication for stratigraphy and the age of red beds. S. Afr. Jnl. Geol., v. 90, pp. 378-394.

Beukes, NJ. (1989). Report on the stratigraphic correlation of a sequence of shale, lava and mafic intrusive intersected in Borehole 2217 near Vostershoop, Northern Cape Province. Unpubl. report for Gencor, 6 p.

Beukes, NJ, Klein, C, Kaufman, AJ and Hayes, JM. (1990). Carbonate petrography, kerogen distribution and carbon and oxygen isotope variation in an Early Proterozoic transition from limestone to iron-fortmation depostion, Transvaal Supergroup, South Africa. Econ. Geol., v. 85, pp. 663-668.

Beukes, NJ, Burger, AM and Gutzmer, J. (1995). Fault-controlled hydrothermal alteration of Paleoproterozoic manganese ore in Wessels Mine, Kalahari Manganese field. S. Afr. Jnl. Geol., v. 98, No. 4, pp. 430-451.

Bishoff, JL, and Dickson, FW. (1975). Seawater-basalt interaction at 200°C and 500 bars: implications for origin of sea-floor heavy-metal deposits and regulation of sea-water chemistry. Earth Planet. Sci. Lett., v. 25, pp. 385-397.

Boardman, LG. (1964). Further geological data on the Postmasburg and Kuruman Manganese ore deposits, Northern Cape Province. In: Haughton, SH (ed.). The geology of some ore deposits in Southern Africa, v. II, Geological Soc. S.A., pp. 415-439.

Bonatti, E. (1967). Mechanism of deep sea volcanism in the South Pacific. In: Abelson, PH (ed.) Researches in geochemistry, v. 2, John Wiley and Sons Inc., New York, pp. 453-491.

Bonatti, E., Kraemer, T. and Rydell, HS. (1972). Classification and genesis of submarine iron-manganese deposits In: Horn, DR (ed) Ferromanganese deposits on the ocean floor. National Science Foundation, Washington, pp. 159-166.

Bonatti, E, Zerbi, M, Kay, R and Rydell, H. (1976). Metalliferous deposits from the Apennine Ophilites: Mesozoic equivalents of modern deposits from oceanic spreading centres. Geol. Soc. of America Bulletin, v. 87, pp. 83-94.

Boström, K. (1973). The origin and fate of ferromanganoan active ridge sediments. Stockholm Contrib. Geol., v. 24, pp. 149-243.

Boström, K. (1976). Particulate and dissolved matter as sources for pelagic sediments Acta Univ. Stockholm., Stockholm Contrib. Geol., v. 30, pp. 17-79.

Boström, K. (1976a). Submarine volcanism as a source for metalliferous deposits of iron and manganese. Geology and Geochemistry of manganese, Symposium 104.3, 25Th. Int. Geol. Congr., Abstracts, v. 3, pp. 761-762.

Boström,.K, Joensuu, O, Valdés, S., Charm, W, and Glaccum, R. (1976). Geochemistry and origin of East Pacific sediments samples during DSDP Leg34. In: Yeats, RS (eds). Initial reports of the deep sea drilling projects, v. 34, Washingtron, pp. 559-574.

Bott, M.P.H. (1976). Formation of sedimentary basins of graben type by extention of continental crust. Tectonophysics, 36, pp. 77-86.

Bott, M.P.H. (1982). Origin of the lithospheric tension causing basin formation. Philos. Trans. R. Soc. London, A305, pp. 319-324.

Bouma, AH (1962). Sedimentology of some flysch deposits. Amsterdam, Elsevier, 168 p.

Brown, LF, Fisher, WL. (1977). Seismic-stratigraphic interpretation of depositional systems: examples from the Brazilian rift and pull apart basins. In: Paton, CE (ed.). Seismic stratigraphy applications to hydrocarbon exploration. AA. PG, Memoir 26, pp. 213–248.

Burger, AM and Beukes, NJ. (1995). Fault controlled hydrothermal alteration of Proterozoic manganese ore in Wessels Mine, Kalahari manganese field, South Africa, Ext. Abstr., Geocongress '95, Geol. Soc. S. Afr., pp. 60-62.

Button, A. (1976). Iron-formation as an end member in carbonate-sedimentary cycles in the Transvaal Supergroup, South Africa. Econ. Geol., v. 71, pp. 193-2091.

273.

Cann, JR, Winter, CK and Pritchard, RG. (1977). A hydrothermal deposit from the floor of the Gulf of Aden. Min. Mag., v. 41, pp. 193-199.

Cannon, WF and Force, ER. (1983(. Potential for shallow high grade manganese deposits in North America. In: Shanks, WC (ed.). Unconventional mineral deposits. Am. inst. Mining Metall. Petroleum engineers, New York, pp. 175-190.

Carrigan, WJ and Cameron, EM. (1991). Petrological and stable isotope studies of carbonate and sulphide minerals from the Gunflint Formation, Ontario: evidence for the origin of early Proterozoic iron formation. Precambrian Research, v. 52, pp. 347-380.

Castro, LO. (1994). Genesis of banded iron - formations. Econ. Geol., v. 89, pp. 1384-1397.

Chenny, ES, and Winter, H. (1995). The late Archean to Mesoproterozoic major unconformity bounded units of the Kaapvaal Province of Southern Africa. Precam. Res., v. 74, pp. 203-233.

Cilliers, JJ le R. (1961). The nature and origin of the rocks of the Lower Griqualand Stage and the associated deposits of amphibole asbestos in the Northern Cape with special reference to the Koegas-Prieska area. Unpubl. D.Sc thesis, Univ. of Pretoria.

Clendenin, CW and Maske, S. (1986). Indentification of syndepositional tectonics within the Transvaal sedimentary basin. Ext. Abstr., Geocongress '86, Geol Soc. S. Afr., pp. 501-504.

Collins, WH, Quirke, TT and Thomson, E. (1926). Michipicoten iron ranges. Canad. Geol. Survey Mem. 147, pp. 1-161.

Corliss, JB, Lyle, M and Dymond, J (1978). The chemistry of hydrothermal mounds near the Galapagas rift. In: Earth Planet. Sci. Letters, v. 40, pp. 12-24.

Cornell, DH. (1987). Stratigraphy and petrology of the Hartley Hill Basalt Formation, Northern Cape Province. S. Afr. Jnl. Geol., v. 90 pp. 7-24.

Cornell, DH. and Schutte, SS. (1995). A volcani-exhalative origin for the world's largest (Kalahari) manganese field. Mineral Deposita, v. 30, pp146-151.

Crerar, DA and Anderson, GM. (1971). Solubility and solvation reactions of quartz in dilute hydrothermal solutions. Chem. Geology, v. 8, pp. 107-122.

Crockett, RN. (1972). The Transvaal system in Botswana: its geotectonic and depositional environment and special problems. Trans. Geol. Soc. S. Afr., v. 75, pp. 275-292.

Curtis, CD and Spears, DA. (1968). The formation of sedimentary iron minerals. Econ Geol. v. 63, pp. 257-270.

De Villiers, PR. (1970). The geology and mineralogy of the Kalahari manganese field north of Sishen, Cape Province. Mem. Geol. Survey, S. Afr., v. 59, 85 p.

De Villiers, PR and Visser, JNJ. (1977). The glacial beds of The Griqualand West Supergroup as revealed by four deep boreholes between Postmasburg and Sishen: Trans. Geol. Soc. S. Afr., v. 80, pp. 1-8.

De Villiers, JE. (1983). The manganese deposits of Griqualand West, South Africa: some mineralogic aspects. Econ. Geol., v. 78, pp. 1108-1118.

De Vries Klein, G. (1991). Rationale for modern basin analysis applied to ore deposits. In: Force, ER, Eidel, JJ and Maynard, JB (eds). Sedimentary and diagenetic mineral deposits: a basin analysis approach to exploration. Review in Economic Geology, v. 5, Society of Economic Geologists, v. 5, pp. 21-23.

Dimroth, E. (1976). Aspects of sedimentary petrology of cherty iron-formation. In: wolf. KH. (ed) Handbook of strata-bound and strata-form ore deposits, v. 7, Elsevier, Amsterdam, pp. 203-247.

Dimroth, E. (1979). Facies Models 15. Models of physical sedimentation of iron formations. In: Walker, RG. (ed).Facies models. Geoscience Canada, Reprint Series 1, pp. 175-182.

Dimroth, E. (1979a). Facies Models 16. Diagenetic facies of iron formation. In: Walker, RG (ed) Facies Models. Geoscience Canada, Reprint Series 1, pp. 183-190.

Dimroth, E. and Chauvell,JJ. (1973). Petrography of the Sokoman iron formation in part of the Central Labrador Trough, Quebec, Canada. Geol. Soc. Amer. Bull. v. 84, pp 111-184.

Dixon, R. (1989). Sugilite and associated metamorphic silicate minerals form Wessels Mine, Kalahari manganese field. Dep. Min. En. Aff., Geol. Surv., Bull, 93, 44 p.

Drever, JI. (1974). Geochemical model for the origin of Precambrian banded iron-formations. Geol. Soc. of Amer. Bull., v. 85 pp. 1099-1106.

Edwards, AB. (1958). Oolitic iron formations in northern Australia. Geol. Rundschau, v. 47, pp. 668-682.

Eichler, J. (1976). Origin of Precambrian banded iron-formation. In: Wolf, KH (ed.), Handbook of strata-bound and stratiform ore deposits, v. 7., Elsevier, pp. 157-197.

Eidel, JJ. (1991). Basin analysis for the mineral industry. In: Force, ER, Eidel, JJ and Maynard, JB (eds). Sedimentary and diagenetic mineral deposits: a basin analysis approach to exploration. Reviews in Economic Geology, Society of Economic Geologists, v. 5, pp. 1-15.

Eriksson, PG, Meyer, R and Botha, WJ. (1988). A hypothesis on the nature of the Pretoria Group basin. S. Afr. Jnl. Geol. v. 91, pp. 490-497.

Eriksson, PG, Schweitzer, JK, Bosch, PJA, Schereiber, UM, Van Deventer, JL and Hatton, CJ. (1993). The Transvaal sequence an overview. Jnl. of African Earth Sciences, v. 16, no. 1/2, pp 25-51.

Eugster, HP. (1969). Inorganic bedded cherts from the Magadi area, Kenya. Contri. Min. and Petr., v. 22, pp 1-31.

Eugster, HP and Ming Chou, I. (1973). The depositional environments of Precambrian banded iron-formation. Econ. Geol., v. 68, pp. 1144-1168.

Fockema, PD. (1967). Corcidolite and associated rocks of the Kuruman area in the Northern Cape. Unpubl. PhD. Thesis, Univ. of Witwatersrand.

Force, ER and Cannon, WF. (1988). Depositional model for shallow-marine manganese deposits around black shale basins. Econ. Geol., v. 83, pp. 93-117.

Force, ER and Maynard, JB. (1991). Manganese: syngenetic deposits on the margins of anoxic basins. In: Force ER, Eidel JJ, Maynard, JB (Eds). Sedimentary and diagenetic mineral deposits: a basin analysis approach to exploration. Rev. in Econ. Geol. v. 5, Soc. of Econ. Geol., pp. 147-157.

Fournier, RO. (1985). The behaviour of silica in hydrothermal systems. In: Berger, BR and Bethke, PM (eds). Geology and geochemistry of epithermal systems. Reviews in Economic Geol., v. 2, Soc. of Econ. Geol., pp. 45-62.

Frakes, LA and Bolton, BR. (1984). Origin of manganese giants: sea-level change and anoxic-oxic history. Geology, v. 12, pp. 83-86.

Frakes LA. and Bolton, BR. (1992). Effects of ocean chemistry, sea level and climate on the formation of primary sedimentary manganese ore deposits. Econ. Geol., v. 87, pp1207-1217.

French, BM. (1968). Progressive contact metamorphism of the Biwabik iron formation, Mesabi Range, Minnesota. Minnes, Geol. Survey Bull., v. 45, 103 p.

French, BM. (1973). Mineral assemblages in diagenetic and low-grade metamorphic iron-formation. Econ. Geol., v. 68, pp. 1063-1074.

Garrels, RM and Christ, CL. (1965). Solution, minerals and equilibria. Harper and Row and John Weatherhill Inc., 450 p.

Garrels, RM. (1987). A model for the deposition of the microbanded Precambrian iron formations. American Journal of Science, v. 287, pp. 81-106.

Geerthsen, K. Maher, MJ and Meyer, R. (1991). The western edge of the Griqualand West Basin - a geophysical perspective. SA Journ. Geol., v. 94, pp. 96-103.

Gillis, KM and Robinson, PT. (1985). Low temperature alteration of the extrusive sequence Troodus Ophiolite, Cyprus. Canad. Mineral., v. 23, pp. 432-441.

Goodwin, AM. (1956). Facies relations in the Gunflint iron formation. Econ. Geol., v. 51, pp. 565-595.

Goodwin, AM. (1973). Archean iron formations and tectonic basins of the Canadian Shield. Econ. Geol., v. 68, pp. 915-933.

Govett, GJS. (1966). Origin of banded iron-formations. Geol. Soc. American Bull., v. 77, pp. 1191-1212.

Gross, GA. (1965). Geology of iron deposits in Canada, v. 1: General geology and evaluation of iron ore deposits. Cand. Geol. Surv., Econ. Geol. Rept, 22, 181 p.

Gross, GA. (1970). Nature and occurrence of iron deposits: iron ore deposits of Canda and the West Indies. In United Nations survey of world siron ore resources. United Nations Publ. sales no. E. 69, II c.4, New York, pp. 13--31 and 237-269.

Gross, GA. (1973). The depositional environment of principal types of Precambrian iron-formations. In: Genesis of Precambrian iron and manganese deposits. Unesco Earth Sci. 9, Paris, pp. 15-21.

Gross, GA. (1980). A classification of iron formations based on depositional environments. Canadian Mineralogist, v. 18, pp. 215-222.

Gross, GA. (1983). Tectonic system and the deposition of iron-formations. Precamrian Research, v. 20, pp. 171-187.

Gross, GA. (1991). Genetic concepts for iron-formations and associated metalliferous sediments. Economic Geol. Monograph 8, pp. 51-81.

Gruner, JW. (1992). The origin of sedimentary iron-formations: The Biwabik formation of the Mesabi Range. Econ. Geol., v. 17, pp. 407-460.

Gutzmer, J and Beukes, NJ. (1995). Fault controlled metasometic alteration of the early Proterozoic sedimentaryt manganese ores in the Kalahari manganese field. Econ. Geol., v. 90, pp. 823-844.

Hälbich, IW, Lamprecht, D, Alterman, W and Horstman, Ue. (1992). A carbonate-banded iron formation transition in the earlky Proterozoic of South Africa. Jnl. Afr. Earth Sci., v. 15, No. 2, pp. 217-236.

Hälbich, IW, Scheepers, R, Lambrecht, D, Van Deventer, JL, De Kok, NJ. (1993). The Transvaal-Griqualand West banded iron formation: geology, genesis, iron exploration. Jnl. Of Afr. Earth Sci., v. 16, pp. 63 – 120.

Han, TM (1972). Diagenetic-metamorphic replacement in the Negaunee formation of the Marquette iron range, Lake Superior District. Soc. Mining Geologists Japan, Spec. Issue 3, pp. 430-438.

Hannekom, HJ. 1966). The crocidolite deposits of the Northern Cape Province. Unpubl. DSc thesis, Univ of Pretoria.

Hem, JD. (1972). Chemical factors that influenced the availability of iron and manganese in aqueous systems. Geol. Soc. of America Bulletin, v. 83, pp. 443-450.

Holland, HD. (1973). A possible source of iron in iron-formations. Econ. Geol., v. 68, pp. 1169-1172.

Hough, JL. (1958). Fresh-water environment of deposition of Precambrian banded iron formation. Jnl. Sediment petrol., v. 28, pp. 414-430.

Holland, HD. (1984). The chemical evolution of the atmosphere and oceans. Princeton series in Geochemistry, Princ. Univ. Press, 582 p.

James, HL. (1954). Sedimentary facies of iron-formation. Econ. Geol., v. 49, pp. 235-293.

James, HL. (1966). Chemistry of iron-rich sedimentary rocks. U.S. Geol. Sur. Prof Paper 440 - W, 61 p.

James, NP (1979). Facies model 10. Shallowing-upwards sequences in carbonates. In: Walter, RG. (ed.) Facies models, Geological Association of Canada, Geoscience Canada Reprint Series 1, pp. 109-119.

James, NP. (1984a) Introduction to carbonate facies models: shallowing – upward sequences in carbonates. In: Walker, RG (ed.) Facies models, 2nd Edit. Geol. Canada, Reprint Ser. 1, pp. 209-244.

Jansen, E. (1983). Die stratigrafie en sedimentologie van die Volop-Groep Olifantshoek-opeenvolging. Unpubl. M.Sc-thesis, Rand Afriaans Univ.

Kimberley, MM. (1974). Origin of iron formation by diagenetic replacement of calcareous oolite. Nature, v. 250, pp. 319-320.

Kimberley, MM. (1978). Paleoenvironmental classification of iron formations. Econ. Geol., v. 73, pp. 215-229.

Kimberley, MM. (1979). Geochemical distinctions among environmental types of iron-formations. Econ. Geol., v. 25, pp. 185-212.

Kimberley, MM. (1989). Nomenclature for iron formations. Ore Geology Reviews, v. 5, pp. 1-12.

Kimberley, MM. (1989a). Exhalitive origins of iron formations. Ore Geology Reviews, v. 5, pp. 13-145.

Klein, C. (1974). Greenalite, stilpnomelane, minnesotatite, crocidolite and carbonates in a very low-grade metamorphic Precambrian iron formation. Can. Miner., v. 12, pp. 475-498.

Klein, C, and Bricker, P. (1977). Some aspects of the sedimentary and diagenetic environment of Proterozoic banded iron-formation. Econ. Geol., v. 72, pp. 1457-1470.

Klein, C. (1983). Diagenesis and metamorphism of Precambrian banded iron formations. In: Trendall, AF and Morris, RC (eds). Iron formation: facts and problems, Elsevier, pp. 417-469.

Klein, C., Beukes, NJ. and Scopf, JW. (1987). Filamentous microfossils in the early Proterozoic Transvaal Supergroup: their morphology , significance and paleoenvironmental setting. Precambrian, Research, v. 36, pp. 81-94.

Klein, C and Beukes, NJ. (1989). Geochemistry and sedimentology of a facies transition from limetone to iron-formation deposition in the Early Proterozoic Transvaal Supergroup, South Africa. Econ. Geol., v. 84, pp. 1722-1774.

Kleyenstüber, ASE. (1984). The mineralogy of the manganese bearing Hotazel Formation of the Proterozoic Transvaal Sequence in Giqualand West, South Africa. Trans. Geol. Soc. S. Afr., v. 86, pp. 257-272.

Kleyenstüber, ASE. (1985). A regional mineralogical study of the manganese-bearing Voëlwater Subgroup in the Northern Cape Province. Unpubl. PhD thesis, Rand Afrikaans University, Johannesburg. 328 p.

Krauskopf, KB. (1956). Seperation of manganese from iron in the formation of manganese deposits in the volcanic association. 20Th. Int. Geol. Cong. Mexico, 1956, Manganese Symposium, v 1, pp. 119-131.

Krupp, R, Orberthür, T and Hirdes, W. (1994). The early Precambrian atmosphere and hydrosphere: thermodynamic constraints from mineral deposits. Econ. Geol., v. 89, pp. 1581-1598.

La Berge, GL. (1964). Development of magnetite in iron-formations of the Lake Superior region. Econ. Geol. v. 59, pp. 1313-1342.

Lepp, H and Goldich, SS. (1964). Origin of Precambrian iron-formation. Econ Geol., v. 59, pp. 1025-1060.

MacGregor, AM. (1927). Problem of Precambrian atmosphere. South African Jnl. Sci. v. 24, pp. 155-172.

Maynard, JB. (1991). Iron: syngenetic deposition controlled by the evolving ocean - atmosphere system. In: Force, ER, Eidel, JJ and Maynard, JB .

Sedimentary and diagenetic mineral deposits: a basin analysis approach in exploration. Reviews in Economic Geology, v. 5., Soc. Econ. Geol., pp. 141-145.

Miall, AD. (1990). Principles of sedimentary basin analysis. Springer - Verslag, New York, 668 p.

Miyano, T. and Beukes, NJ. (1987). Physiochemical environments for the formation of quartz-free manganese oxide ores from the Early Proterozoic Hotazel Formation, Kalahari Manganese field, South Africa. Econ. Geol., v. 82, pp. 706-718.

Moore, ES and Maynard, JE. (1929). Solution, transportation and precipitation of iron and silica. Econ. Geol., v. 24, pp. 282-303, pp. 365-402, pp. 506-527.

Morris, RC. (1980). A textural and mineralogical study of the relationship of iron ore to banded iron-formations in the Hamersley Iron Province of Western Australia. Econ. Geol., v. 75, pp. 184-209.

Morris, RC. (1993). Genetic modelling for banded iron - formations of the Hamersley Group, Pilbara Craton, Western Australia. Precambrian Research, v. 60, pp. 243-286.

Morris, RC. and Horwitz, RC. (1983). The origin of the iron-formation- rich Hammersley Group of Western Australia - deoposition on a platform. Precambrian Research, v. 21, pp. 273-297.

Nel, CJ. (1984). Die mineralogie en geochemie van die Mamatwan-ertsligaam, Kalaharimangaanveld, Transvaal-Supergroep. Unpubl. M.Sc. thesis, Rand Afrikaans University, Johannesburg, 119p.

Nel, CJ, Beukes, NJ and De Villiers, JPR. (1986). The Mamatwan manganese mine of the Kalahari Manganese field. In: Anhauesser, C and Maske, S. Mineral Deposits of Southern Africa, v. 1, Geol., Soc. S. Afr., pp. 963-978.

Nicholson, K. (1992). Contrasting mineralogical – geochemical signatures of manganese oxides. Guides to metallogenesis. Econ. Geol. V. 87, pp. 1253-1264.

Norrish, K. and Hutton, J.T. (1969). An accurate X-ray spectrographic method for analysis of a wide range of geological samples. Geochim. Cosmochim. Acta, 33, pp. 431-453.

Rona, PA and Scott, SD. (1993). A special issue on sea floor hydrothermal mineralization: new perspectives - preface. Econ. Geol., v. 88, pp. 1933-1976.

Rossignol-Strick, M. (1987). Rainy periods and bottom water stagnation initiating brine accumulation and metal concentrations - Precambrian gold-uranium ore beds and banded iron formations. Paleoceanography, v. 2, pp. 379-394.

Roy, S. (1981). Manganese deposits. London Academic Press, 458 p.

Roy, S. (1992). Environments and processes of manganese deposition. Econ. Geol., v. 87, pp. 1218-1236.

Sakamoto, T. (1950). The origin of Precambrian banded iron ores. Amer. Jnl. Sci., v. 248, pp. 449-474.

Schidlowski, M. (1987). Photoautotrophie und evolution des ivdischen sauerstaffbudgets. In: Joenicke, R. (ed.). Atmosphärische Spurenstaffe. Weinheim, VCH-Verlagsgellschaft pp. 377-396.

Schissel, D. and Aro, P. (1992). The major early Proterozoic sedimentary iron and manganese deposits and their tectonic setting. Econ. Geol., v. 87, pp. 1367-1374.

Schlager W. (1981). The paradox of drowned reefs and carbonate platforms: Geol. Soc. of Amer. Bulletin, v. 92, pp. 197-211.

Schutte, SS. (1992). Ongeluk volcanism in relation to the Kalahari manganese deposits. Unpubl. PhD thesis University of Natal, Durban, 266 p.

Scott, RB and Hajash, A. (1976). Initial submarine alteration of basaltic pillow lavas: a microprobe study. Amer. Jour. Sci., v. 276, pp.480-501.

Sheu, DD and Presley, BJ. (1986). Formation of hematite in the euxinic Orca basin, northern Gulf of Mexico. Marine Geology, v. 69, pp. 309-321.

Sheu, DD, Shakur, A, Pigott, JD, Wiesenburg, DA, Bookes, JM and Krouse, HR. (1988). Sulfur and oxygen isotopic compositions of dissolved sulfate in the Orca Basin: implications for the origin of the high salinity brine and oxidation of sulphides at the brine-seawater interface. Marine Geology, v. 78, pp. 303-310.

Siever, R. (1971). Low temperature geochemistry of silicon. In: wedepohl, KH (ed). Handbook of geochemistry, vii - 7, section 14. Springer - Verlag, Heidelberg.

Simonson, BM. (1985). Sedimentology of cherts in the early Proterozoic Wishardt Formation, Quebec - Newfoundland, Canada. Sedimentology, v. 32, pp. 23-40.

Svitalski, N. (1937). Kriv Rog and the iron ores of this district. 17th. Internat. Geol. Cong., Moscow, Handbook No. 4, pp. 51-77.

Thomas, RJ, Van Veh, MW and Macourt. (1993). The tectonic evolution of South Africa: an overview. Jnl. of African Earth Science, v. 16, No. 1/2, pp. 5-24.

Toth, JR. (1980). Deposition of submarine crust rich in manganese and iron: Geol. Soc. America Bull, v. 91, pp. 44-54.

Trendal, AF. (1973). Precambrian iron-formations of Australia. Econ. Geol. v. 68, pp. 1023-1034.

Trendal, AF. (1973a). Time distribution and type-distribution of Precambrian iiron-formations in Australia. In: Genesis of Precambrian iron and manganese deposits, Proc. Kief. Symp., 1970. Unesco, Paris, pp.49-57.

Trendal AF. (1973). Precambrian iron-formations of Australia. Econ. Geol., v. 68, pp. 1023-1034.

Trendall, AF and Blockley, Jg. (1970). The iron-formations of the Precambrian Hamersley Group, Western Australia, with special reference to the associated crocidolite. West. Aust. Geol. Sur., Bull. 119, 366 p.

Tsikos, H. (1994). The mineralogy and geochemistry of the Voëlwater banded iron-formation, Northern Cape Province. Unpbl. Msc. thesis, Rhodes University,m 152 p.

Van Hise, CR and Leith, CK. (1911). Geology of the Lake Superior region. US Geol. Survey Mon. 52, 641 p.

Van Schalkwyk, JF and Beukes, NJ. (1986). The Sishen iron ore deposit, Griqualand West. In: Anhaeusser, C and Maske, S (eds). Mineral deposits of Southern Africa, v. 1, Geol. Soc. s. Afr., pp. 931-956.

Visser, JNJ. (1971). The deposits of the Griqualand glacial member in the Transvaal Supergroup. Trans. Geol. Soc. S. Afr., v. 74, pp. 187-199.

Walther, JV and Helgeson, HC. (1977). Calculation of the thermodynamic properties of aqueous silica and the solubility of quartz and its polymorphs at high pressures and temperatures. Am. Jnl. Sci., v. 277, pp. 1315-1351.

Williams, TM and Owen, RB. (1992). Geochemistry and origins of lacustrine ferromanganese nodules from the Malawi rift, Central Africa. Geochem. Cosmochim, Acta, v. 56, pp. 2703-2712.

Wilson, J.L. (1975). Carbonate facies in geologic history. Springer-verlag, 471 p.

Zelenov, NK. (1958). On the discharge of iron in solution into the Okhotzk Sea by thermal springs of the Ebeko Volcano (Paramushir Island). Akad. Nauk SSSR Doklady, v. 120, pp. 1089 - 1092.

APPENDIX

ANALYSIS OF BOREHOLES

	1	1	1	1	1	2	2	2	2	2	3	3
	Bif 1/OLP2	LBH1/OLP2	LBP1A/OLP2	RBCHP/OLP2	UBH2/OLP2	Bif1/EMP5	OX1/EPM5	OX2/EPM5	UBH2/EPM5	UBH1/EPM5	Bif1/OLW7	UBH-2/OLW7
SiO2	27.13	19.62	29.22	38.74	16.07	42.03	47.9	38.03	52.02	12.81	20.45	18.07
TiO2	0.03	0.04	0.04	0.04	0.04	0.04	0.03	0.04	0.04	0.04	0.04	0.05
Al2O3	0.28	0.19	0.25	0.18	0.24	0.37	0.13	0.14	0.39	0.21	0.29	0.26
Fe2O3	34.85	42.08	57.18	44.12	31.19	55.49	50.8	61.06	46.36	46.67	52.08	47.08
MnO	7.07	14.35	2.02	0.23	12.07	0.13	0.05	0.05	0.48	13.03	4.97	12.62
MgO	4.07	9.18	1.22	2.2	2.94	0.47	0.2	0.19	1.5	6.8	3.08	4.25
CaO	12	2.07	4.2	6.53	15.18	0.38	0.27	0.14	0.2	4.39	7.31	4.92
Na2O	0	0	0	1.43	0.05	0	0	0	0	0	0	0
K2O	0.05	0	0.04	0.05	0.05	0.01	0	0	0.01	0	0	0.02
P2O5	0.1	0.06	0.12	0.08	0.06	0.25	0.19	0.1	0.02	0.08	0.13	0.08
H2O-	0.17	0.13	0.14	0.09	0.21	0.11	0.09	0.06	0.1	0.27	0.05	0.18
LOI	13.49	12.08	5.78	6.04	19.94	0.15	0.11	0.12	0.84	15.09	11.01	12.14
TOTAL	99.24	99.8	100.21	99.73	98.04	99.43	99.77	99.93	101.96	99.39	99.41	99.67
V	8	14	13	6	9	40	20	13	21	9	9	5
Cr	2	0	52	25	0	79	85	66	78	35	24	3
Co	0	28	0	0	66	0	0	0	0	0	0	0
Rb	17	6	24	16	20	17	15	20	34	22	19	23
Sr	75	27	28	317	452	21	22	25	47	110	27	63
Y	25	26	32	24	26	31	24	29	51	43	32	33
Zr	32	39	43	19	13	42	38	40	62	4	40	41
Nb	17	20	24	16	19	21	19	23	41	27	23	25
Zn	14	18	1	15	20	8	0	0	44	121	0	13
Cu	94	146	77	86	21	31	66	116	252	104	118	12
Ni	10	17	19	14	11	25	22	29	35	23	17	8

APPENDIX

ANALYSIS OF BOREHOLES

	1	1	1	1	1	2	2	2	2	2	3	3
	Bif 1/OLP2	LBH1/OLP2	LBP1A/OLP2	RBCHP/OLP2	UBH2/OLP2	Bif1/EMP5	OX1/EPM5	OX2/EPM5	UBH2/EPM5	UBH1/EPM5	Bif1/OLW7	UBH-2/OLW7
SiO2	27.13	19.62	29.22	38.74	16.07	42.03	47.9	38.03	52.02	12.81	20.45	18.07
TiO2	0.03	0.04	0.04	0.04	0.04	0.04	0.03	0.04	0.04	0.04	0.04	0.05
Al2O3	0.28	0.19	0.25	0.18	0.24	0.37	0.13	0.14	0.39	0.21	0.29	0.26
Fe2O3	34.85	42.08	57.18	44.12	31.19	55.49	50.8	61.06	46.36	46.67	52.08	47.08
MnO	7.07	14.35	2.02	0.23	12.07	0.13	0.05	0.05	0.48	13.03	4.97	12.62
MgO	4.07	9.18	1.22	2.2	2.94	0.47	0.2	0.19	1.5	6.8	3.08	4.25
CaO	12	2.07	4.2	6.53	15.18	0.38	0.27	0.14	0.2	4.39	7.31	4.92
Na2O	0	0	0	1.43	0.05	0	0	0	0	0	0	0
K2O	0.05	0	0.04	0.05	0.05	0.01	0	0	0.01	0	0	0.02
P2O5	0.1	0.06	0.12	0.08	0.06	0.25	0.19	0.1	0.02	0.08	0.13	0.08
H2O-	0.17	0.13	0.14	0.09	0.21	0.11	0.09	0.06	0.1	0.27	0.05	0.18
LOI	13.49	12.08	5.78	6.04	19.94	0.15	0.11	0.12	0.84	15.09	11.01	12.14
TOTAL	99.24	99.8	100.21	99.73	98.04	99.43	99.77	99.93	101.96	99.39	99.41	99.67
V	8	14	13	6	9	40	20	13	21	9	9	5
Cr	2	0	52	25	0	79	85	66	78	35	24	3
Co	0	28	0	0	66	0	0	0	0	0	0	0
Rb	17	6	24	16	20	17	15	20	34	22	19	23
Sr	75	27	28	317	452	21	22	25	47	110	27	63
Y	25	26	32	24	26	31	24	29	51	43	32	33
Zr	32	39	43	19	13	42	38	40	62	4	40	41
Nb	17	20	24	16	19	21	19	23	41	27	23	25
Zn	14	18	1	15	20	8	0	0	44	121	0	13
Cu	94	146	77	86	21	31	66	116	252	104	118	12
Ni	10	17	19	14	11	25	22	29	35	23	17	8

	3	3	3	3	3	4	4	4	4	5	5	5	5	5
	Bif3/OLW7	OX2/OLW7	LBH1/OLW7	LBH2/OLW7	UBH2/OLW7	Bif1/U17	Bif3/U17	LBH1/U17	UBH1/U17	Bif2/OLW3	Bif3/OLW3	OX1/OLW3	LBH1/OLW3	LBH2/OLW3
SiO2	36.41	42.29	25.73		17.64	33.14	40.15	16.45	9.27	35.29	44.07	34.33	24.49	6.98
TiO2	0.04	0.03	0.05		0.05	0.03	0.03	0.03	0.05	0.03	0.03	0.04	0.04	0.05
Al2O3	0.16	0.21	0.043		0.24	0.18	0.18	0.21	0.29	0.18	0.14	0.18	0.3	0.37
Fe2O3	43.84	56.82	57.74		47.59	48.46	42.83	39.33	39.45	45.16	43.16	54.19	48.05	58.16
MnO	1.81	0.05	3.59		13.05	0.29	0.23	17.85	19.15	0.28	0.16	0.3	9.31	1.35
MgO	2.78	0.18	2.14		4.13	1.26	2.16	8.5	4.76	1.86	1.52	1.58	5.19	4.1
CaO	6.57	0.15	4.13		4.85	8.74	7.13	2.55	8.58	8.55	5.39	3.24	3.68	17.07
Na2O	0	0	0		0	0	0	0	0.2	0	0	0	0	0
K2O	0	0.01	0		0.02	0.01	0.04	0	0.05	0.01	0	0	0	0
P2O5	0.13	0.11	0.11		0.08	0.11	0.1	0.08	0.07	0.1	0.13	0.09	0.1	0.08
H2O	0.05	0.02	0.13		0.18	0.15	0.2	0.13	0.49	0.12	0.16	0.05	0.22	0.16
LOI	8.19	0.16	6.43		12.14	7.35	6.68	13.96	17.55	8.51	5.4	6.06	8.78	11.93
TOTAL	99.98	100.03	100.093		99.97	99.72	99.73	99.09	99.91	100.09	100.16	100.06	100.16	100.25
V	7	12	13	11	14	6	7	12	20	6	11	8	11	13
Cr	24	53	45	0	0	29	27	0	0	46	48	37	10	0
Co	0	0	0	20	64	0	0	37	53	0	0	0	19	44
Rb	14	21	21	9	22	17	17	18	25	15	11	17	19	21
Sr	22	24	29	49	62	244	312	30	234	238	46	29	34	46
Y	28	25	35	19	31	28	25	26	30	29	25	32	31	31
Zr	35	38	46	27	39	26	18	40	31	24	34	38	41	40
Nb	17	21	25	9	24	18	16	22	23	17	15	21	23	24
Zn	6	0	0	14	16	25	28	39	54	20	9	4	14	23
Cu	35	23	95	60	23	31	59	18	168	105	117	155	111	232
Ni	15	22	17	10	18	15	12	20	20	9	13	15	21	20

	3	3	3	3	3	4	4	4	4	5	5	5	5	5
	Bif3/OLW7	OX2/OLW7	LBH1/OLW7	LBH2/OLW7	UBH2/OLW7	Bif1/U17	Bif3/U17	LBH1/U17	UBH1/U17	Bif2/OLW3	Bif3/OLW3	OX1/OLW3	LBH1/OLW3	LBH2/OLW3
SiO2	36.41	42.29	25.73		17.64	33.14	40.15	16.45	9.27	35.29	44.07	34.33	24.49	6.98
TiO2	0.04	0.03	0.05		0.05	0.03	0.03	0.03	0.05	0.03	0.03	0.04	0.04	0.05
Al2O3	0.16	0.21	0.043		0.24	0.18	0.18	0.21	0.29	0.18	0.14	0.18	0.3	0.37
Fe2O3	43.84	56.82	57.74		47.59	48.46	42.83	39.33	39.45	45.16	43.16	54.19	48.05	58.16
MnO	1.81	0.05	3.59		13.05	0.29	0.23	17.85	19.15	0.28	0.16	0.3	9.31	1.35
MgO	2.78	0.18	2.14		4.13	1.26	2.16	8.5	4.76	1.86	1.52	1.58	5.19	4.1
CaO	6.57	0.15	4.13		4.85	8.74	7.13	2.55	8.58	8.55	5.39	3.24	3.68	17.07
Na2O	0	0	0		0	0	0	0	0.2	0	0	0	0	0
K2O	0	0.01	0		0.02	0.01	0.04	0	0.05	0.01	0	0	0	0
P2O5	0.13	0.11	0.11		0.08	0.11	0.1	0.08	0.07	0.1	0.13	0.09	0.1	0.08
H2O	0.05	0.02	0.13		0.18	0.15	0.2	0.13	0.49	0.12	0.16	0.05	0.22	0.16
LOI	8.19	0.16	6.43		12.14	7.35	6.68	13.96	17.55	8.51	5.4	6.06	8.78	11.93
TOTAL	**99.98**	**100.03**	**100.093**		**99.97**	**99.72**	**99.73**	**99.09**	**99.91**	**100.09**	**100.16**	**100.06**	**100.16**	**100.25**
V	7	12	13	11	14	6	7	12	20	6	11	8	11	13
Cr	24	53	45	0	0	29	27	0	0	46	48	37	10	0
Co	0	0	0	20	64	0	0	37	53	0	0	0	19	44
Rb	14	21	21	9	22	17	17	18	25	15	11	17	19	21
Sr	22	24	29	49	62	244	312	30	234	238	46	29	34	46
Y	28	25	35	19	31	28	25	26	30	29	25	32	31	31
Zr	35	38	46	27	39	26	18	40	31	24	34	38	41	40
Nb	17	21	25	9	24	18	16	22	23	17	15	21	23	24
Zn	6	0	0	14	16	25	28	39	54	20	9	4	14	23
Cu	35	23	95	60	23	31	59	18	168	105	117	155	111	232
Ni	15	22	17	10	18	15	12	20	20	9	13	15	21	20

	5	5	6	7	8							
	UBH1/OLW3	UBH2/OLW3	Bif2/EPM5	OX1/OUN7	LBH1A/U7	HB1	HB2	HB3	HB4	HB5	HB6	HB7
SiO2	26.12	24.16	47.03	33.15	29.81	61.43	38.6	7.42	17.06	11.56	15.78	13.19
TiO2	0.04	0.04	0.04	0.03	0.05	0.04	0.04	0.08	0.04	0.05	0.04	0.04
Al2O3	0.36	0.22	0.24	0.16	0.57	0.7	0.32	0.64	0.32	0.25	0.22	0.28
Fe2O3	40.29	53.49	51.87	39.57	64.01	37.16	60.15	90.16	33.35	36.7	43.37	39.41
MnO	2.31	1.31	0.18	1.1	0.86	0.15	0.04	0.26	14.18	14.89	12.67	19.04
MgO	1.74	2.39	0.41	4.11	1.63	0.55	0.41	0.64	3.86	7.21	3.41	5.61
CaO	15.12	7.92	0.08	9.01	1.74	0.09	0.19	0.16	11.35	10.2	9.94	6.4
Na2O	0	4.11	0	0	0.01	0	0	0	0	0	0	0
K2O	0.01	0.06	0.01	0	0.15	0.01	0.02	0	0	0.01	0	0.01
P2O5	0.08	0.08	0.04	0.11	0.09	0.03	0.15	0.04	0.07	0.06	0.08	0.06
H2O-	0.25	0.21	0.17	0.11	0.21	0.05	0.04	0.15	0.18	0.16	0.42	0.24
LOI	13.43	5.9	0.19	12.9	0.85	0.37	0.44	0.22	18.5	18.73	13.37	15.56
TOTAL	**99.75**	**99.89**	**100.26**	**100.25**	**99.98**	**100.58**	**100.4**	**99.77**	**98.91**	**99.82**	**99.3**	**99.84**
V	9	15	13	8	13	20	12	18	14	14	11	15
Cr	29	31	53	30	60	81	60	93	0	0	0	0
Co	2	0	0	0	0	0	0	0	75	57	18	28
Rb	18	22	15	12	39	11	21	35	14	16	21	18
Sr	1124	421	21	31	26	78	31	52	71	57	135	56
Y	27	29	60	24	29	20	29	209	26	27	32	26
Zr	0	21	38	32	45	34	41	54	36	36	35	37
Nb	20	24	19	15	27	14	25	39	18	20	24	22
Zn	22	23	0	3	18	7	1	0	8	22	22	24
Cu	158	24	22	123	157	51	54	343	107	175	241	62
Ni	14	17	17	11	24	19	21	44	12	14	18	21